Analysis of Doppler Experiments (III)

—SEFOR—

August, 1974

POWER REACTOR AND NUCLEAR FUEL DEVELOPMENT CORPORATION

N251 74-20
August, 1974

Analysis of Doppler Experiments (III)*

- SEFOR -

Shigeki Fukutomi** Tsutomu Otsuka**
Shigeaki Tunoyama** Yoshitaka Sueoka**
and Kazuo Monta**

Abstract

The SEFOR (Southwest Experimental Fast Oxide Reactor) project in the United States was undertaken in order to evaluate the Doppler reactivity effect, which is an important parameter for Fast Reactor Safety, and demonstrated the usefulness of the Doppler effect for the inherent safety and stability of LMFBR.

This report describes the results of analysis performed to evaluate the Doppler reactivity effect from experimental data on the super-prompt critical transients of the project.

The super-prompt critical transient tests were performed on two different cores: Core I and Core II. Following the previous report (J201 73-03), this report describes the analysis performed on Core I.

The objective of the analysis is to evaluate the usual method of dynamic analysis for these severe transients by comparing the result of analysis with the experimental data. The objective is also to clarify the parameters and the method of approximation which have an important effect on the analysis.

This is the translation of the report, No.J201 74-03, issued in February, 1974

* Work performed by Tokyo Shibaura Electric Co., Ltd. under contract with Power Reactor and Nuclear Fuel Development Corp.
** Nippon Atomic Industry Group Co., Ltd.

This analysis is first performed with a one point model for reactor kinetics. It is found that the analytical results agree well with the experimental data and that the dynamic analysis model and the theory of Doppler coefficient are sound.

Next, the model for reactor kinetics is replaced with a one dimensional space-time model, and the effects of variations of neutron flux distribution are analyzed.

Analysis of Doppler Experiments (III)

Table of Contents

1. Introduction

The Southwest Experimental Fast Oxide Reactor (SEFOR) project in the United States was undertaken in order to evaluate the Doppler reactivity effect, which is an important parameter for fast reactor safety, and demonstrated the usefulness of the Doppler effect for inherent safety and stability of LMFBR.[10]

Compilation of the data from this project,[1] and an analysis of the static experimental data, such as power vs. the Doppler feedback,[2] were performed, and reported by Tokyo Shibaura Electric Co., Ltd. (Toshiba) under contracts with the Power Reactor and Nuclear Fuel Development Corporation (PNC). This report describes the results of evaluation study of the Doppler effect based on the transient data from the SEFOR super-prompt critical tests.

The SEFOR is a 20 MWt fast spectrum reactor fueled with mixed PuO_2-UO_2 and cooled with sodium. The SEFOR transient tests were performed on two different cores; Core I and Core II. Core I contained six volume per cent BeO, which was replaced with stainless steel in Core II to harden the neutron spectrum. This report, following the previous report (J201 73-03), describes the analysis of the transient test results performed on Core I.

In these tests, the reactor power was brought to an initial steady state power level of either 1, 2, 5 or 8 MW, whereupon a B_4C rod with positive reactivity less than 1.3 $ was ejected from the center of the core in approximately 0.1 second. The resulting power transients were accompanied with rapid fuel temperature rises, and the negative Doppler reactivity effect produced by fuel temperature changes moderated the power levels up to 10,000 MWt and a maximum fuel temperature rise of 340 °C. The SEFOR Core I super-prompt critical transients

demonstrated, for the first time at the sodium cooled fast reactor, the capability of the Doppler effect to turn the power around and to shut down the reactor safely, even in the cases of super-prompt critical reactivity insertions.

The program started with familiarization transients, which involved reactivity insertions of 0.5 $ or less. Through sub-prompt critical transients which involved reactivity insertions greater than 0.5 $, but less than 1.0 $, the program was completed with super-prompt critical transient tests that resulted from reactivity insertions in excess of 1.0 $. The SEFOR Core I transient test program included 27 cases in all.

The purpose of this report is to evaluate the analysis method and to make sure of approximation methods and parameters, which have an important influence upon such analyses.

In this report, these transient test results are simulated by a usual transient analysis method.

Analyses are mainly focused on the super-prompt critical transients with large nominal reactivity insertions. This is because, in these cases, the Doppler reactivity feedback must be larger and experimental errors would be small. Therefore, it is considered to be more favorable for the evaluation of the analysis method.

The analysis performed by using a space independent kinetics model gave a very good agreement between calculated results and data measured qualitatively on the transient tests. This showed the correctness of the dynamic analysis model and of the Doppler effect theory. There remain, however, a few problems to be examined; in approximate methods employed in the calculations of local and core averaged fuel temperatures, in the determination of the value of effective delayed

neutron fraction, Beff, etc. A one dimensional space-time model was applied to investigate especially an influence of radial neutron flux distributions upon the local Doppler reactivity effect of the core.

2. Summary of SEFOR Transient Experiments

The SEFOR transient experiments were performed on two different cores. One is Core I, which contained six volume per cent BeO, and the other is Core II, in which the BeO was replaced by stainless steel in order to harden the neutron spectrum. In addition, the experimental program was divided into three groups, depending upon the ranges of reactivity inserted (see Table 2.1).

In this analytical work, attention was focused on the super-prompt critical experiments, because the Doppler feedback was the most prominent in these cases and there were relatively many data on these test cases.

Input reactivity for transient test was provided by the fast reactivity excursion device (FRED), as shown in Fig. 2.1. This device, consisting of a B_4C rod, was ejected from the center of the core in approximately 0.1 second and produced a rapid insertion of positive reactivity. The resulting rapid power transient was moderated by the Doppler feedback, due to the fuel temperature change, until a delayed scram terminated the test at about 0.35 sec.

Neutron flux signals during a transient test, as well as fuel temperature, coolant temperature and flow signals, were digitized with an analog-to-digital converter and stored on magnetic tapes. The raw data obtained during the tests were treated to reduce spurious fluctuations. In addition, the treated data were used for the calculation of reactivity and energy release (see Fig. 2.2).[3] These data were compiled and described in a series of AEC Reports on the SEFOR program. In this analysis work, however, an attempt was made to examine only a limited number of data, which could be obtained in time.

The Core I transient tests, as shown in Table 2.1, were divided

into familiarization, sub-prompt critical and super-prompt critical tests by the ranges of inserted reactivities. The familiarization transient tests involved reactivity insertions of 40¢ and 50¢ from initial power levels of 1 and 10 MW. Eight transients were performed during the familiarization test sequence. It is difficult to analyze the Doppler effect of these transients because the reactivity feedback was small during the tests.

Eleven tests were performed under the heading of the sub-prompt critical transients. Two of these tests involved reactivity insertions of about 80¢ from nominal initial power levels of 1 MWt. The reactivity feedback produced during tests was small. The other tests involved reactivity insertions of about 97¢, which resulted in appreciable reactivity feedback. These transients, as well as the familiarization experiments, were performed to test the experimental equipment and instruments. Results of these transients, which involved reactivity insertions of 96 ~ 97¢ from initial power levels of 2, 5 and 10 MW, are tabulated in Table 2.2. The table shows energy coefficients and peak power levels, as well.

Under the heading of the super-prompt critical transients, in which reactivity insertions were greater than 1 $, eight tests were performed. The transients involved reactivity insertions of ~ 1.18 $ and 1.28 $ by the FRED rod from initial power levels of 2, 5 and 8 MW. Each published report gives slightly different values for data on the FRED worth and experimental data. For example, a HEDL report (HEDL-TME 73-42) presents 1.16 $ and 1.26 $ as values of the FRED worth.[12] In these transients, the reactor power increased rapidly just after the time when inserted reactivity crossed the value of 1 $. The peak power level reached about 1,000 times as high as the

initial power level. However, the Doppler feedback lowered the power to the level of a twentieth of the peak power level within 10 msec. Figure 2.3 shows an example of the power history during the transient tests. Experimental data on the super-prompt critical transients are summarized in Table 2.3.

TABLE 2-1

SEFOR TRANSIENT TEST PROGRAM

Test	Reactivity Range ($)	Power Level Initial (MW)	Power Level Peak (MW)	Maximum Increase in Fuel Temperature (°C)	Maximum Reactivity Feedback ($)
Core I					
Familiarization	$\Delta k \lesssim 0.5$	1,10	< 20	<10	-0.01
Sub-Prompt Critical	$0.5 < \Delta k < 1.0$	1,2,5,10	250	70	-0.15
Super-Prompt Critical	$1.0 < \Delta k < 1.3$	2,5,8	9000	280	-0.45
Core II					
Sub-Prompt Critical	$0.5 < \Delta k < 1.0$	2,5,10	180	60	-0.12
Super-Prompt Critical	$1.0 < \Delta k < 1.2$	2,5,8	10000	340*	-0.48
Reactivity Insertion Time	~0.1 seconds				
Test Terminated by Scram	~0.35 seconds after transient initiation				

* Peak fuel temperature reached in the transient tests was ~1800 °C (~1000 °C core average), Reprinted from GEAP-13929

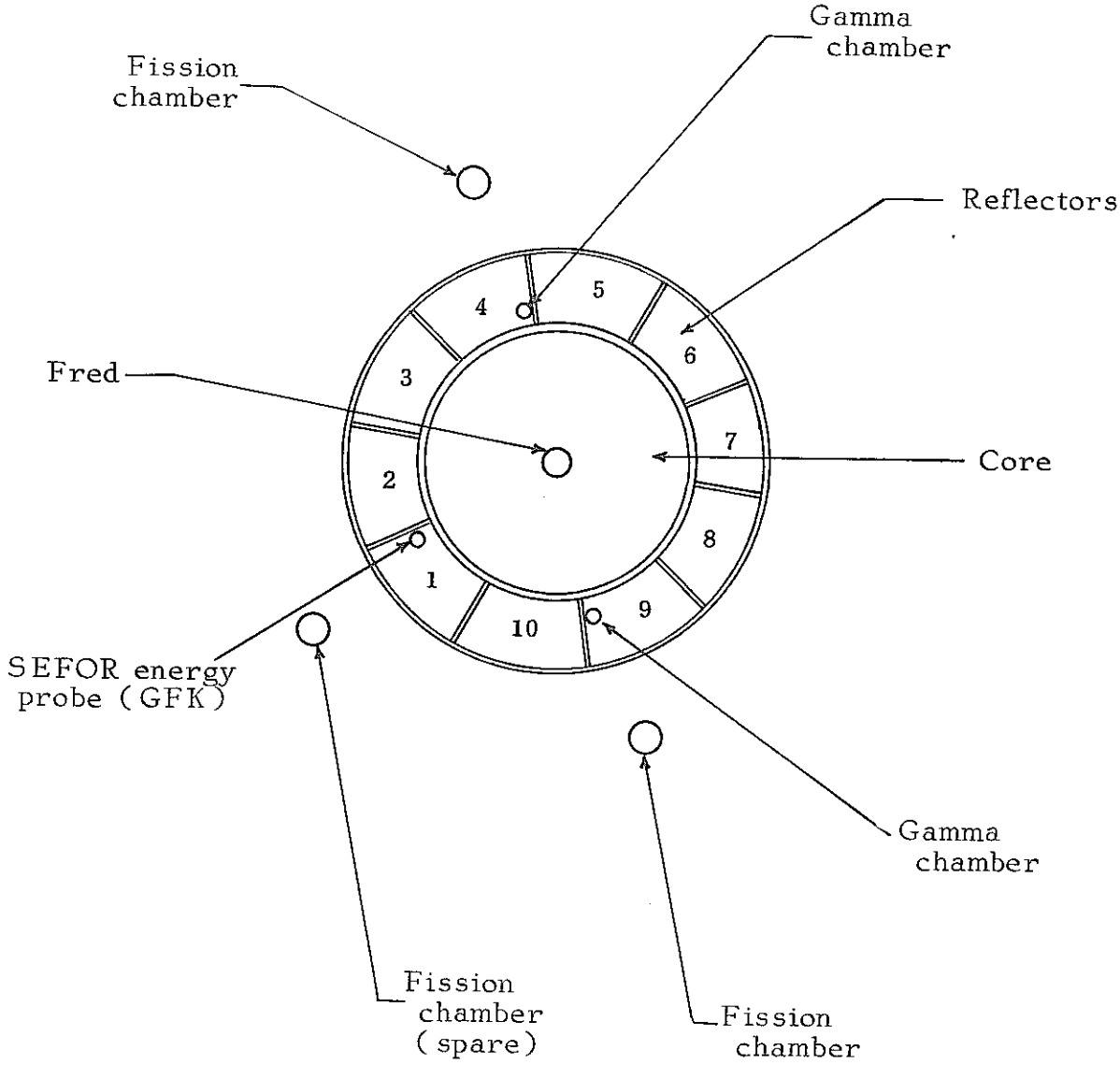

Reprinted from GEAP 10010-30

Fig. 2.1 Transient Detector Locations

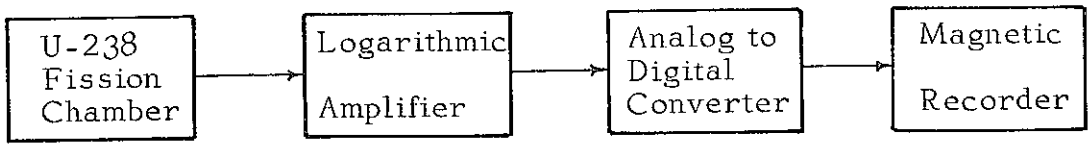

(1) Recording Experimental Data

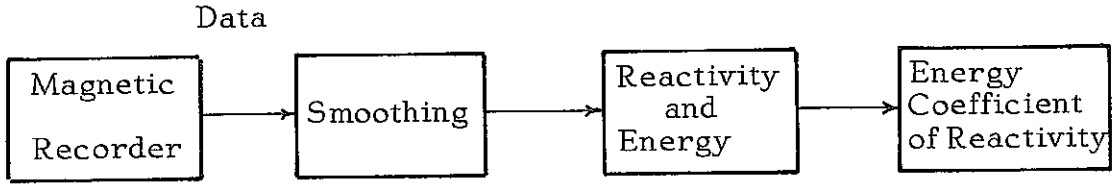

(2) Data Treatment

Fig. 2.2 Flow Diagram of Recording and Treatment of SEFOR Experimental Data

Table 2.2 Results of Sub-Prompt Critical Transients

Test	Initial Power (MW)	Maximum FRED Worth		Energy Coefficient		Maximum Peak Power	
		Detector A (cents)	Detector B (cents)	A (cents/MW-sec)	B	A (MW)	B
2	2	96.6	96.6	-0.57	-0.56	80	85
3	2	96.7	96.5	-0.54	-0.58	85	80
4	5	96.4	96.5	-0.46	-0.45	140	150
5	5	96.6	96.6	-0.45	-0.45	150	150
6	5	96.9	96.8	-0.43	-0.44	160	160
7	10	96.6	96.7	-0.36	-0.37	260	250
8	10	-	96.6	-	-0.36	-	260
9	10	96.9	-	-0.34	-	270	-
10	10	-	-	-	-	-	-

Reprinted from GEAP 10010-29

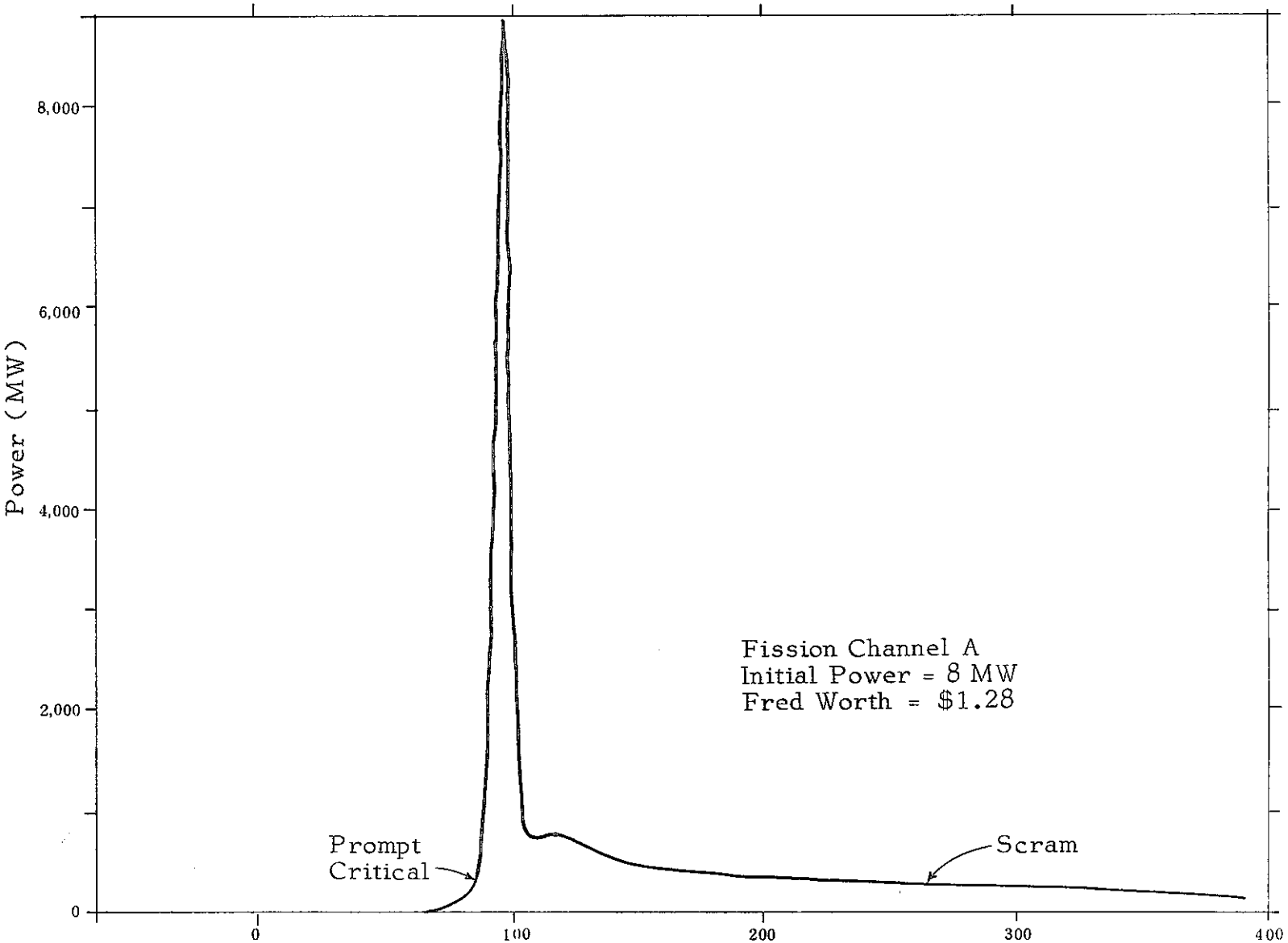

Reprinted from
GEAP 10010-30

Fig. 2.3 Time Dependent Power for Super-Prompt Transient No.8

Table 2.3 Super-prompt Transient Power, Energy and Energy Coefficients

From GEAP-10010-30
Table 5-1 ~ 5.3

Test	Initial Power (MW)	Slug Worth ($)	Peak Power (WM)	Energy Release to 0.3 sec (MJ)	Energy Coefficient (¢/MJ)
1	2	1.18	5300	82	-0.47
2	2	1.28	9000	108	-0.45
3	2	1.28	8800~9300	106	-0.45
4	5	1.18	4900~5100	93	-0.42
5	5	1.28	8200~8700	120	-0.42
6	8	1.18	5100~5500	108	-0.39
7	8	1.28	8300~8700	135	-0.39
8	8	1.28	8400~8800	136	-0.38

3. Analysis Procedure

Among the series of the SEFOR experiments, attention was focused on the super-prompt critical tests, which were considered to be the most suitable for examining the Doppler effect. In the first place, transient number 8 was studied because data on this case was easier to obtain. The data on this experiment were reported in part by General Electric (GE) and Hanford Engineering Development Laboratory (HEDL).

Data on maximum peak power level, energy released, fuel temperature and power trace were taken to be compared with calculations. The net reactivity inserted into the core, Kn(t), can be determined from the recorded power trace, P(t), using the following equation,[3]

$$Kn(t) = 1 + \frac{\ell}{\beta}\cdot\frac{1}{P(t)}\cdot\frac{dP(t)}{dt} + \frac{P(t) - P(o)}{P(t)} - \frac{1}{P(t)}\int_o^t [P(u) - P(o)]\cdot D(t-u)du$$

where ℓ/β is the ratio of the prompt neutron lifetime to the effective delayed neutron fraction, P(o) is the initial power and D(t) is the delayed neutron kernel defined as

$$D(t) = \sum_i \sum_j B_{ij}\lambda_{ij} e^{-\lambda_{ij}t}$$

In this expression, λ_{ij} is the decay constant for delayed neutrons in decay group i from fissionable isotope j, and B_{ij} is defined as $B_{ij} = \beta_{ij}/\beta$eff, $(\sum_i \sum_j B_{ij} = 1)$

The feedback reactivity, K_fb, is the difference between the net reactivity, Kn, and the input reactivity, K_F, generated by the FRED, that is,

$$K_fb\ (t) = Kn(t) - K_F(t).$$

The feedback reactivity thus determined cannot avoid inclusion of uncertainties in ℓ/β. To avoid the above uncertainties, the feedback reactivity to energy release was analyzed during the time interval following the complete ejection of the FRED from the reactor regions of reactivity influence. During this time interval, the input reactivity, K_F, is equal to a constant, K_o, and any change in net reactivity, Kn(t), is a result of change only in feedback reactivity. In this interval (between ~ 140 msec and ~ 250 msec after the transient initiation), the net reactivity may be expressed as a polynominal in energy release, E(t), of the form,

$$Kn(t) = Ko + \Sigma a_j \cdot E(t)^j.$$

By the data fit, an essentially linear relationship exists between the net reactivity and energy release for the limited energy range under consideration. When the slope of this linear relation, a_1, is defined as the reactivity energy coefficient, this can be treated as one of the experimental data. In this analysis study, the energy coefficient was regarded as one of the promissing measured values. Comparison was made with calculated values to demonstrate the validity of this analytical method. The energy coefficient data during transients are listed in Tables 2.2 and 2.3.

The experimental analysis was performed by the use of a point reactor kinetics computer code, backed up by a one-dimensional space-time kinetics code.

In the point reactor kinetics model, the core is divided into 10 radial annuli and 10 axial increments. Any fuel rod is also divided into 10 anular rings. For each core sub-region, thermo-hydro dynamics calculations were performed and the Doppler reactivity for

a change in fuel temperature, as well as other feedback reactivities, were evaluated. Calculated results were evaluated by comparison with experimental data, such as the maximum peak power level, initial fuel ttemperature, power trace, energy release and reactivity energy coefficient.

The analysis was performed on all of the super-prompt critical experiments and on a few typical cases of the sub-prompt critical tests. The sensitivity study of calculated results to variation in parameters, such as nuclear kinetics data and thermodynamic parameters, was conducted about one of the super-prompt critical transients.

The one-dimensional space-time kinetics model was used to calculate changes in radial power distribution after the withdrawal of the FRED. Calculated results of peak power and feedback reactivity were compared and evaluated with those calculated by the point reactor kinetics code.

4. Analysis by the Point Reactor Kinetics Model

4-1. Outline of the Point Reactor Kinetics Code (VODGIN)

Thermo-hydro dynamics model

A typical coolant flow channel is selected, as shown in Fig. 4-1.1. The fuel rod and clad temperature distributions and the coolant behavior are assumed to satisfy the following equations.

Only the radial heat conduction in fuel rod and clad is taken into consideration. Then, the Fourier heat conduction equation for a cylindrical element can be written as

$$\frac{\partial}{\partial t}(\alpha\theta) = \frac{1}{r}\frac{\partial}{\partial r}\left(rK\frac{\partial\theta}{\partial r}\right) + g \qquad (4\text{-}1.1)$$

Laws of conservation of mass, momentum and energy, and an equation of state may be written as

$$\frac{\partial\rho}{\partial t} + \frac{\partial G}{\partial Z} = 0 \qquad (4\text{-}1.2)$$

$$\frac{\partial G}{\partial t} + \frac{\partial}{\partial Z}\left(\frac{G^2}{\rho}\right) + \frac{\partial\rho}{\partial Z} = -\left(\rho g + \frac{2f_F G|G|}{D_h'\rho}\right) \qquad (4\text{-}1.3)$$

$$\rho\frac{\partial H}{\partial t} + G\frac{\partial H}{\partial Z} = \frac{1}{V_c}\left(A_E\phi_{E\to C} - A_S\phi_{C\to S}\right) \qquad (4\text{-}1\text{-}4)$$

$$\rho = \rho(H) \qquad (4\text{-}1.5)$$

These equations describe the behaviors of coolant flow through a channel.

The Crank-Nicolson method is applied to integrate the equation (4-1.1) numerically. For the radial nodes, i = 1, 2, ---, I-1, the following finite-difference approximation of the temperature is derived.

$$-U^{j+1}_{i-\frac{1}{2}}\cdot\theta^{j+1}_{i-1}+(U^{j+1}_{i-\frac{1}{2}}+W^{j+1}_{i}+U^{j+1}_{i+\frac{1}{2}})\,\theta^{j+1}_{i}-U^{j+1}_{i+\frac{1}{2}}\,\theta^{j+1}_{i+1}$$

$$=U^{j}_{i-\frac{1}{2}}\,\theta^{j}_{i-1}+(-U^{j}_{i-\frac{1}{2}}+W^{j}_{i}-U^{j}_{i+\frac{1}{2}})\,\theta^{j}_{i}+U^{j}_{i+\frac{1}{2}}\,\theta^{j}_{i+1}$$

$$+\frac{\Delta t}{2}(R^{(-)}_{i}\,g^{j+\frac{1}{2}}_{i-\frac{1}{2}}+R^{(+)}_{i}\,g^{j+\frac{1}{2}}_{i+\frac{1}{2}}) \qquad (4\text{-}1.6)$$

The boundary conditions at points i = 0, I, I + 1, and I + 2, are given as follows,

$$\frac{\partial\theta}{\partial r}\Big|_{i=0}=0 \qquad (4\text{-}1.7)$$

$$-K\frac{\partial\theta}{\partial r}\Big|_{i=I}=h_{F\to g}(\theta_{I}-\theta_{I+1}) \qquad (4\text{-}1.8)$$

$$-Ke\frac{\partial\theta_{e}}{\partial r}\Big|_{i=I+1}=\frac{R_{F}}{Re}\,h_{F\to g}(\theta_{I+1}) \qquad (4\text{-}1.9)$$

$$-Ke\frac{\partial\theta_{e}}{\partial r}\Big|_{i=I+2}=h_{E\to C}\,(\theta_{I+2}-\theta_{C}) \qquad (4\text{-}1.10)$$

where

$$U_{i}=\frac{\Delta t}{\Delta r^{2}}\,r_{i}\,K_{i}$$

$$W_{i}=R^{(-)}_{i}\,\alpha_{i-\frac{1}{2}}+R^{(+)}_{i}\,\alpha_{i+\frac{1}{2}}$$

$$R^{(-)}_{i}=r_{i}-\Delta r/4$$

$$R^{(+)}_{i}=r_{i}+\Delta r/4$$

and

θ_{C} : Coolant temperature.

Thus, temperature θ_{i} at any point i (i = 0, ---- , I + 2) can be

obtained by a set of simultaneous equations from Eqs. (4-1.6) through (4-1.10).

For transient coolant flow treatment, in order to eliminate the sonic effect, a momentum integral model is applied, i.e., the momentum equation (Eq. 4-1.3) is therefore integrated over the entire channel length;

$$\frac{\partial \bar{G}}{\partial t} = \frac{1}{L_C} (\Delta P - R) \qquad (4\text{-}1.11)$$

This equation yields the behavior of the average mass velocity with time. From Eqs. (4-1.2) to (4-1.5), the space mass velocity distribution can be obtained by integrating the equation

$$\frac{\partial G}{\partial Z} = \frac{\psi(H)}{\rho} \left(G \frac{\partial H}{\partial Z} - \hat{q} \right) \qquad (4\text{-}1.12)$$

where

$$\psi(H) = \frac{d\rho}{dH}$$

$$\hat{q} = \frac{1}{V_C} (A_E \phi_{E \to C} - A_S \phi_{C \to S})$$

a) When the channel inlet fluid velocity is given, the coolant velocity in each axial section is solved directly from Eq. (4-1.12)

$$\left.\begin{aligned} G_o^{j+1} &= G_{inlet}^{j+1} \\ G_n^{j+1} &= \frac{1}{2-\delta} \left[(2+\delta) G_n^{j+1} - 2\Delta Z \hat{q}_{n+\frac{1}{2}}^{j+1} \left(\frac{\psi}{\rho} \right)_{n+\frac{1}{2}}^{j+1} \right] \\ \delta &= \left(\frac{\psi}{\rho} \right)_{n+\frac{1}{2}}^{j+1} \left(H_{n+1}^{j+1} - H_n^{j+1} \right) \end{aligned}\right\} \qquad (4\text{-}1.13)$$

And b), when the total pressure drop over the entire channel is provided, the coolant mass velocity is given as follows,

$$
\left.
\begin{aligned}
&G_0^{j+1} = \alpha \sum_{n=1}^{N} \left(\rho_{n-1}^{j+1} \Gamma_{n-1} + \rho_n^{j+1} \Gamma_n \right) \\
&G_n^{j+1} = \left(\frac{\rho_n}{\rho_0}\right)^{j+1} \left(G_0^{j+1} - \Gamma_n \right) \qquad (n=1, \cdots, N) \\
&-\alpha = 2 \sum_{n=1}^{N-1} \rho_{n+\frac{1}{2}}^{j+1} \\
&\Gamma_0 = \sum_{n=1}^{N} \left(G_{n-1}^{j} + G_n^{j} \right) + \frac{2\Delta t}{\Delta Z} \left(\Delta P^{j+\frac{1}{2}} + R^{j+\frac{1}{2}} \right) \\
&\Gamma_n = \Delta Z \, \rho_0^{j+1} \sum_{n=1}^{N-1} \left[\psi \left(\frac{\hat{q}}{\rho^2} \right) \right]_{n+\frac{1}{2}}^{j+1}
\end{aligned}
\right\} \qquad (4\text{-}1.14)
$$

In this case, however, as R is a function of G, an iterative method would be needed.

For the coolant enthalpy calculation, the box method is applied to Eq. (4-1.4). Then the coolant enthalpy in each node is given by

$$
\left.
\begin{aligned}
&H_0^{j+1} = H_{\mathrm{inlet}}^{j+1} \\
&H_{n+1}^{j+1} = H_n^{j} + \frac{1}{1+\gamma} \left[(1-\gamma) \left(H_{n+1}^{j} - H_n^{j+1} \right) + 2\Delta t \left(\frac{\hat{q}}{\rho} \right)_{n+\frac{1}{2}}^{j} \right] \\
&\gamma = \frac{\Delta t}{\Delta Z} \left(\frac{G}{\rho} \right)_{n+\frac{1}{2}}^{j}
\end{aligned}
\right\} \qquad (4\text{-}1.15)
$$

Neutronics

The point reactor kinetics formulation, with G groups of delayed neutrons, can be written as

$$
\frac{d\psi}{dt} = R\,\psi \qquad (4\text{-}1.16)
$$

where

$$R = \begin{bmatrix} \frac{1}{A}(K-1), & \lambda_1 & \cdots\cdots & \lambda_G \\ \frac{a_1}{A} & -\lambda_1 & & \\ \vdots & & \ddots & \\ & & & 0 \\ \frac{a_G}{A} & 0 & & -\lambda_G \end{bmatrix}$$

$$\psi = \mathrm{Col}(n, C_1, \cdots\cdots, C_G)$$

It is well known that E_g (4-1.16) is a "stiff" differential equation, and skill is needed in order to solve this equation efficiently. Here, the following technique is selected for this purpose. When the R in E_g. (4-1.16) is approximated by $R^{j+\frac{1}{2}}$, the integration of E_g. (4-1.16) performed over the time interval between tj and tj+1 gives

$$\psi^{j+1} = \exp(R^{j+1/2}\,\Delta t)\,\psi^j \equiv \exp(M)\,\psi^j \qquad (4\text{-}1.17)$$

An application of the second order diagonal Pade approximation to the exponential term in E_g. (4-1.17) leads to the following linear algebraic equation

$$\psi^{j+1} = \left(E - \frac{M}{2} + \frac{M^2}{12}\right)^{-1}\left(E + \frac{M}{2} + \frac{M^2}{12}\right)\psi^j \qquad (4\text{-}1.18)$$

E : unit matrix

It is easy to obtain the inverse of the matrix of this equation set and, in addition, it may be possible to apply a larger integration time step.

Integration time step size, Δt, is to be adjusted so as to satisfy the condition of truncation error limit in each time step.

When a time step size is decreased, it may reduce to the lowest minimum by a half until the error limit condition is satisfied. On the other hand, an increase of any time step size is achieved by doubling it at one integration cycle. It is not so easy to estimate the truncation error and, in this code, the Richardson Extrapolation method[17] is applied. By this method, truncation error, E^j, at any integration cycle is written by

$$E^j \doteqdot \frac{i^P}{i^P-1} \left(\psi^j_{(i)} - \psi^j \right) \qquad (4\text{-}1.19)$$

where $\psi^j_{(i)}$ is a solution of Eq. (4-1.18) for time step size, $\Delta t/i$ ($i>1$), and P is degree of accuracy.

Reactivity Feedback Model

The reactivity feedback model of the reactor includes such terms as feedbacks due to density changes in fuel, clad, coolant and structure and the Doppler reactivity feedback. Each feedback reactivity, except the Doppler effect, is assumed to be proportional to the average temperature change of each material. Three different models are available for the average fuel temperature to evaluate the Doppler effect of reactivity:

1) Based on the unweighted, core volume average fuel temperature,

$$\delta K^{(1)}_{DOP} \propto \ell_n \left(\frac{\int_{core} \theta_{fuel}(r, Z)\, dV}{\int_{core} dV} \right) \qquad (4\text{-}1.20)$$

2) Based on the unweighted, volume average fuel temperature in the average channel,

$$\delta K^{(2)}_{DOP} \propto \ell_n \bar{\theta}_{fuel} \qquad (4\text{-}1.21)$$

$\bar{\theta}_{fuel}$: average fuel temperature in the average channel

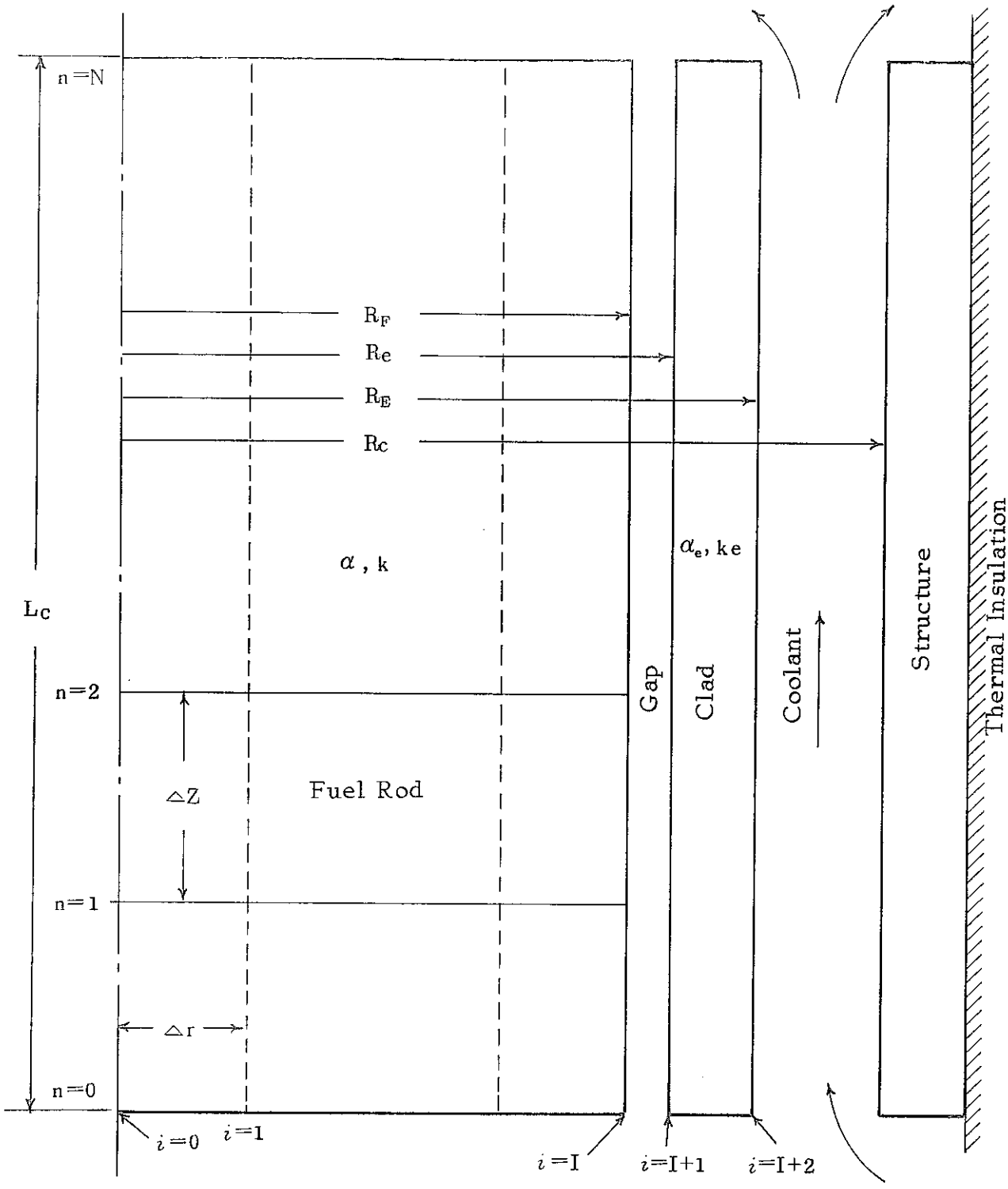

Fig. 4.1.1 Flow Channel

3) Based on the weighted, core average fuel temperature.

$$\delta K_{DOP}^{(3)} \propto \frac{\int_{core} W(r, Z)\ \ell_n \theta_{fuel}(r, Z)\, dV}{\int_{core} W(r, Z)\, dV} \qquad (4\text{-}1.22)$$

using the square of the local power density as the weighting function $W(r, Z)$.

The initial core temperature distribution is calculated by using the time invariant flux (or power) distribution function.

4-2. Significant Data Used

1. Core Element Description

The SEFOR hexagonal fuel channel contains six fuel rods (22.2 mm in diameter) and a central BeO rod (19.7 mm in diameter). The SEFOR Core I was made up of 109 such channels. Figure 4.2.1 shows a cross-sectional view of the fuel channel. Significant information on the core element components follows:[7]

Core equivalent diameter	0.88135 m
Core height	0.92865 m
Number of core elements	109
Fuel rods per core element	6
Tightener rods per core element	1
Rod pitch	2.781×10^{-2} m
Fuel channel material	Type 304 SS
Channel outside dimension across flats	0.08 m
Channel wall thickness	1.542×10^{-3} m
Side rod diameter	6.350×10^{-3} m
Fuel rod overall length	1.2604 m
Fuel rod diameter	2.4688×10^{-2} m

Fuel length	0.8588 m
Cladding material	Type 316 SS
Cladding inside diameter	2.2605×10^{-2} m
Cladding wall thickness	1.041×10^{-3} m
Fuel pellet material	PuO_2 - UO_2
Fuel pellet diameter	2.2224×10^{-2} m
Fuel pellet density	10200 Kg/m^3
Fuel theoretical density	92.6 %
Tightening rod cladding material	Type 316 SS
Tightening rod cladding outside diameter	2.2224×10^{-2} m
Tightening rod cladding wall thickness	1.016×10^{-3} m
Tightening rod BeO pellet diameter	1.9735×10^{-2} m
Tightening rod BeO pellet density	2900 Kg/m^3
Tightener sleeve material	Type 304 SS

2. Kinetics Parameters

The values of the effective delayed neutron fraction, β_{eff}, differs from one another depending on the original nuclear data used. In Ref. (2), Analysis of Doppler Experiments (II), the values in Table 4.2.1 are reported. Reference (13) reports the values shown in Table 4.2.2, based on the Keepin data and Evans and Thorpe's data, where the value of β_{eff} is 0.00309. In Ref. (10), it is reported that, through the SEFOR experimental program, the analysis has been performed using the Keepin data. In this analysis, the value of 0.00309 was used for the effective delayed neutron fraction, β_{eff}. Table 4.2.2 also shows the values of the delayed neutron precursor decay constants, λ_i, used.

1.60×10^{-4} sec was used for the value of ℓ/β_{eff}. It was reported that this value gave a good fit for the reactivity insertion curve produced by FRED rod ejection (see Fig. 4.2.2).[10]

3. Coolant Conditions

Since each transient test terminated in a short time, mass flow rate and reactor inlet temperature of coolant can be assumed to be constant during the test. The initial conditions for each test of the super-prompt critical and the sub-prompt critical transients were almost the same, except for the initial power level. Table 4.2.3 summarizes the reactor heat balance data for the super-prompt critical tests.

Coolant flow in fuel channels differed depending on the core orifice zones.[7] Coolant flow area of each channel was assumed to be same. From data on the mass flow rate and velocity of coolant in each channel (Table I-4 in Ref. (7)), the coolant flow area could be found to be 1.482×10^{-3} m^2. About 87 per cent of the rated vessel flow constituted the core flow and the rest became a leakage flow.

4. Power Density Distribution

Values of the local power density or the flux distributions were needed in order to evaluate feedback reactivities and fuel temperatures in the core. The calculated result of flux distribution was provided in the report[2] in this series of the analysis work. The radial flux distribution is shown in Fig. 4.2.3 and that of the axial direction in Fig. 4.2.4. The radial and axial distributions of local power density are shown in Figs. I-5 and

3-2 of Ref. (7), respectively. Based on these data, the power density distributions were roughly approximated by Jo function in radial direction and Sine function in axial direction, with extrapolation distances of 0.1453 meter and 0.1721 meter, respectively.

The point reactor kinetics code (VODGIN) can treat two fuel channels, an average fuel channel and a hot channel. Power and flow peaking factors of the hot channel relative to the average are listed in Table 4.2.4.

In fast transients, the total energy generated is not immediately deposited as sensible heat. This arises because of the decay of fission products. Assuming that the fission product gamma and β rays are delayed longer than the transients ($\sim$ 0.2 sec.), it was found that only about 91 per cent of the energy generated was deposited in fuel, fuel clad and coolant.[11] Of this prompt energy, the fractions deposited in the fuel, fuel clad and coolant are listed in Table 3-5 and 3-6 in Ref. (7). These values are summarized again in Table 4.2.5. Thus, in this transient analysis, 9.03 per cent of power generated was assumed to be delayed.

5. Reactivity Effects

The -0.0081 Doppler coefficient, $T\frac{dK}{dT}$, was used in this analysis work. This value was used in the analysis by GE and was concluded to be reasonable.[16] , [4] , [8]

In addition to the Doppler effect, reactivity feedbacks due to expansions of fuel, fuel clad and structures and change in coolant density were taken into account. These values are listed in Table 4.2.5. A sum of feedback reactivities, except for the

Doppler effect, was estimated to be about 12 per cent of total feedback reactivity.[4]

6. FRED Rod Reactivity Worth

The FRED rod reactivity worth can be found in Fig. 10 of Ref. (11). First, the value of 125.7¢ was used in this analysis. The time dependence of the reactivity insertion by the FRED rod during a test is shown in Table 4.2.7. These values correspond to those for transient number 8. The FRED worth takes different values between 1.25 and 1.29 $, depending on the reports. Since, in Ref. (4) and others, the value of 1.28 $ for transient number 8 was used as a standard, this value was also used in survey calculations in this analysis.

Data on the FRED rod are summarized in Table 4.2.6. The position-versus-time relation and the reactivity insertion as a function of axial position were combined to generate the reactivity insertion as a function of time. The combined FRED worth-versus-time curve is shown in Fig. 4.2.5. Using values taken from this curve, the FRED worth-vs.-time relations corresponding to the maximum reactivity insertions of 1.18 $ and 1.28 $ were obtained, and are listed in Table 4.2.7. In this analysis, the values in Table 4.2.7 were used as input reactivity dependent on the transient test case.

The reactivity-versus-time relations to be used for the sub-prompt critical transients were obtained in the same manner as shown in Fig. 4.2.6 by using values in Table 4.2.8.

7. Thermodynamic Properties

Below are summarized the major thermodynamic properties of material, such as thermal conductivity, specific heat, density and heat transfer coefficient, used for temperature calculations of core constituents, such as fuel, fuel clad, structure and coolant. Heat transfer coefficient from fuel to clad ($W/cm^2 - {}^\circ F$)[8]

$$h_{fe} = 0.04109 + 5.521 \times 10^{-4} Q + 8.738 \times 10^{-6} Q^2$$

Q : power density (W/cm^3)

Heat transfer coefficient from clad to coolant[8]

$$h_{EC} = 6.78 \quad Kcal/m^2\text{-}sec\text{-}℃$$

Fuel

Density $\rho_f = 10200 \quad Kg/m^3$[7]

Specific heat $C_{pf} = 0.0773 \quad Kcal/Kg\text{-}℃$

Thermal conductivity ($W/cm\text{-}℃$)[8]

$$K_f = 0.011 + [T(0.4848 - 0.4465D)]^{-1}$$

D : Theoretical density = 0.92

T : fuel temperature (℃)

Fuel clad (Type 316 SS)

Density $\rho_c = 7700 \quad Kg/m^3$

Specific heat $C_{pc} = 0.115 \quad Kcal/kg\text{-}℃$

Thermal conductivity $Ke = 0.00393 \quad Kcal/m\text{-}sec\text{-}℃$

Sodium

Density (g/cm^3)[19]

$$\rho_c = 0.9490 - 2.23 \times 10^{-4} T - 1.75 \times 10^{-8} T^2$$

T : sodium temperature (℃)

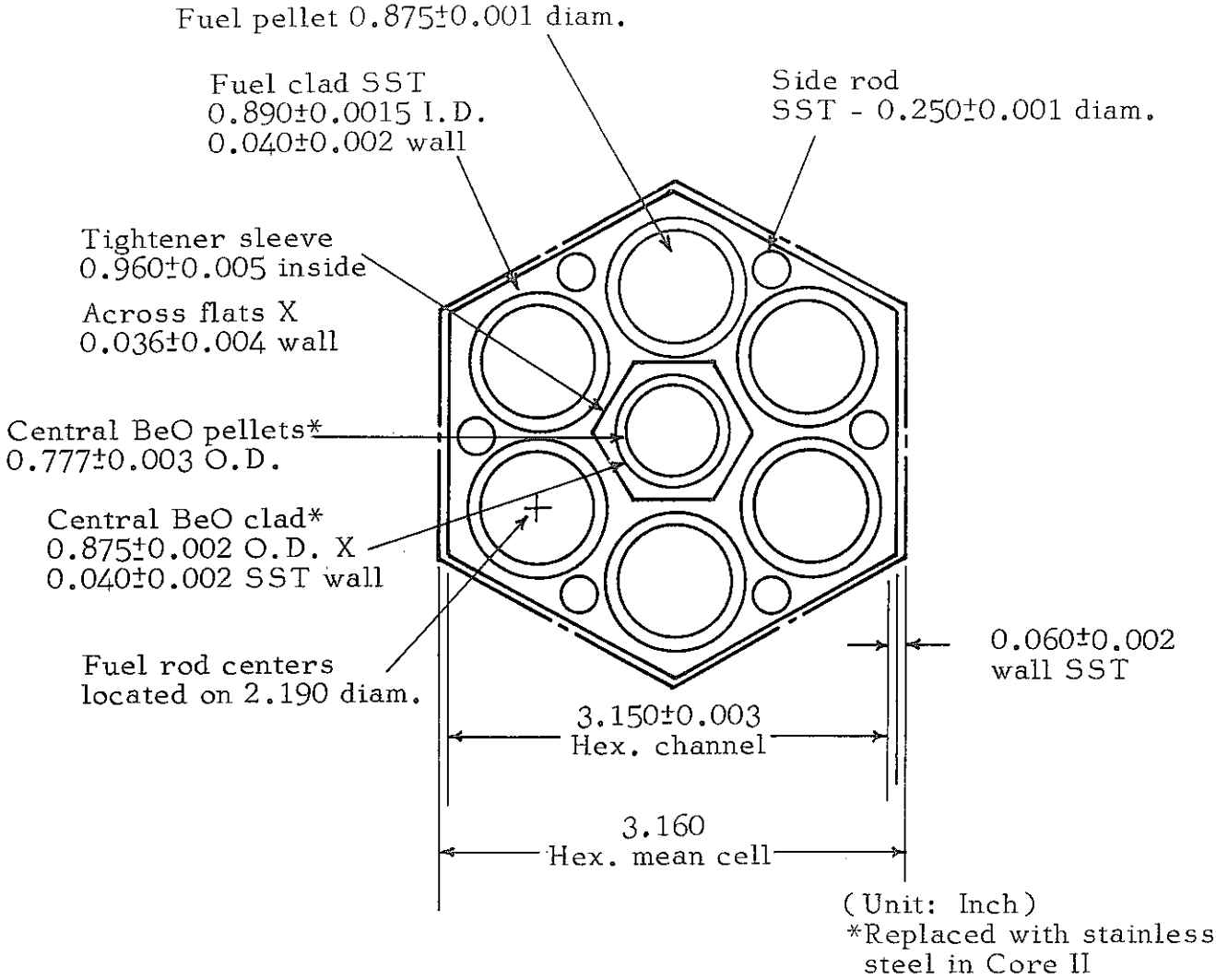

(Reprinted from GEAP-13588)

Fig. 4.2.1 SEFOR Core I Fuel Channel

Table 4.2.1 SOFER Core I Kinetics Parameters

	Keepin	Tomlinson	Krick & Evance
β_{eff}	0.00309	0.00330	0.00350
ℓ/β_{eff} (sec)	1.78×10^{-4}	1.67×10^{-4}	1.57×10^{-4}

$\ell = 5.4938 \times 10^{-7}$

From J201 73-03

Table 4.2.2 Delayed Neutron Data used in Analysis

i	$\beta_{eff}(i)$ *	λ_i (sec^{-1})
1	0.0000822	0.0130
2	0.00067285	0.0311
3	0.0005881	0.1330
4	0.00109943	0.1340
5	0.00048576	1.34
6	0.00016136	3.92
Total	0.0030896	

$\ell/\beta^*_{eff} = 1.60 \times 10^{-4}$ sec ($\ell = 4.944 \times 10^{-7}$ sec)

* From ORNL-TM-4244

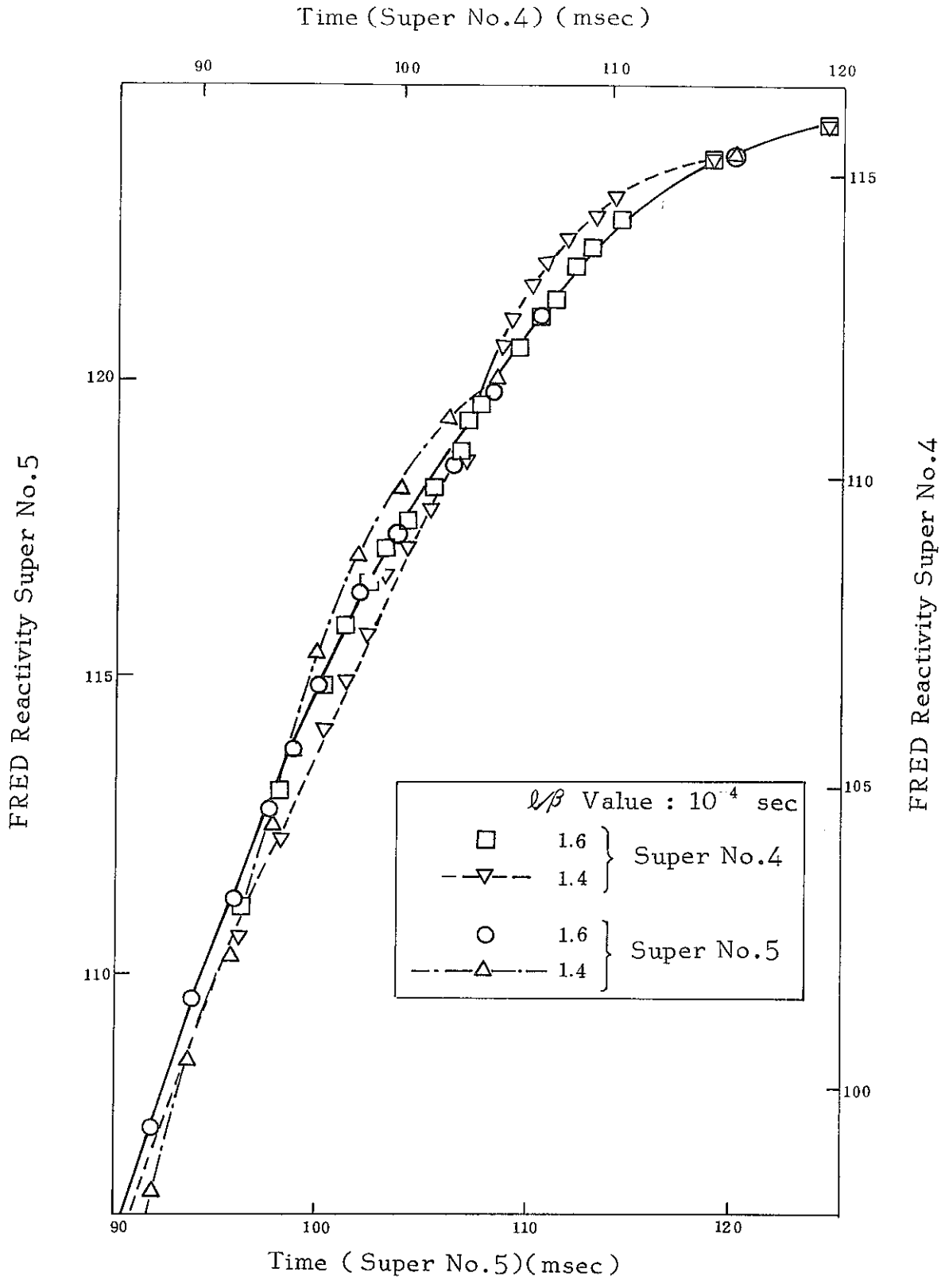

Fig. 4.2.2 FRED Reactivity versus Time Obtained by Superposition

Reprinted from GEAP-13929

Table 4.2.3 Heat Balance Data

From Table 5-5 GEAP 10010-30

Superprompt Transient Test	Date (1971)	Thermal Power (MW)	Average Coolant Temperature	Main Primary System Temperature (℃) Inlet	Outlet	Flow (kg/sec)	Auxiliary Primary System Temperature (℃) Inlet	Outlet	Flow (kg/sec)
1	Aug. 14	1.99	404.4	401.5	407.3	265.0	405.3	407.5	12.4
2	Aug. 17	1.96	405.9	403.1	408.7	261.9	401.1	407.7	12.5
3	Aug. 19	2.12	406.5	403.5	409.4	265.6	401.3	408.9	12.7
4	Aug. 21	5.24	407.1	399.6	414.4	268.2	399.7	413.6	13.0
5	Aug. 23	5.17	406.6	399.1	414.1	262.6	402.1	413.4	12.5
6	Aug. 26	8.05	405.2	393.6	416.7	265.4	396.4	414.3	13.0
7	Aug. 28	8.08	407.2	395.6	418.9	262.8	395.8	416.6	12.8
8	Aug. 30	7.99	406.7	395.1	418.3	263.1*	395.7	415.7	12.3*

Flow Area .162 m^2/Rated Flow ($^{Main}_{+ Aug}$) 273.8 kg/sec/Rated Core Flow 237.9 kg/sec

* From Table 5-6 GEAP 10010-31 /Rated Inlet Temp.404.4 ℃

Table 4.2.4 Power and Flow Peaking Factors

Location	Power Peaking Factors	Flow Peaking Factors
Hot Rod	1.485	1.55
Average Rod	1.0	1.0

From GEAP-13598

Table 4.2.5 Fraction of Energy Produced and Reactivity Coefficients

	Fraction of Energy Produced* That is Promptly Absorbed	Reactivity** Coefficient (¢/℃)
Fuel	0.879	-0.0162
Na	0.0039	-0.1368
Fuel Cladding	0.0077	-0.1296
Other Stainless Steel	0.0191	-0.2682
Total	0.9097	

* From GEAP 13598
** From GEAP 13588

Fig. 4.2.3 Neutron Flux Radial Distribution (1-D)

Reprinted from J201 73-03

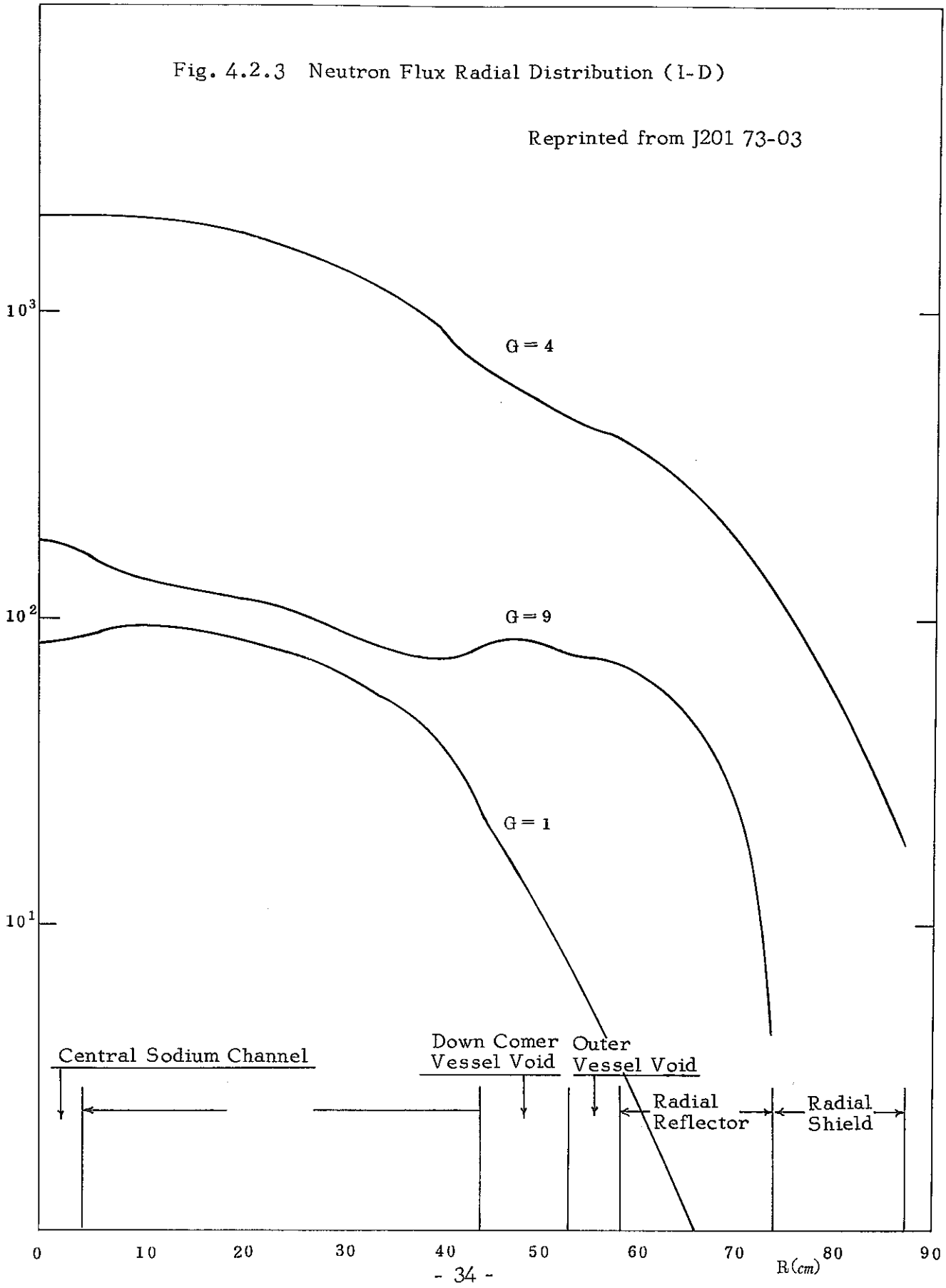

Fig. 4.2.4 Neutron Flux Axial Distribution (I-D)

Reprinted from J201 73-03

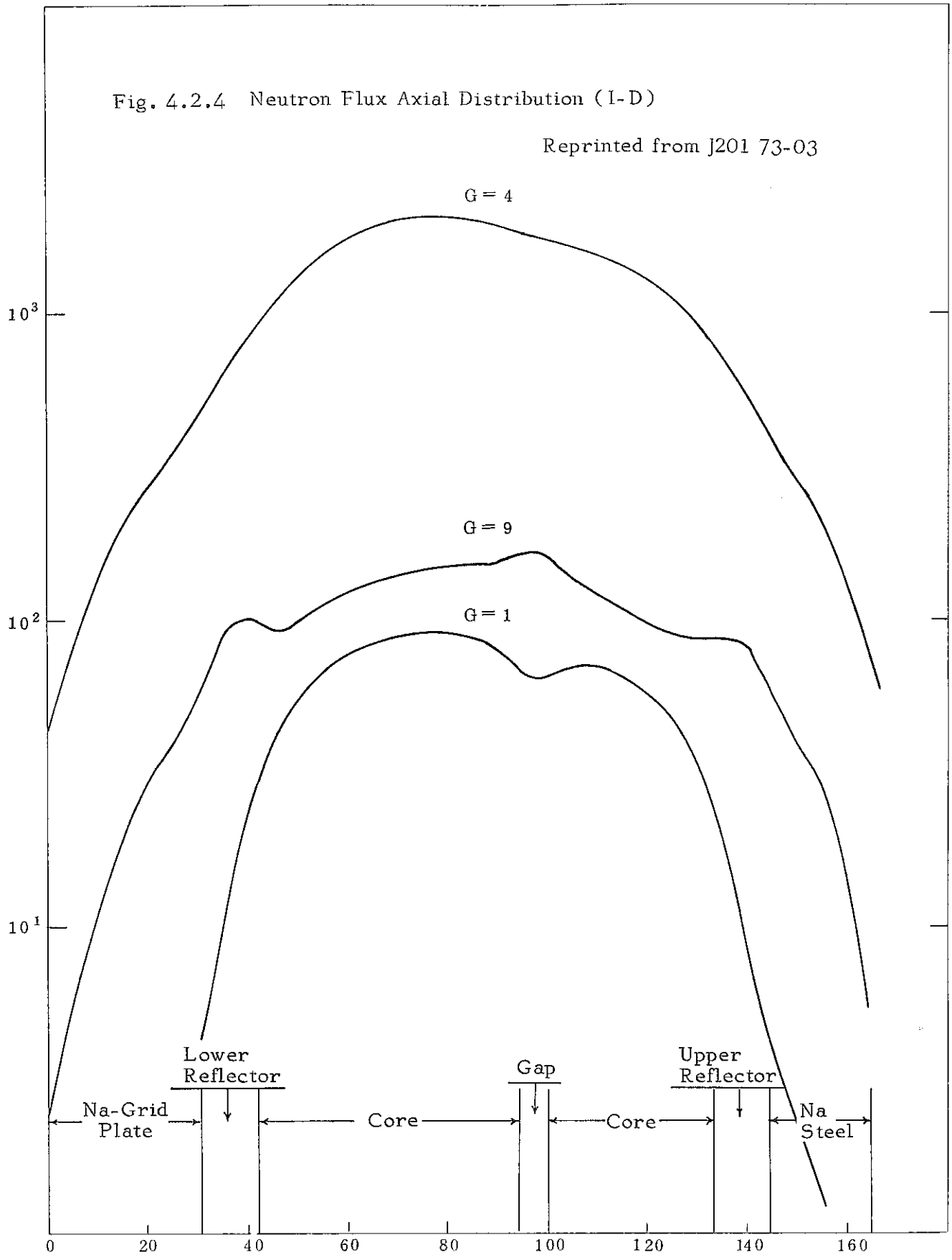

Table 4.2.6

Average FRED Position Data

Distance (inches)	Time from Lift-Off Average (msec)
0	0
1	20.6
2	29.0
3	35.5
4	41.1
5	46.3
8	60.0
9	64.1
10	68.0
12	76.1
13	79.9
14	83.5
15	87.0
16	90.9
17	94.6
20	105.3
21	108.4
22	112.3
25	122.9
28	133.8

From GEAP 10010-29
Table 6-14

Averaged Slug Worth vs Position

FRED Position (inches)	Averaged Measured Worth (¢)
0.05	0.00
1.0	5.76
2.0	11.67
3.0	19.92
4.0	26.94
5.0	34.19
6.0	41.18
7.0	47.83
8.0	54.49
9.0	62.78
10.0	68.15
11.0	74.86
12.0	80.77
13.0	86.40
14.0	92.10
15.0	96.95
16.0	101.69
17.0	105.28
18.0	109.10
19.0	111.08
20.0	114.08
21.0	115.72
25.0	119.02
29.7	119.08

From GEAP 10010-31
Table 5-3

Table 4.2.7 FRED Input Data

Time (msec)	FRED Worth (¢)	Time (msec)	Normalized Data 118¢ Data	Normalized Data 128¢ Data
0.	0.	0.	0.	0.
5.952	0.8571	5.	0.59	0.64
11.905	2.3810	10.	1.65	1.792
17.500	4.7407	15.	3.304	3.584
23.810	9.5238	20.	5.664	6.144
26.667	11.8500	25.	9.676	10.496
34.722	20.0	30.	12.980	14.080
41.304	28.8889	40.	24.780	26.880
50.0	40.0	50.	39.294	42.624
62.5	60.0	60.	54.870	59.520
74.167	80.0	70.	71.036	77.056
80.556	90.0	80.	86.140	93.440
83.888	94.0740	90.	99.946	108.416
85.227	97.1850	95.	105.138	114.048
88.890	100.0	100.	109.504	118.784
97.238	112.8571	105	113.044	122.624
103.190	117.7143	110.	115.640	125.440
109.143	121.3333	115.	116.820	126.720
115.095	123.8095	120.	117.646	127.160
121.048	124.9524	125.	117.882	127.872
127.0	125.7143	127.	118.0	128.0
132.952	125.7143	150.	118.0	128.0
250.0	125.7143	500.	118.0	128.0

From HEDL-TME 72-78
Fig. 10.

Fig. 4.2.5 FRED Worth-vs.-time relation
for Super-Prompt Critical Transients

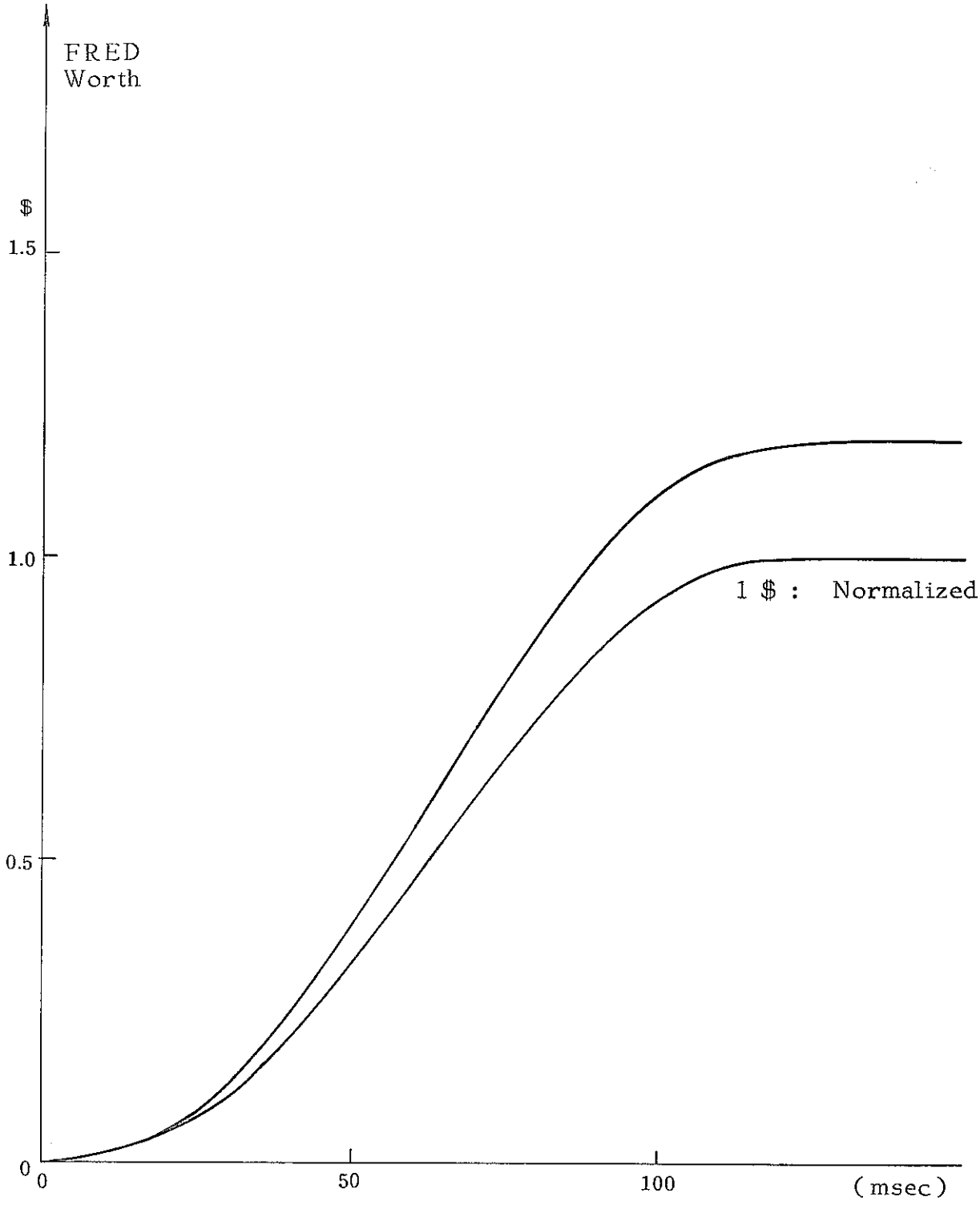

Table 4.2.8

Subprompt Slug Worth vs Position

FRED Position (in.)	Averaged Measured Worth (cents)
0.0	0.0
2.0	11.3
4.0	23.5
6.0	35.7
8.0	47.7
10.0	58.9
12.0	69.3
14.0	77.8
15.7	83.8
16.0	85.1
17.7	89.5
18.0	90.2
20.0	94.0
20.7	95.0
22.0	96.2
24.0	97.0
25.0	97.1
26.0	97.3
29.7	97.0

From GEAP-10010-29
Table 6-13

Table 4.2.9

Subprompt FRED Worth vs Time

Time (msec)	FRED Reactivity ($)
0.0	0.0
10.0	0.011
20.0	0.050
30.0	0.123
40.0	0.227
50.0	0.345
60.0	0.476
70.0	0.615
80.0	0.737
90.0	0.842
100.0	0.914
105.0	0.940
110.0	0.957
115.0	0.965
120.0	0.966
125.0	0.966
10,000.0	0.966

Fig. 4.2.6 FRED Worth-vs.-time relation
for Sub-Prompt Critical Transients

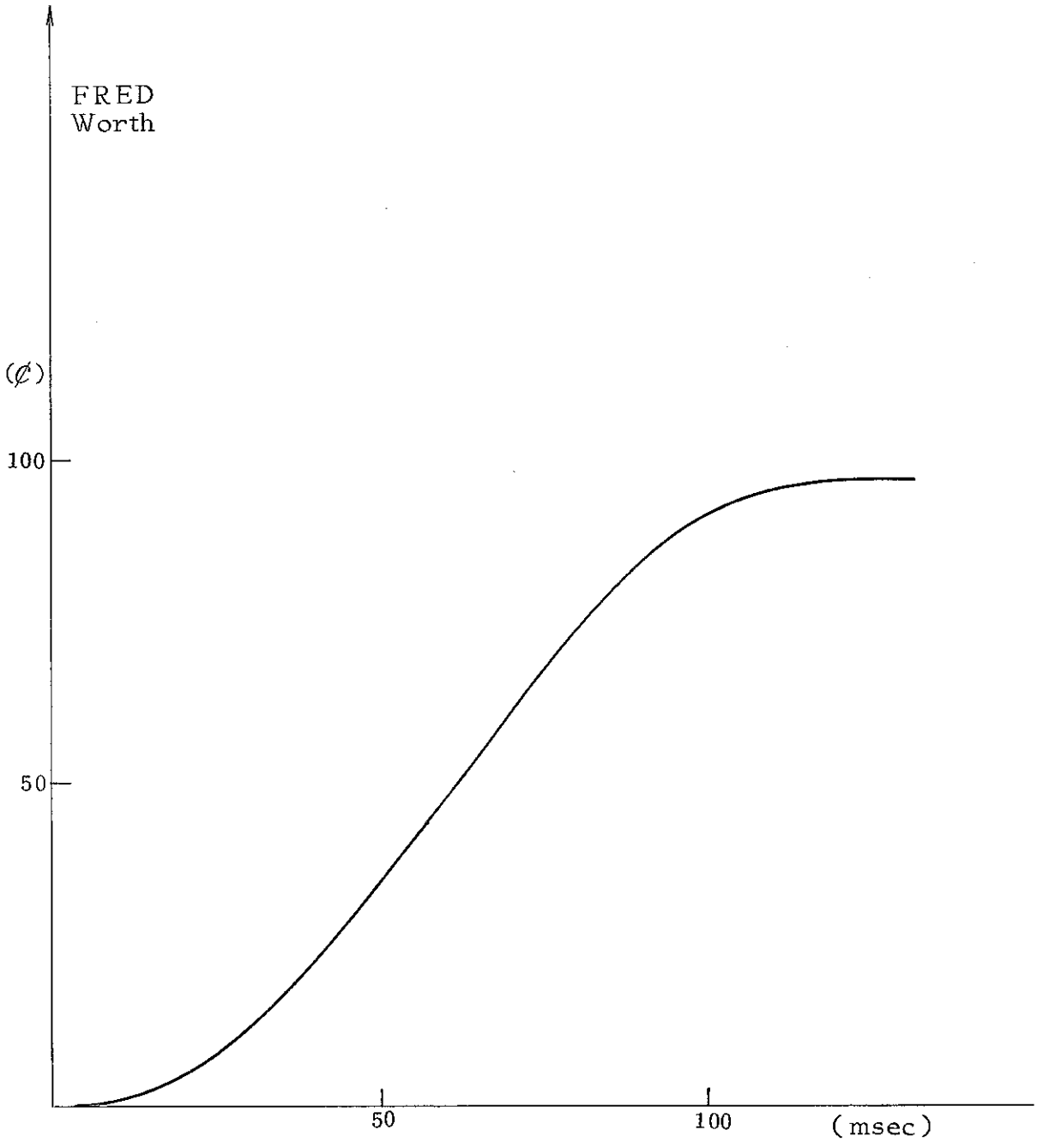

Specific heat (J/g - ℃)[18]

$$C_{pc} = \frac{1.4367 - (5.9605 \times 10^{-4} - 4.62 \times 10^{-7}\,\Gamma)\,T}{1 - 1.2637 \times 10^{-5} \times T}$$

T : sodium temperature (℃)

Thermal conductivity (W/cm- ℃)[14]

$$Kc = 0.93 - 0.581 \times 10^{-3}\,T + 1.173 \times 10^{-7}\,T^2$$

T : sodium temperature (℃)

Dynamic viscosity μ (centipoise)[14]

$$\log_{10}\mu\,(T) = 0.5108 + 220.65/T - 0.4925\,\log_{10}T$$

T : sodium absolute temperature (°K)

4-3. Measurement and Calculation Comparison

Experimental results of the super-prompt critical transients are summarized mainly in Ref.'s (4) and (11). It seems to be difficult, however, to compare calculated results with measured results shown in these references except for the energy coefficients of reactivity. Reference (9) was assumed to describe the transient experiments in more detail, but there was no opportunity to refer to the report during this analysis work.

In References (4) and (11), there are figures which show the power level, net reactivity and energy release versus time of the super-prompt critical transient number 8 (the initial power level is 8 MW and FRED reactivity insertion is 1.28 $). These are reprinted in Figs. 4.3.1 to 4.3.3. Calculated results were compared with data in these figures, which were regarded as the results of transient number 8.

Available numerical data on these transients are the peak power level, energy release to 0.3 sec and energy coefficient as

shown in Table 2.3. Of these data, the energy coefficients are considered the most reliable measurements.

Calculated results of the power level, reactivities, energy release and reactivity energy coefficient for the super-prompt critical transient number 8 (the conditions of which were the same as for number 7) are shown in Figs. 4.3.4 to 4.3.7. The initial power level of this test was 8 MW and the value of 1.257 $ from Fig. 10 of Ref. (11) was used for the FRED worth in the calculation.

The relation between net reactivity and energy release is a straight line, as shown in Fig. 4.3.7. As described in Chap. 3 this relation is written by

$$Kn(t) = Ko + a_1 E(t)$$

Reactivity energy coefficient, a_1, can be easily determined from the slope of this straight line. A value of energy coefficient determined in this manner is -0.3825¢/MW·sec and shows an excellent agreement with the measured value in Table 4.3.1. Calculated energy and net reactivity values are also in good agreement with measured values. However, the power history calculated is fairly sharp, as compared with measurements, the maximum peak power level is higher and the second maximum peak is lower, as compared with measurements. These differences between the calculated and measured power histories could be almost eliminated by a little change of the FRED reactivity insertion curve, as described later. It is found that the power vs. time history would be sensitively influenced by the reactivity insertion magnitude and rate.

Calculations of all the cases of the super-prompt critical

transients were performed by fixing all parameters except the FRED worth, which took values of 1.18 and 1.28 $. These calculated results are summarized in Table 4.3.1 and the power time traces are shown in Figs. 4.3.8 through 4.3.13.

The initial power levels of these transients were 2, 5 and 8 MW. Calculated average initial fuel temperatures in the average fuel channel are listed in Table 4.3.2, corresponding to the initial power levels. On the other hand, the average fuel temperature vs. initial power levels reported in Ref. (2) are shown in Fig. 4.3.16. From these data, the core average fuel temperature at each initial power level was estimated, as shown in Table 4.3.2. These value are in good agreement with values taken from Fig. 2-2 of Ref. (8). Since fuel temperature calculations are sensitively influenced by changes in fuel thermal conductivity and fuel-to-clad heat transfer coefficient, it is important to examine the adequacy of these values. The initial conditions of fuel temperature are also assumed to have a great influence on the Doppler reactivity and the reactivity energy coefficient.

A comparison of calculated and experimental values is made in Table 4.3.1. A good agreement is seen between the calculated and experimental values of reactivity energy coefficient at the initial power level of 8 MW. As the initial power level becomes lower, the difference between the calculated and measured values becomes larger. The calculated values are larger than those measured at the lower initial power levels. The calculated energy release to 0.3 sec from the initial power level of 5 MW agreed comparatively well with the measurement. Calculated results were smaller in the cases of lower initial power level and larger in the cases of higher

initial power level. For the maximum peak power level, a good agreement was obtained in the cases of lower initial power level. The calculated peak power level got higher than the measured value, as the initial power level became larger. Since measured values of the maximum peak power level, which had been reported were fairly different from one another, depending on the reports, figures and tables, it was difficult to decide the standard values for comparison. Generally, every figure of power time history in the references at hand could be considered to exhibit the characteristics of transient tests. Logarithmic indications of power time history for transient numbers 1 and 8 were obtained from Ref. (11). For other cases, only linear graphical representations[4] were available for comparison with calculated results.

One of the reasons why the calculated and measured energy coefficients at lower initial power levels did not agree well was assumed to be due to the differences in initial average fuel temperatures. Using thermodynamic parameters shown in Table 4.3.2, calculated average fuel temperature at the initial power level of 8 MW agreed within 8 ℃ with that estimated from the measurement. However, calculations using the same parameters gave 12 ℃ lower average fuel temperature at 5 MW and 18 ℃ lower at 2 MW. Furthermore, since the Doppler coefficient, $T\frac{dK}{dT}$, was fixed constant at a value of −0.0081, the reactivity feedback effect was greater at lower fuel temperature. By this effect, it was considered that the power level was calculated lower and, consequently, the energy release was lower compared with the measured value. Thus, the reactivity energy coefficient, which indicated the ratio of the feedback reactivity change to the change in energy release,

was concluded to be larger. It is necessary to further examine an effect of change in initial average fuel temperature, which can be adjusted by an appropriate selection of thermodynamic parameter values.

Calculated reactivity time history results are shown in Fig. 4.3.14 and energy time relation results are shown in Fig. 4.3.15 for the case of an initial power level of 8 MW and a FRED worth of 1.28 $. In this transient, the calculated power time history (in Fig. 4.3.13) coincides very well with the measured curve in Fig. 4.3.1. The net reactivity similar to the power history agrees well, except for a time difference of about 2 msec. On the other hand, energy release results differ in magnitude significantly from each other. The calculated result is found larger than the other. This trend coincides with that described in Ref. (11) and is a point to be examined in more detail.

As an example of sub-prompt critical test analysis, Fig. 4.3.17 shows the calculated power history with initial power level conditions of 10 MW and a FRED worth of 96.6¢. Table 4.3.3 shows a calculated result of reactivity energy coefficient for this test, as well as the measured values. It can be seen that the maximum peak power level was calculated slightly lower, but that the calculated reactivity energy coefficient agrees well. Calculated value of initial average fuel temperature is 803.2 ℃, which shows good agreement with the value of 802 ℃ obtained from Fig. 4.3.16. The power time history also coincides well with the experiment shown in Fig. 6-16 of Ref. (3). It is understood that the adequacy of calculations was proved by these results.

Table 4.3.1 Analysis Results of Super-Prompt Critical Experiments

Initial Power (MW)	FRED Worth ($)	Peak Power Level		Energy Release to 0.3 sec		Energy Coefficient	
		Measured (MW)	Calculated (MW)	Measured (MW-sec)	Calculated (MW-sec)	Measured (¢/MW-sec)	Calculated (¢/MW-sec)
2	1.18	5300	5562.7	82	74.7	-0.47	-0.585
2	1.28	8800 ~ 9300	8989.0	106 ~ 108	97.3	-0.45	-0.54
5	1.18	4900 ~ 5100	5786.7	93	96.2	-0.42	-0.46
5	1.28	8200 ~ 8700	9927.8	120	125.2	-0.42	-0.4475
8	1.18	5100 ~ 5500	6237.7	108	115.8	-0.39	-0.39
8	1.28	8300 ~ 8800	10709.3	135 ~ 136	150.3	-0.38	-0.38
8	1.257		11642.7		142.9		-0.3825

Fig. 4.3.1 Time Dependent Power for Super-Prompt Critical Transient No.8

(Experimental)

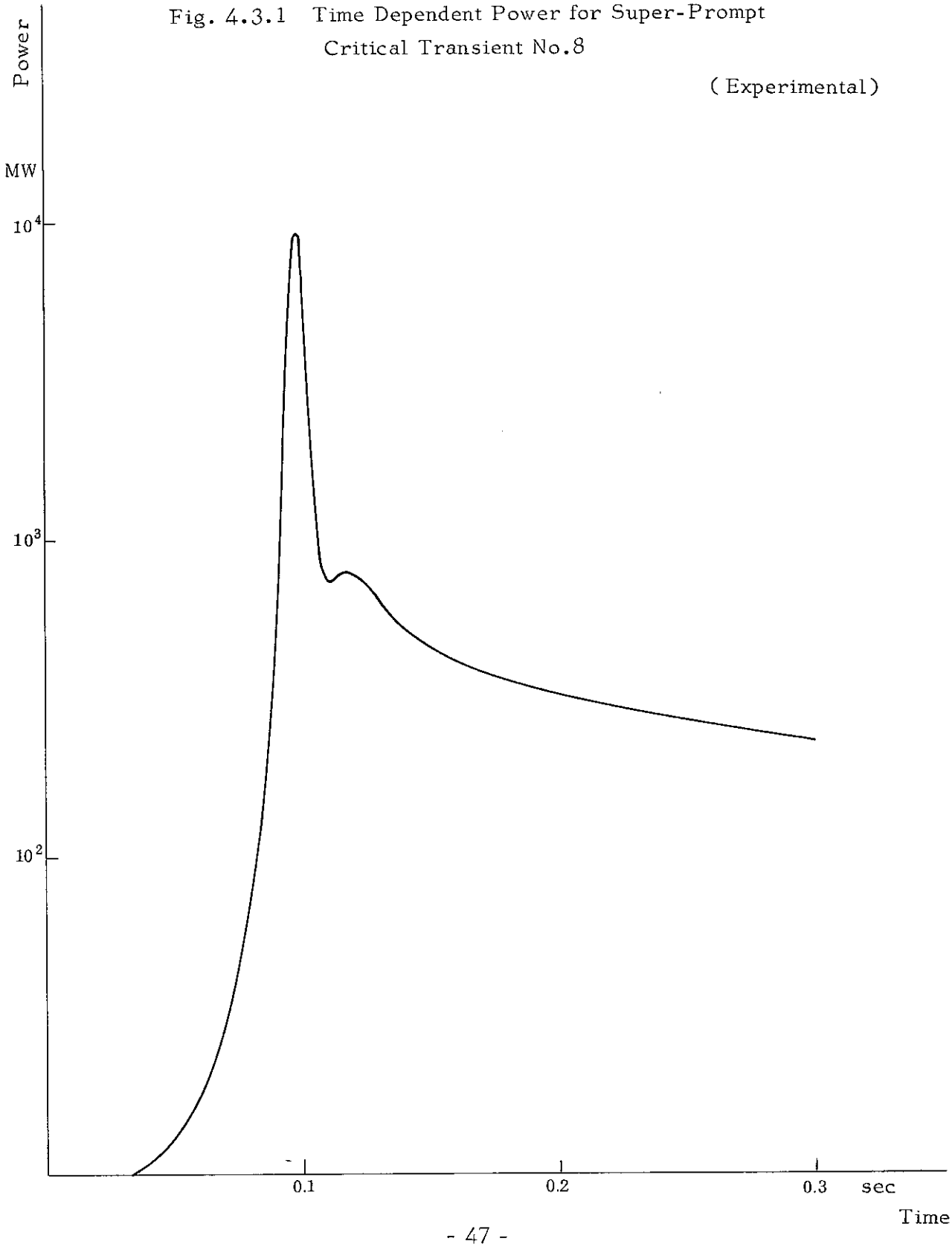

Fig. 4.3.2 Time Dependent Net Reactivity for Super-Prompt Critical Transient No.8
(Experimental)

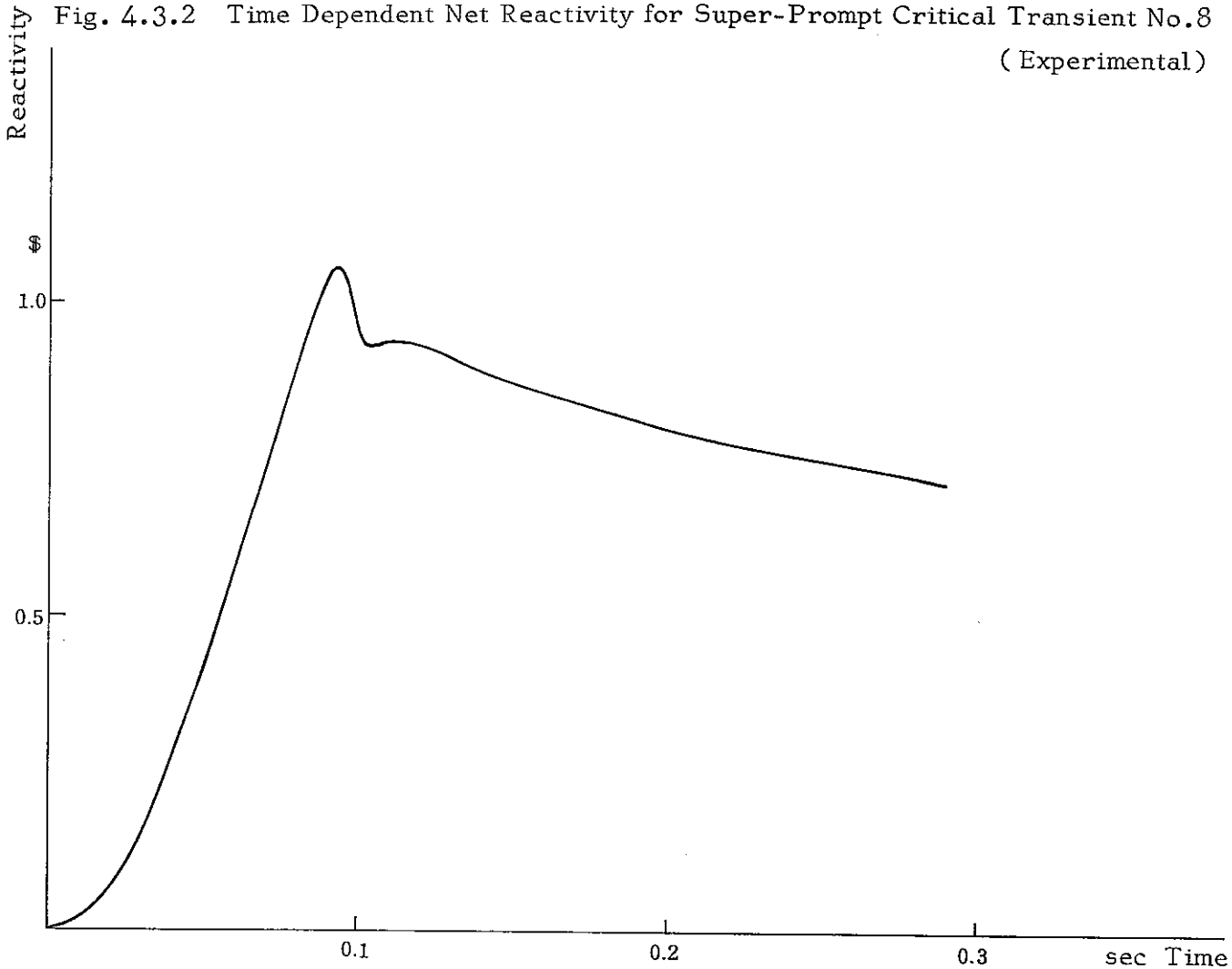

Fig. 4.3.3 Time Dependent Energy Release for Super-Prompt Critical Transient No.8
(Experimental)

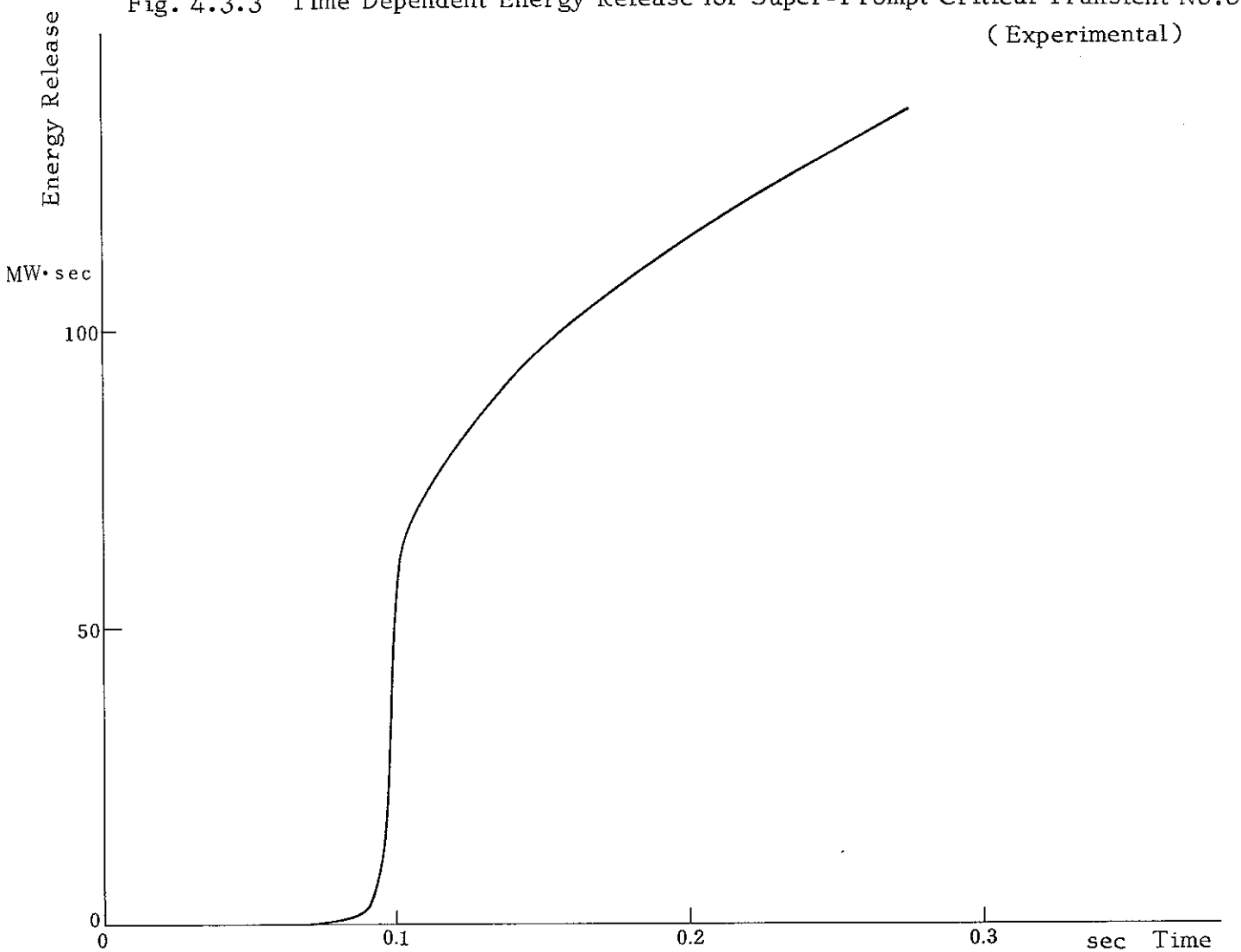

Fig. 4.3.4 Time Dependent Power for
Super-Prompt Critical Transient No.8
(Calculated)

Initial Power 8 MW
FRED Worth 1.257 $

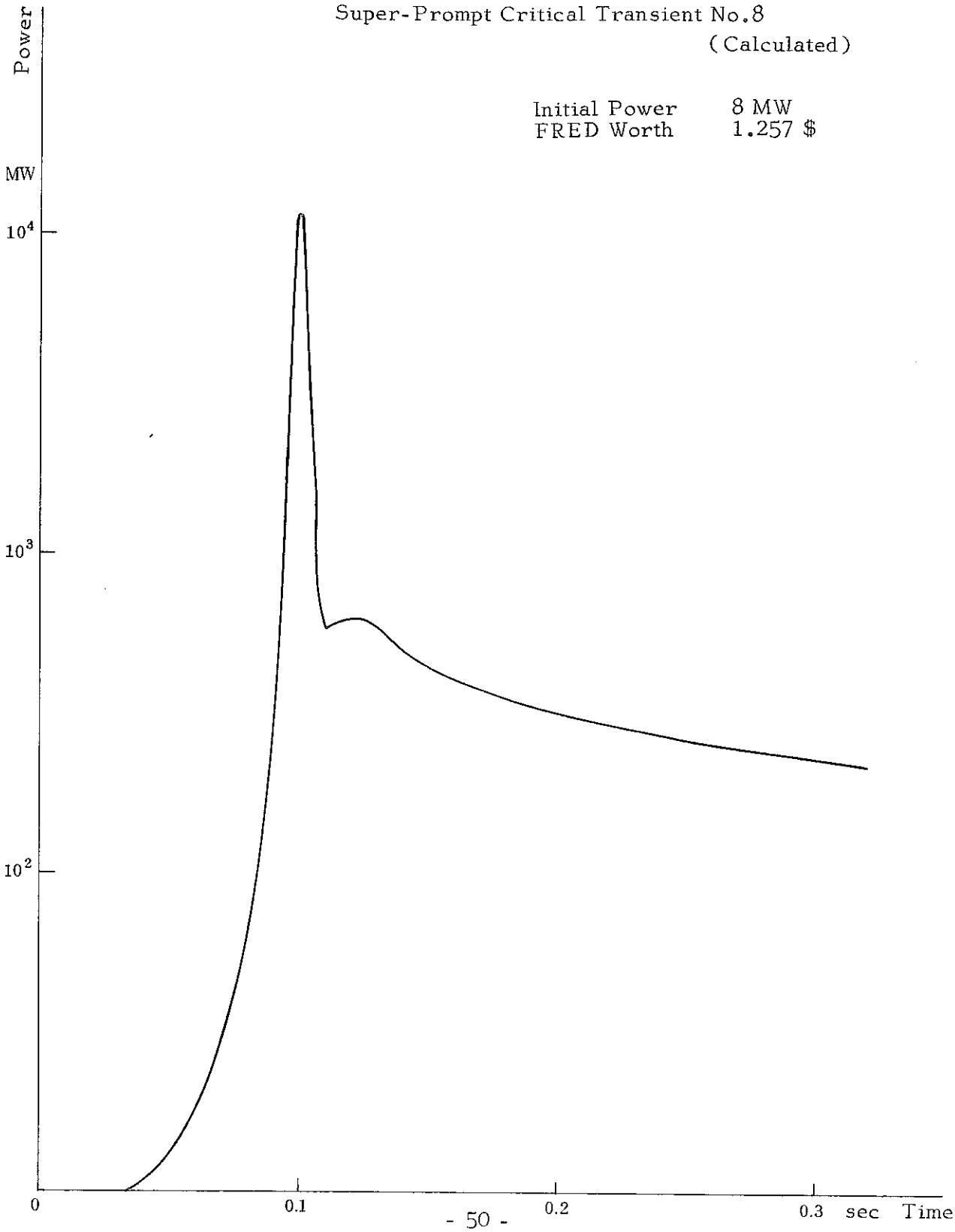

Fig. 4.3.5 Time Dependent Reactivities for Super-Prompt Critical Transient No.8
(Calculated)

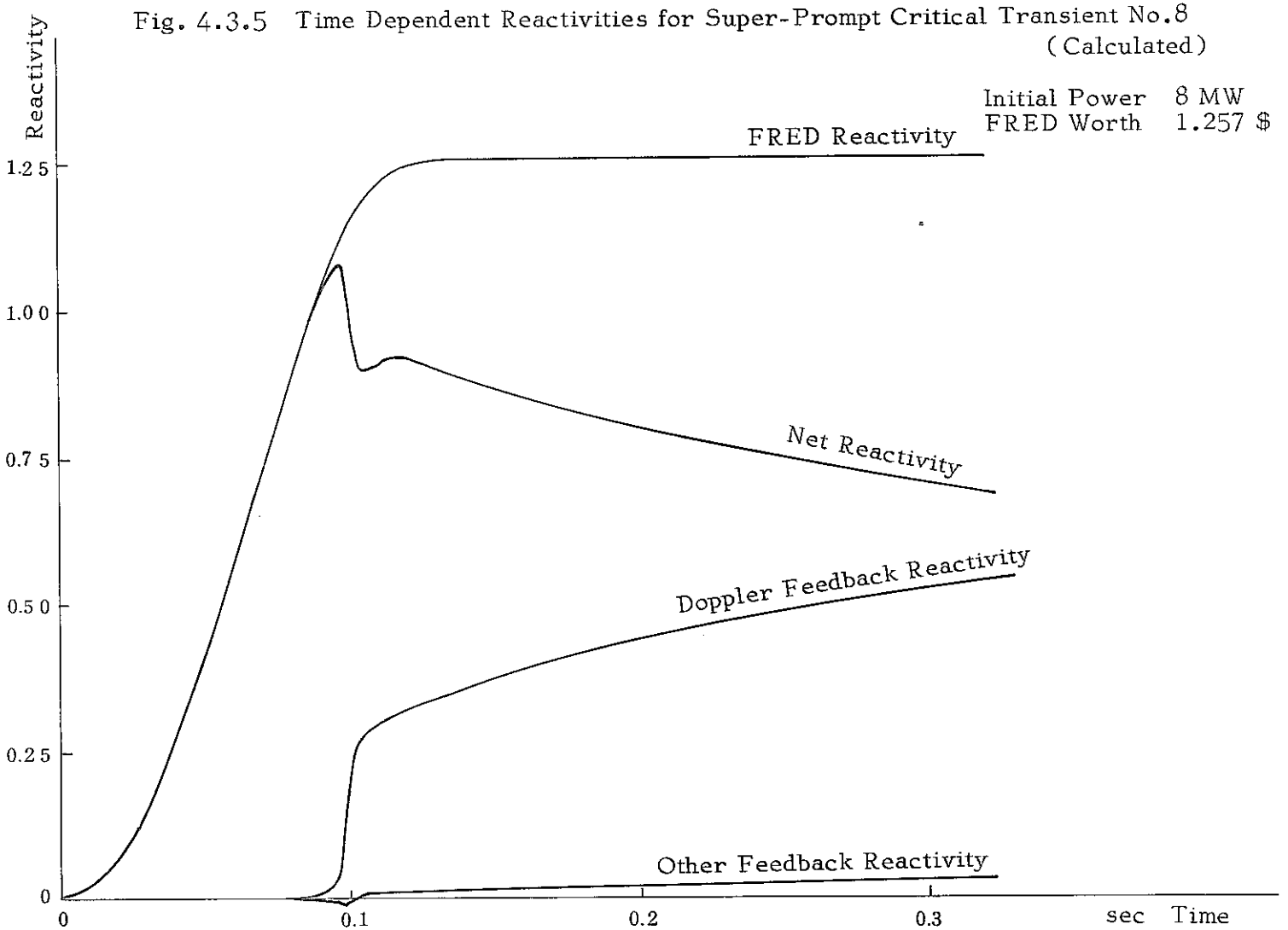

Fig. 4.3.6 Time Dependent Energy Release for Super-Prompt Critical Transient No.8

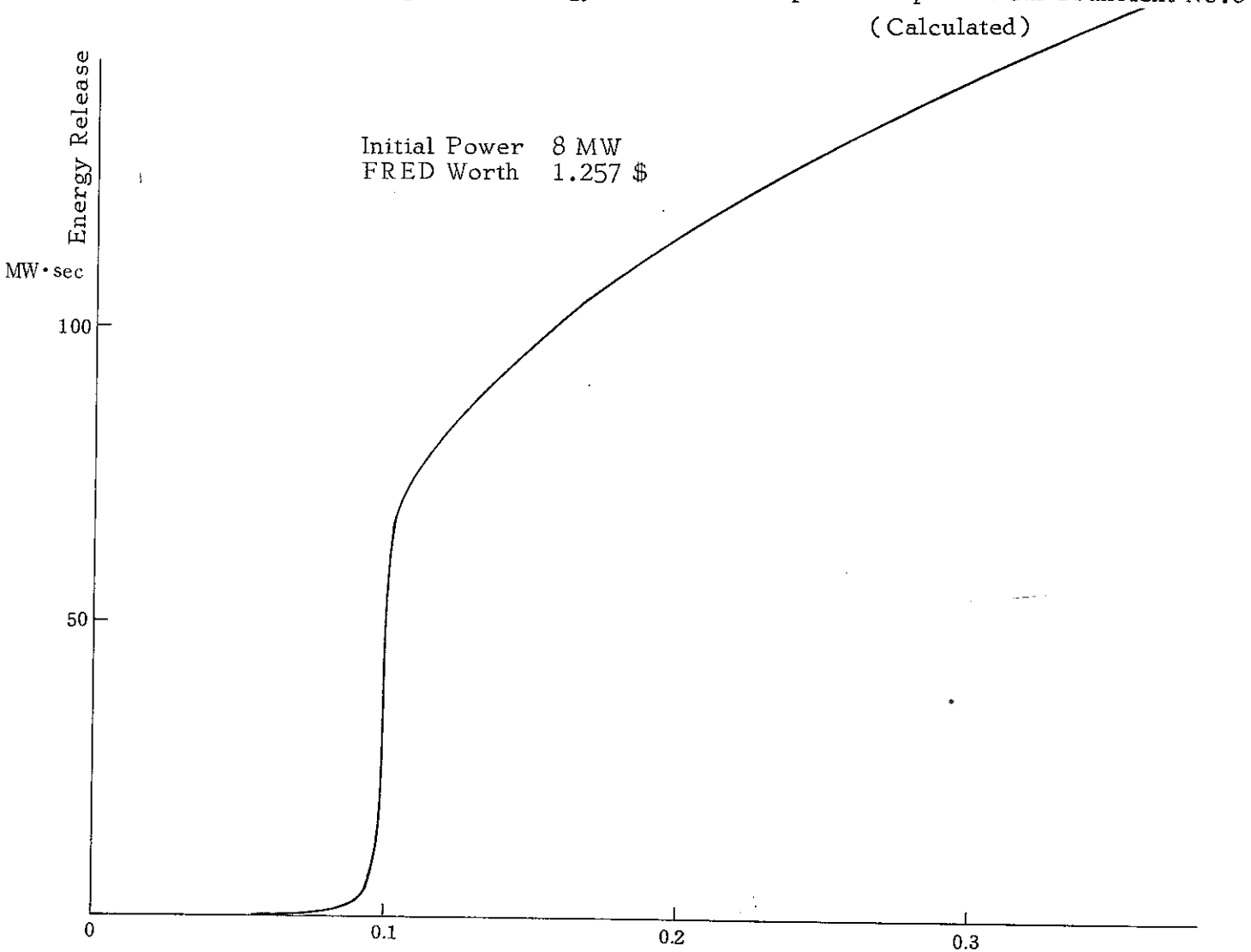

Fig. 4.3.7 Calculated Energy Coefficient for Super-Prompt Critical Transient No.8

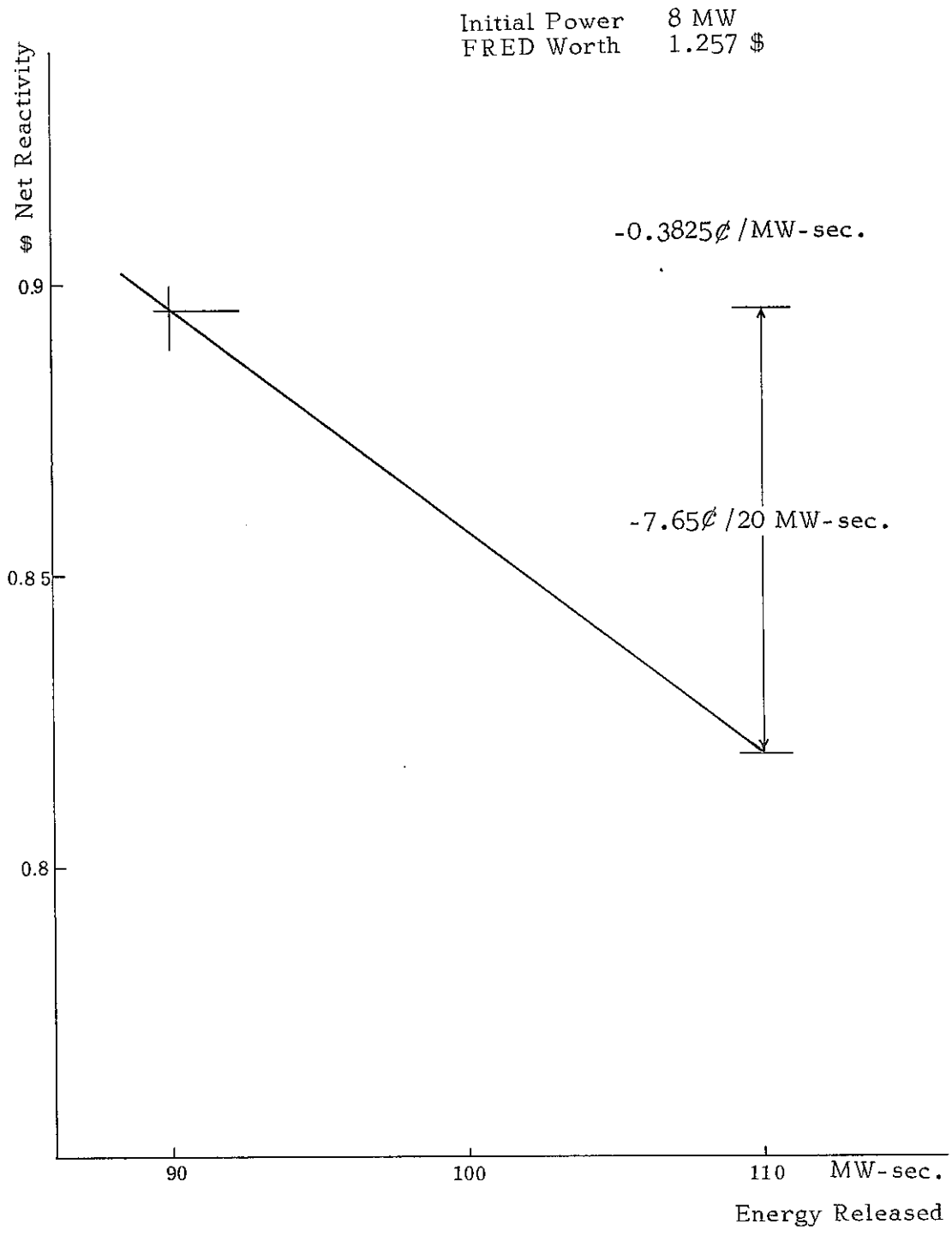

Fig. 4.3.8 Time Dependent Power for Super-Prompt Critical Transient No.1
(calculated)

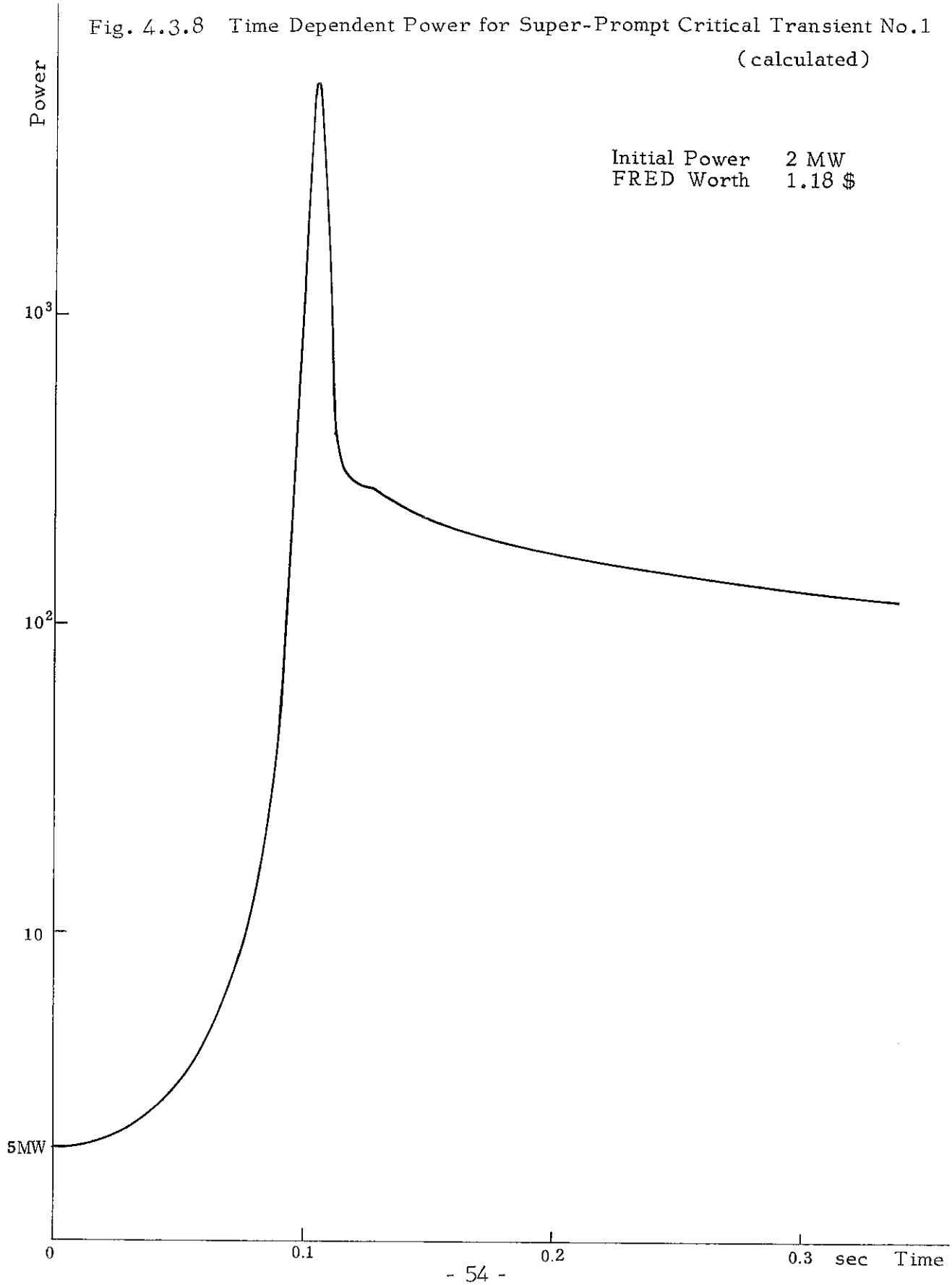

Fig. 4.3.9 Time Dependent Power for Super-Prompt Critical Transients No.2 and No.3 (Calculated)

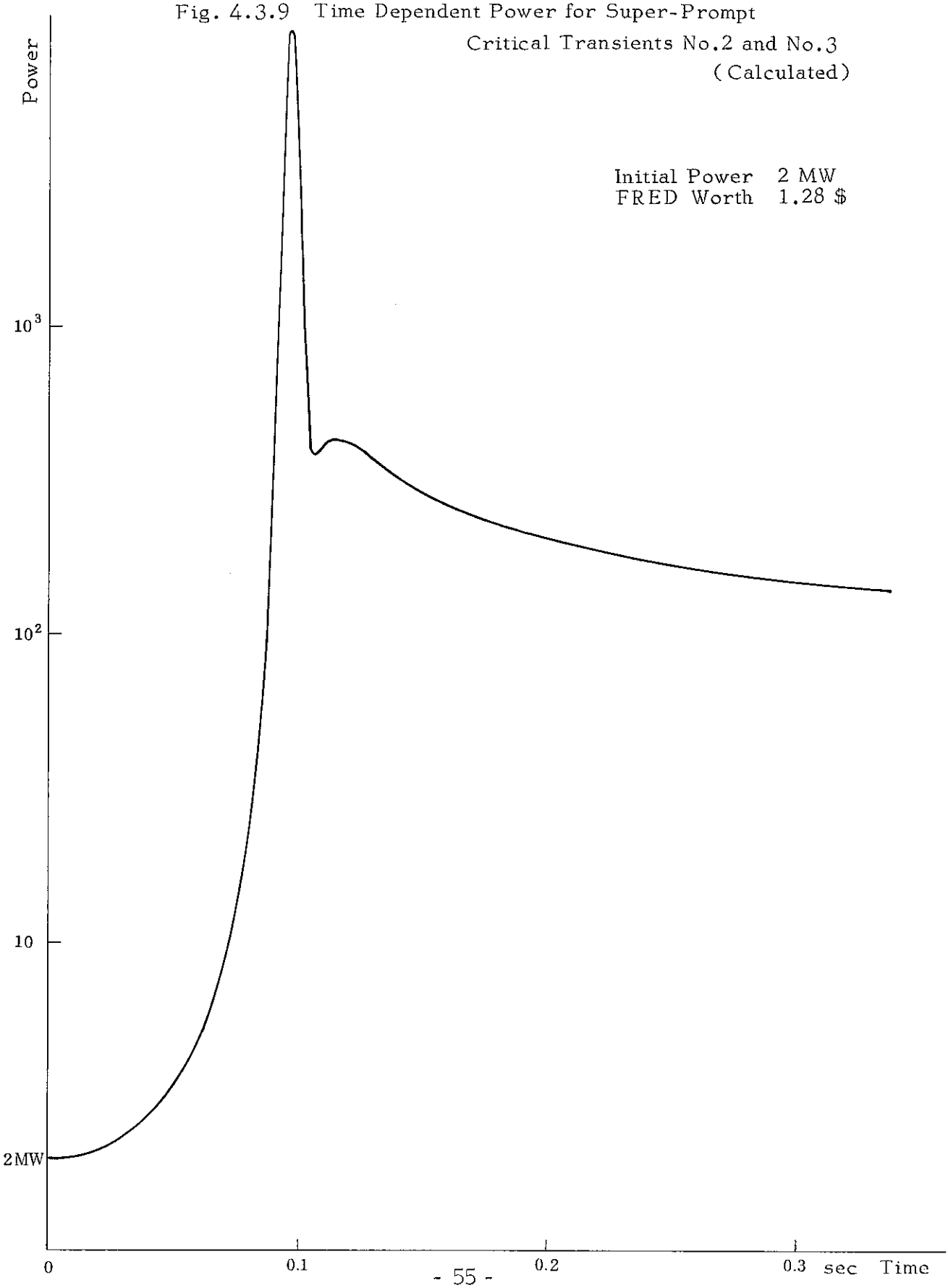

Fig. 4.3.10 Time Dependent Power for Super-Prompt Critical Transient No.4
(Calculated)

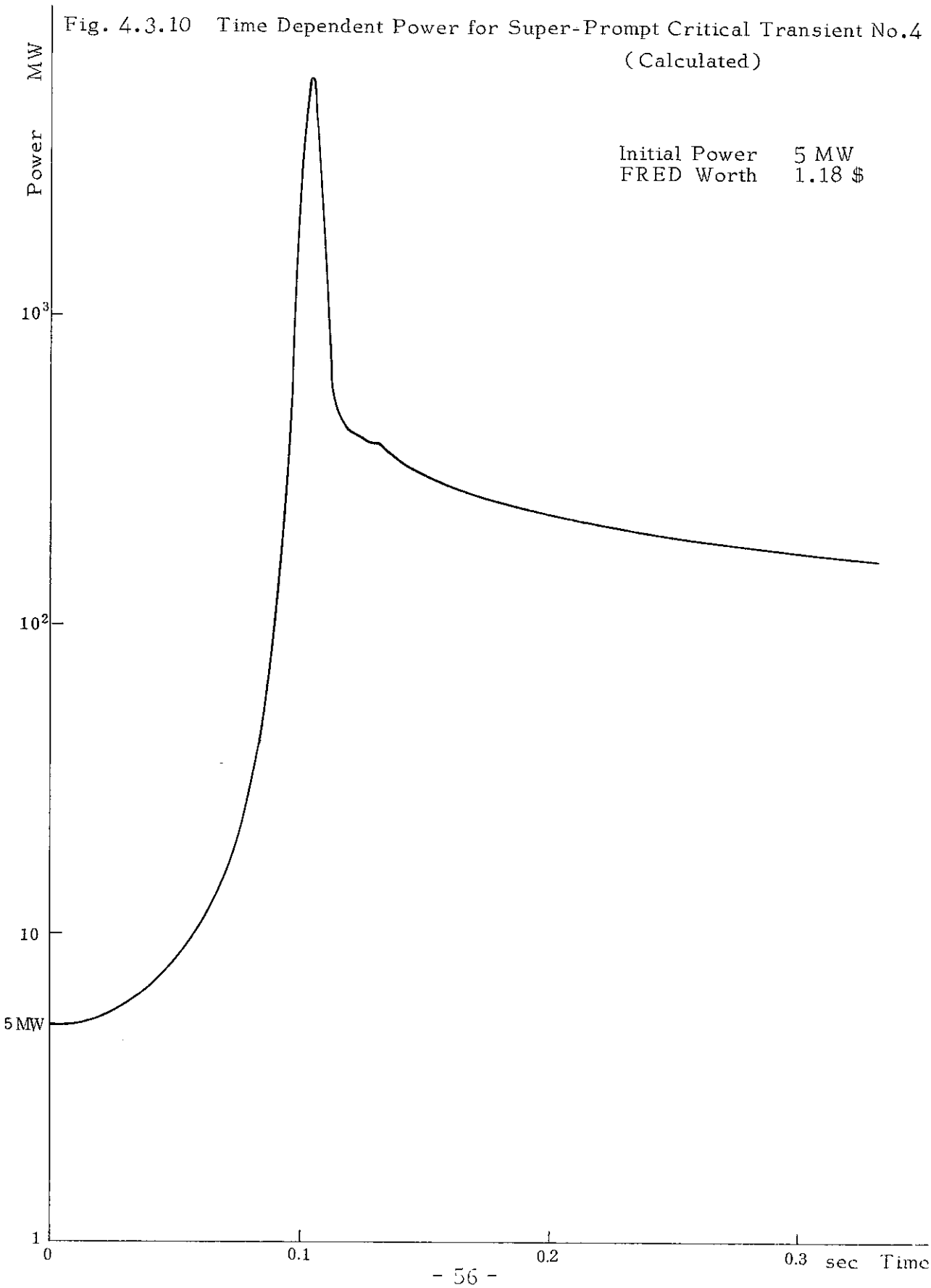

Fig. 4.3.11 Time Dependent Power for Super-Prompt Critical Transient No.5
(Calculated)

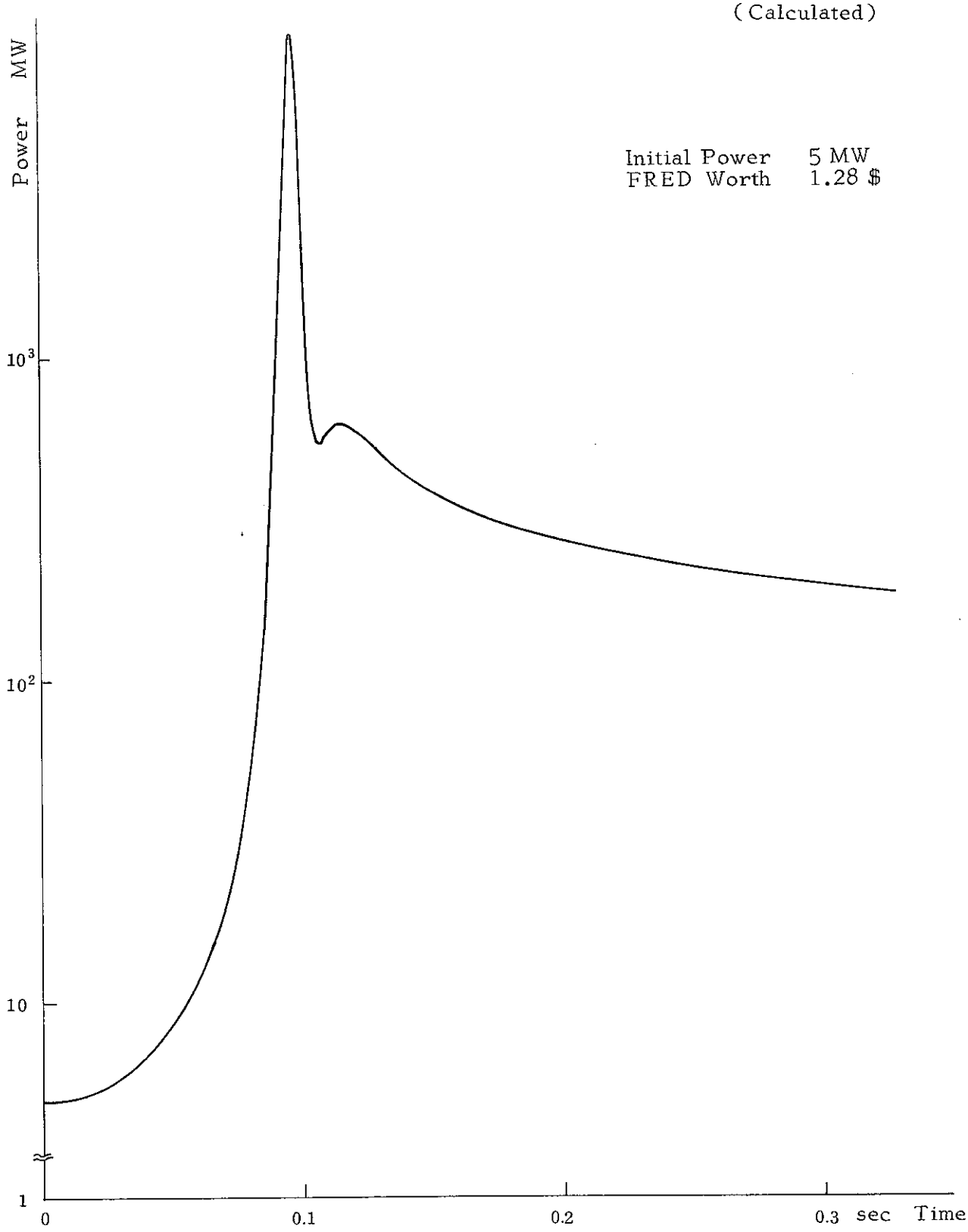

Fig. 4.3.12 Time Dependent Power for
Super-Prompt Critical Transient No.6
(Calculated)

Initial Power 8 MW
FRED Worth 1.18 $

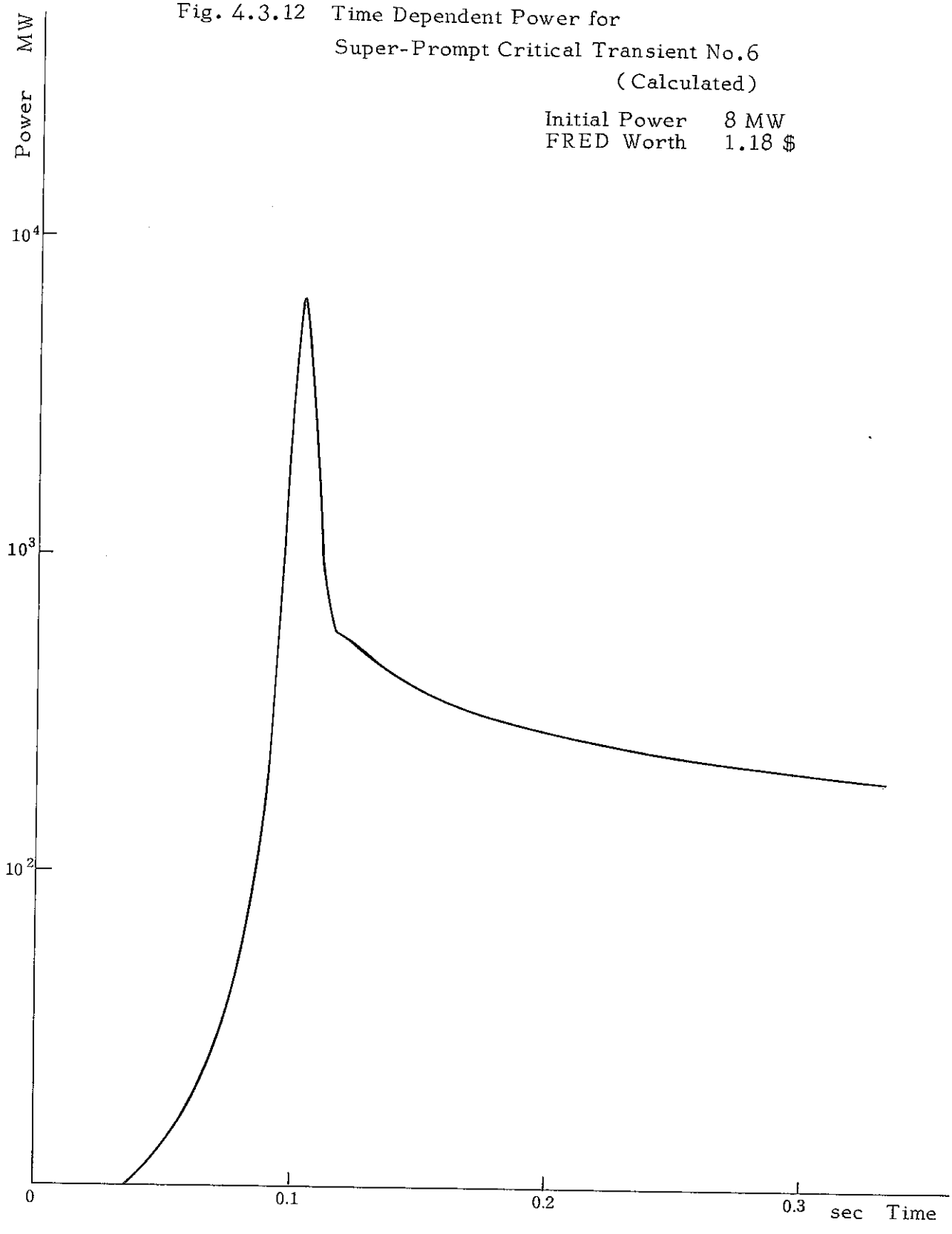

Fig. 4.3.13 Time Dependent Power for Super-Prompt Critical Transients No. 7 and No.8

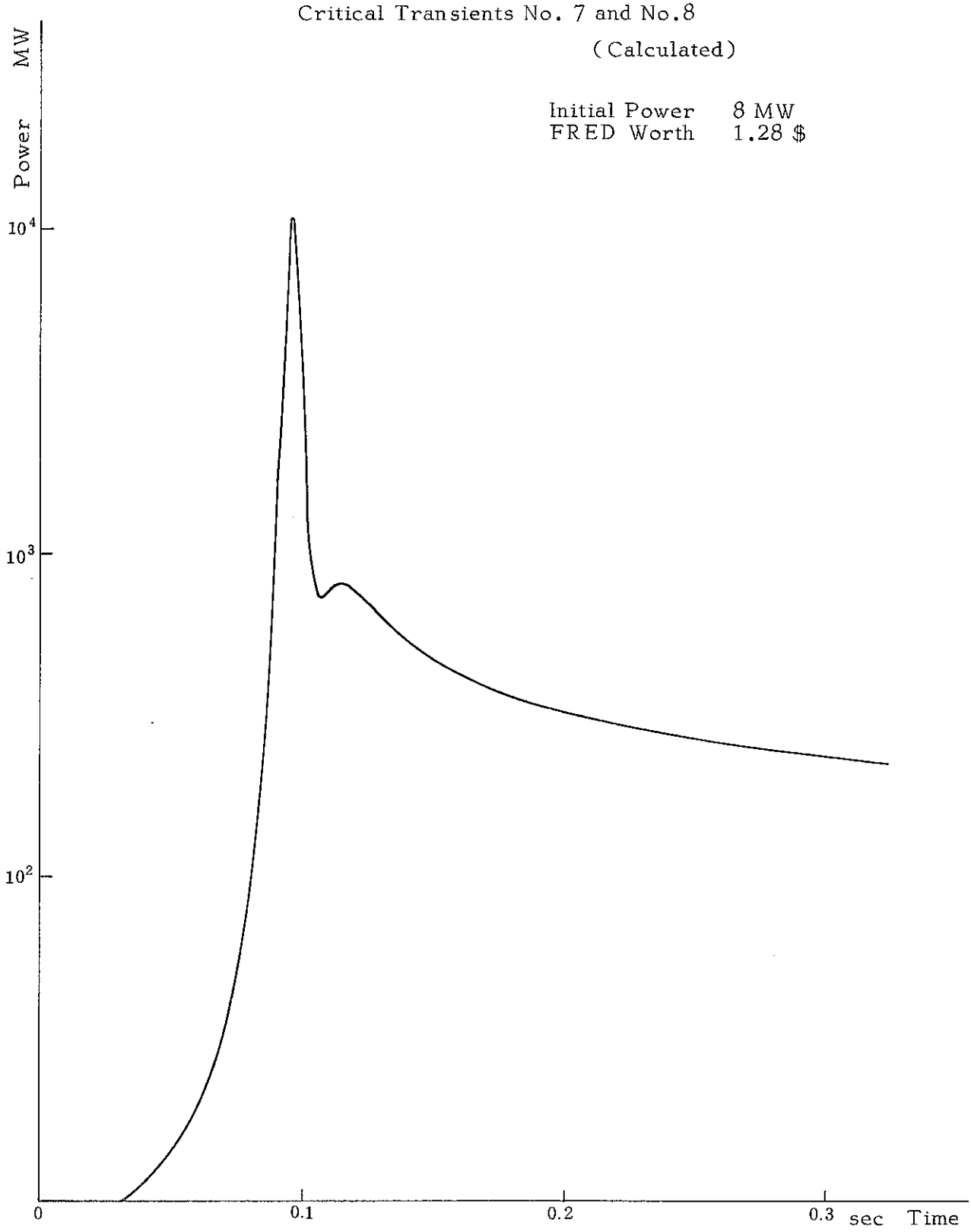

Fig. 4.3.14 Time Dependent Reactivities for Super-Prompt Critical Transients No.7 and No.8 (Calculated)

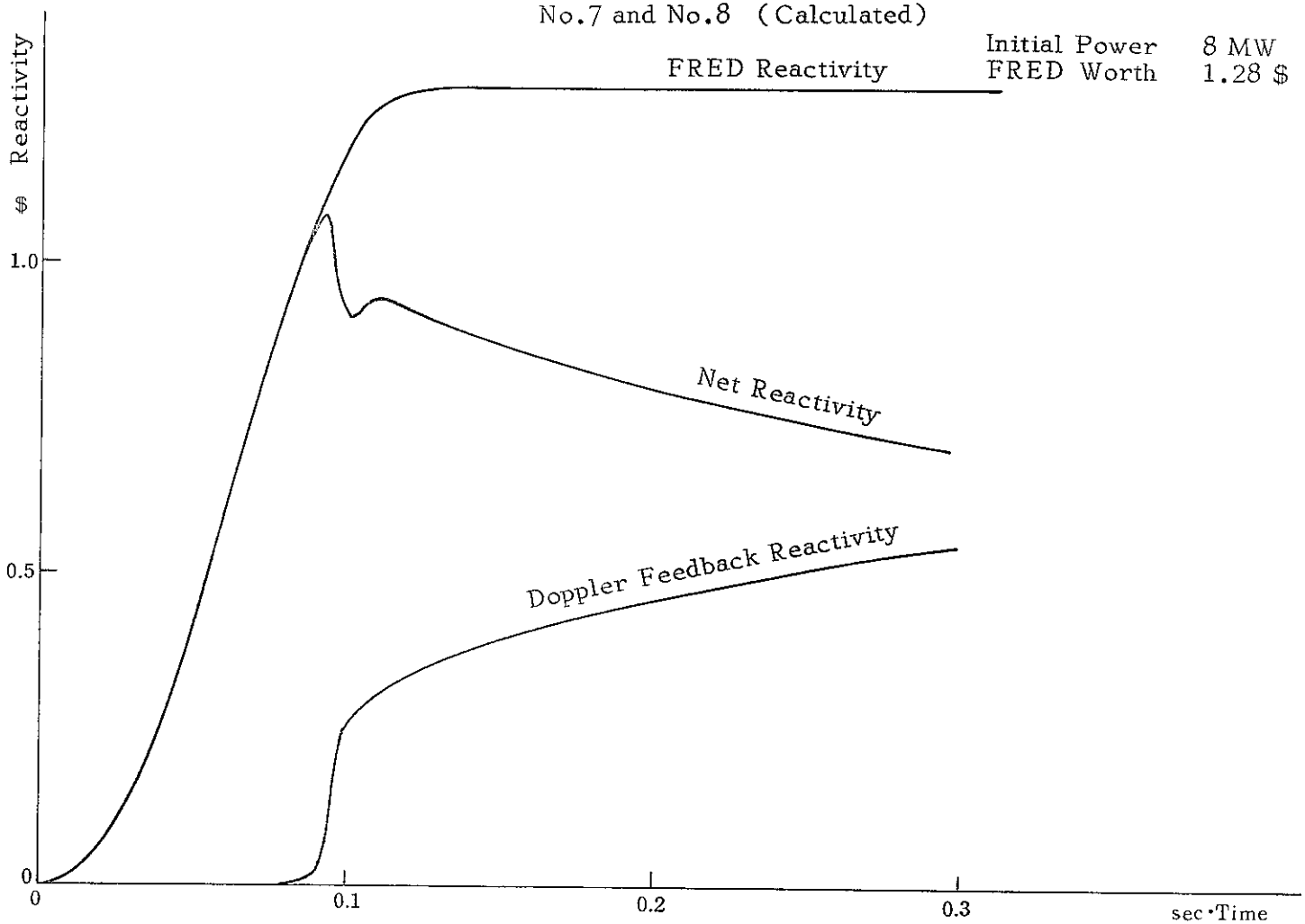

Fig. 4.3.15 Time Dependent Energy Release for Super-Prompt Critical Transients No.7 and No.8 (Calculated)

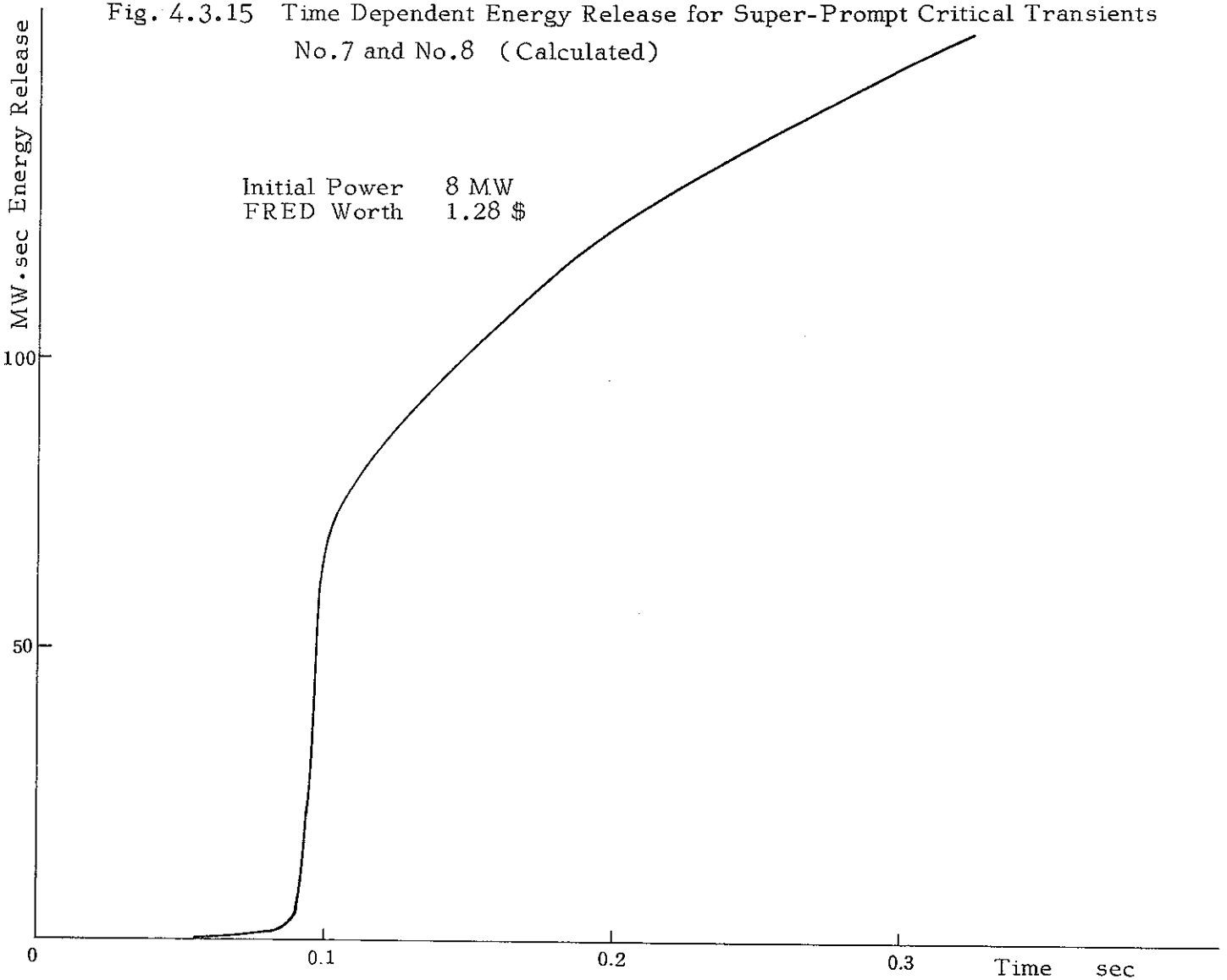

Table 4.3.2 Initial Core Averaged Fuel Temperature for Transient Tests

Initial Power (MW)	Average Fuel Temperature	
	Calculated *	Calculated **
2	504 ℃	485.4 ℃
5	627 ℃	614.8 ℃
8	738 ℃	730.9 ℃

* Estimated from Data of J201 73-03 & GEAP 13702
** Calculated in this Analysis

Table 4.3.3 Results of Subprompt Critical Transients

Initial Power (MW)	FRED Worth (averaged) (cents)	Nominal Peak Power (MW)		Energy Coefficient (¢/MW-sec)	
		Measured *	Calculated	Measured *	Calculated
2	96.6	-0.56 ±0.08		80 ~ 85	
5	96.6	-0.45 ±0.06		140 ~ 160	
10	96.6	-0.36 ±0.05	-0.38	250 ~ 270	242.9

* From GEAP 10010-29
Table 6-6 & 6-7

Fig. 4.3.16 Average Fuel Temperature

From J201 73-03
Table 5.1.3

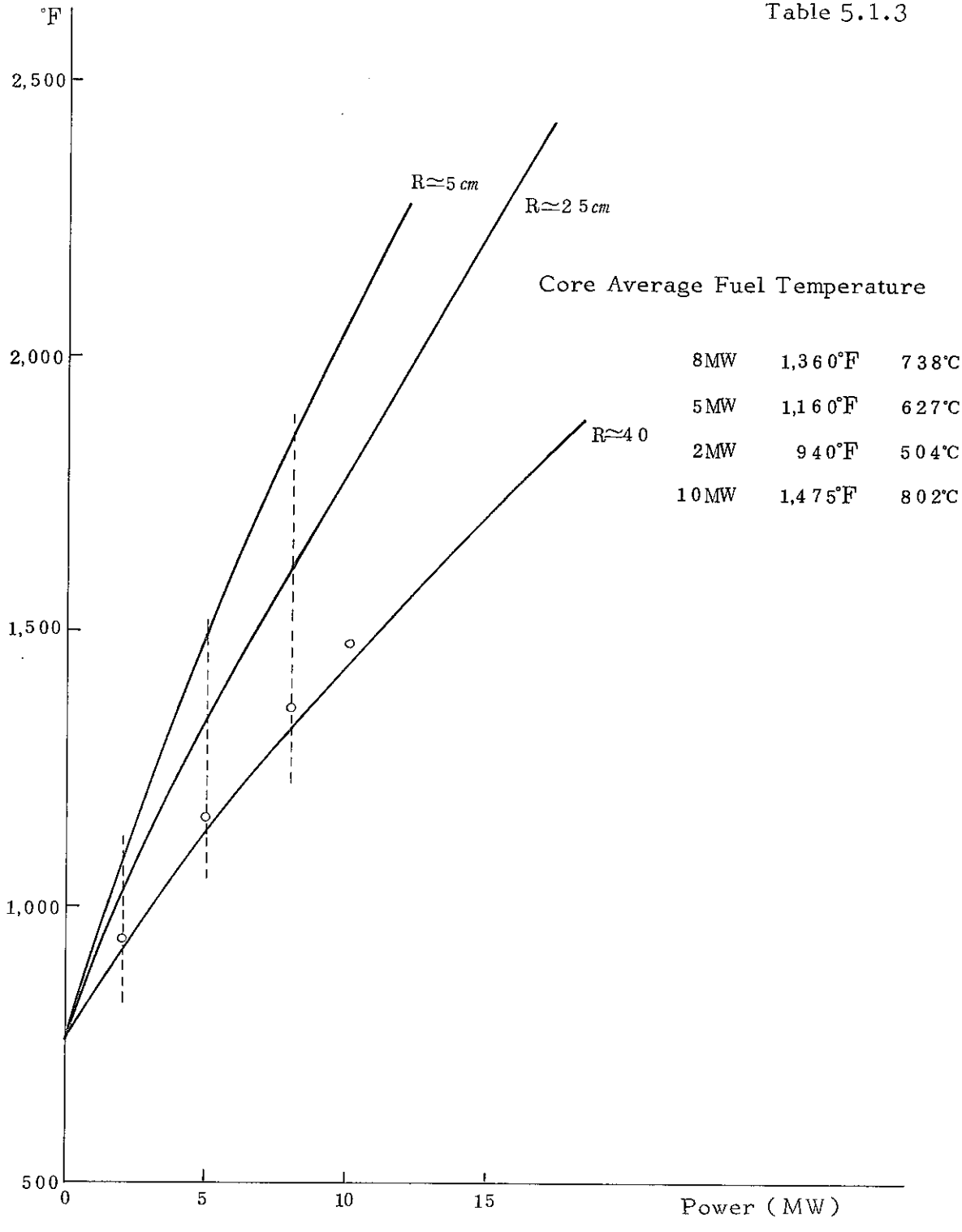

Fig. 4.3.17 Time Dependent Power for Sub-Prompt Critical Transient

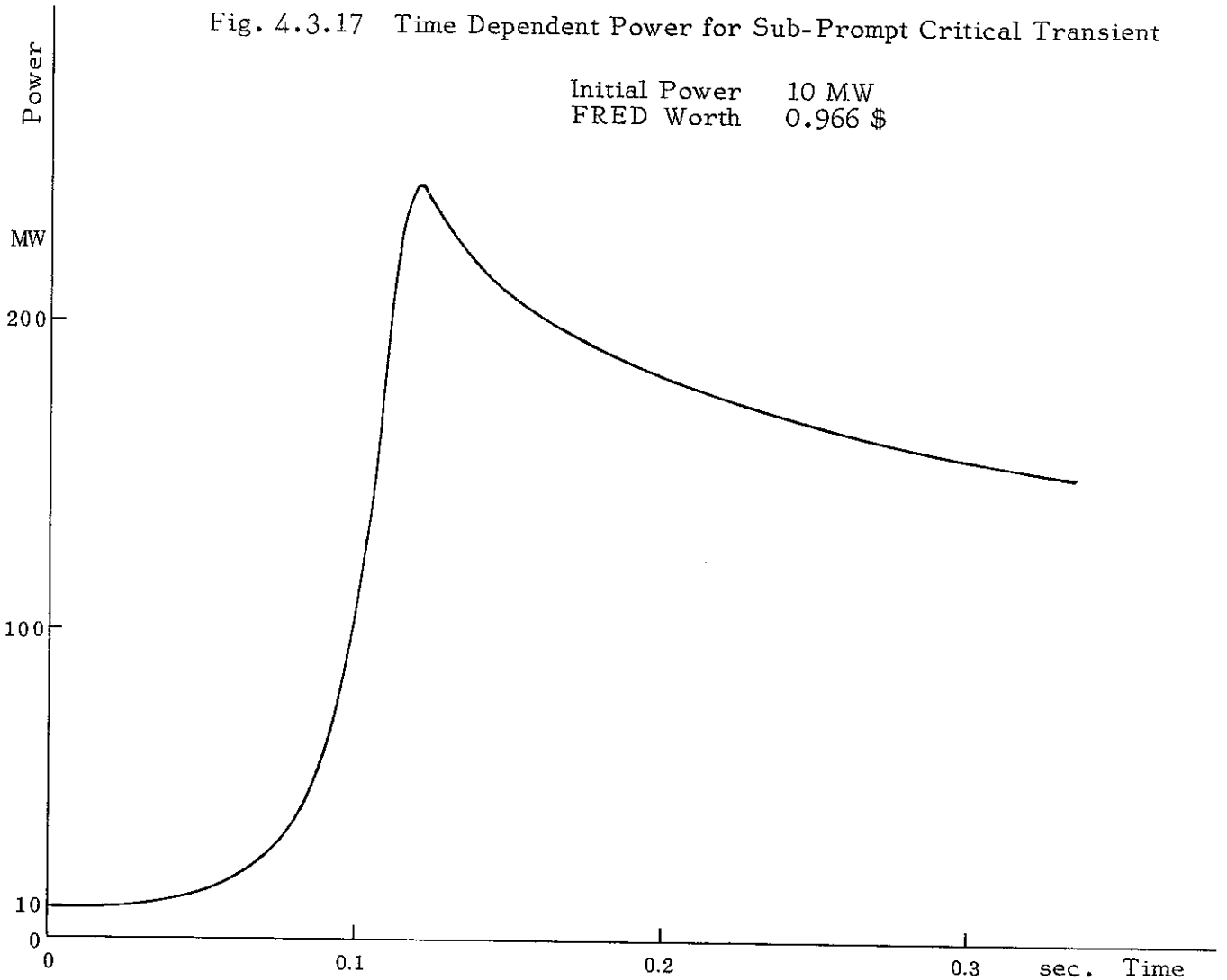

4-4. Parameter Sensitivity Analysis

In order to examine the sensitivity of reactivity energy coefficient to variations in parameters, calculations were performed, taking the transient test case in Figs. 4.3.4 to 4.3.7 in Section 4.3 as a basis of comparison. Results are summarized in Table 4.4.1, in which calculated basic test results are rewritten in the top line.

Ten per cent increase in β value caused a decrease in Doppler feedback effect calculated in terms of dollars, and also provided a decrease in neutron kinetics times constant ℓ/β. The change resulted in an enhancement of the power and an decrease of ~10 per cent in the reactivity energy coefficient.

The effects of an increase in the Doppler coefficient, $T\frac{dK}{dT}$, of 10 per cent were opposite to those of the increase in β. Here, it followed that the power peak became lower and the reactivity energy coefficient was increased by ~ 10 per cent.

Any increase in thermodynamic parameters, such as fuel-to-clad heat transfer coefficient, h_{fe}, fuel thermal conductivity, K_f, and fuel clad-to-coolant heat transfer coefficient, h_{EC}, resulted in a decrease in initial average fuel temperature, which, in turn, caused an increase in Doppler reactivity feedback for the same value of the Doppler coefficient, $T\frac{dK}{dT}$. Thus, an increase in reactivity energy coefficient resulted. Since the value of h_{EC} is much greater in magnitude than that of h_{fe}, heat transfer from fuel clad to coolant is good and temperature difference between them is small. The effect of a change in h_{EC} on the reactivity energy coefficient may, therefore, be small. Variations in h_{fe} and K_f cause great effects on the evaluation of fuel temperature. Especially, the

value of h_{fc} has many uncertainties and it is difficult to determine. Usually in reactor design, the value of h_{fe} is chosen from the safety point of view. It is also an important problem to evaluate the values of h_{fe} and K_f from experimental data with many measured fuel temperatures. In calculation of the basic test case, as mentioned before, one of these values, or both, might have been determined to be too large and, consequently, the initial fuel temperature is considered to have been estimated lower, as listed in Table 4.3.2.

The effect of specific heat of fuel, C_{pf}, becomes considerable, especially for a rapid transient such as in the super-prompt critical experiment. Ten per cent increase in C_{pf} resulted in 9 per cent decrease in reactivity energy coefficient. The main reason for this is that a change in fuel temperature is slower compared with the power variation. This, of course, affects the reactivity effect.

As mentioned above, the thermodynamic parameters have especially great effects on the Doppler reactivity. Therefore, when performing an analysis like this, it is highly important to choose and use these parameters carefully.

Mentioned here are methods of averaging fuel temperature for evaluation of the Doppler feedback. As pointed out in Ref. (2), calculation of the Doppler reactivity based on the simple, unweighted, core volume averaged fuel temperature underestimated the Doppler effect. As described in Section 4.1, methods using Eqs. (4-1.20) to (4-1.22) were examined to obtain the Doppler reactivity. The method based on Eq. (4-1.22) employed the weight of the square of local power density. On the other hand, the other two methods did not consider the weighting factor and used only the simple core averaged fuel temperature to evaluate the Doppler effect. These

Table 4.4.1 Sensitivity of the Energy Coefficient to Parameter Changes in Transient No. 8

Parameter	Change in Parameter	Initial Average Fuel Temperature (℃)	Peak Power (MW)	Energy Release to 0.3 sec (MW·sec)	Energy Coefficient (¢/MW·sec)
Nominal values	*	730.9	11642.7	142.9	-0.3825
β	+10%	730.9	13235.6	155.8	-0.35
$T(\frac{dK}{dT})$	+10%	730.9	10248.3	130.1	-0.425
h_{fe}	+100%	644.9	9869.8	127.3	-0.4275
K_f	+20%	702.3	10927.3	136.8	-0.40
C_{pf}	+10%	730.9	13020.2	156.2	-0.3475
h_{EC}	+100%	727.5	11570.9	142.0	-0.385
Doppler Evaluation					
Eq. (4-1.20)		730.9	17092.5	192.7	-0.2775
Eq. (4-1.21)		730.9	17470.3	195.9	-0.275

* Initial Power Level 8MW, FRED Worth 1.257 $ Doppler Evaluation (4-1.22)

results are summarized in Table 4.4.1. Unweighted calculation underestimated the Doppler effect and resulted in 25 per cent smaller value for the reactivity energy coefficient. Ref. (20) also points out that the method based on the unweighted, core volume averaged fuel temperature is the most approximate.

4-5. Comparison with Results from Other Reports

Analytical studies of the SEFOR super-prompt critical experiments have been accomplished hitherto by General Electric (GE) and Hanford Engineering Development Laboratory (HEDL). The reactivity energy coefficients calculated by GE and HEDL are listed in Table 4.5.1, together with results of this analysis.

The calculated results of this analysis, on the whole, proved to be larger. As mentioned before, this is assumed to be because thermodynamic parameters used in this analysis might not have been optimized. Results by HEDL are generally small, judging from the limited amount of data obtained. It is found that results reported by GE show the closest correspondence to the experimental data. GE results, however, show a tendency, compared with the measurements, for the energy coefficient to be larger for a case with low initial power level, and vice versa. This tendency, as well as the measured results, should be examined in more detail.

Table 4.5.1 Comparison of Calculated Energy Coefficients

Initial Power (MW)	FRED Worth ($)	Energy Coefficients Calculated (¢/MW-sec)			
		Measured *	GE *	HEDL **	VODGIN
2	1.18	-0.47	-0.49	-0.47	-0.585
2	1.28	-0.45	-0.46		-0.54
5	1.18	-0.42	-0.42		-0.46
5	1.28	-0.42	-0.40		-0.4475
8	1.18	-0.39	-0.37		-0.39
8	1.28	-0.38	-0.36	-0.33	-0.38
10	0.97	-0.35	-0.37		-0.38

* GEAP 10010-30

** HEDL-TME 72-78

5. Analysis by One Dimensional Kinetics Code

5-1. Outline of One Dimensional Kinetics Code

The computer code "NAKIN" used in this analysis is divided into two parts; space-time neutron kinetics and feedback calculation parts.

The space-time kinetics part was developed based on a one dimensional multigroup kinetics code "GAKIN".[15] Effect of a control rod is simulated by a time change in cross section in the control rod region.

In the feedback system, the reactor fuel region is divided into an arbitrary number (within the limit) of thermo-hydraulic (T-H) regions. In the SEFOR transient analysis, the fuel region was divided into three T-H regions. Taking an average fuel rod in a T-H region, average fuel rod temperature was calculated. Thus the Doppler effect in the region was simulated by a change in macroscopic cross sections, according to the calculated fuel temperature. The fuel temperature was calculated by the following equations, on the assumption that the power density distribution was approximated by a time independent Sine function.

$$(\rho C)_f \frac{\partial \theta}{\partial t} = \frac{1}{r}\left\{ \frac{\partial}{\partial r}\left(r K \frac{\partial \theta}{\partial r} \right) \right\} + g \qquad (5\text{-}1.1)$$

$$(\rho CS)_{c\ell} \frac{\partial \theta_{c\ell}}{\partial \theta} = (UA)_{f,c\ell}(\theta_f - \theta_{c\ell}) - (UA)_{c\ell,c}(\theta_{c\ell} - \theta_c) \qquad (5\text{-}1.2)$$

$$(\rho CS)_c \frac{\partial \theta_c}{\partial t} = (UA)_c(\theta_{c\ell} - \theta_c) - W \frac{\partial (C_c \theta_c)}{\partial Z} \Big|_{Z=H/2} \qquad (5\text{-}1.3)$$

where subscripts f, $c\ell$ and c represent fuel, fuel clad and coolant, respectively. The other symbols are defined as;

θ : temperature

C : specific heat

W : mass flow

H : core height

$\mathcal{g}$: heat generation per unit volume

S : cross section area

A : area

U : overall heat transfer coefficient

θ_f : fuel surface temperature

ρ : density

The UA's can be written as

$$(UA)_{f,c\ell} = \frac{1}{\frac{1}{\pi \cdot (R_f + Re) C_G} + \frac{\ell n (Ra/Re)}{2\pi Kc\ell}} \qquad (5\text{-}1.4)$$

$$(UA)_{c\ell,c} = \frac{1}{\frac{\ell n (R_E/R_a)}{2\pi Kc\ell} + \frac{1}{2\pi R_E h_c}} \qquad (5\text{-}1.5)$$

where

R_f : fuel rod radius

R_e : fuel clad inner radius

R_a : fuel clad effective radius

R_E : fuel clad outer radius

C_G : gap conductance

$Kc\ell$: fuel clad thermal conductivity

h_c : coolant heat transfer coefficient

5-2. Analysis Results

1. One Dimensional Reactor Model

This analysis was performed by using a one dimensional cylindrical model. The reactor was divided into nine regions, which included three fuel regions, two FRED rod (B_4C and Ar) regions as well as a down comer inner vessel void, an outer vessel void, a radial reflector and a radial shield region. In addition, 59 subdivided mesh points were considered in this model, as shown in Fig. 5.2.1.

The reactivity insertion by the FRED rod is simulated by changes in neutron cross sections in the B_4C region. Three neutron energy groups and six delayed neutron groups were taken into account in calculation.

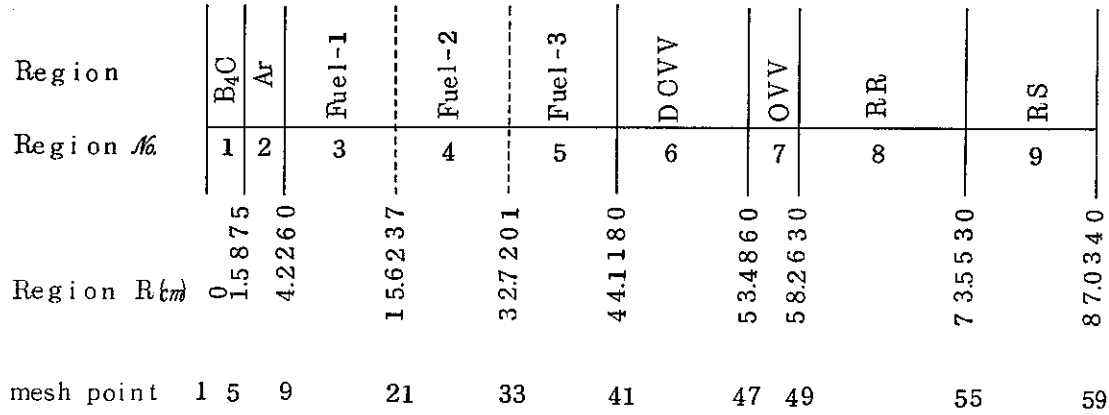

Fig. 5.2.1 Reactor Configuration

2. Data Used

Data used in temperature feedback calculation were practically the same as those used in the point kinetics model. Core coolant flow rate in each of three fuel regions was assumed constant, and the following values were used,[7]

Region Number 3 : 246.9 cm/sec

Region Number 4 : 210.6 cm/sec

Region Number 5 : 152.4 cm/sec

Before the transient analysis, variations in neutron cross sections, corresponding to the FRED rod in and out of the core region and due to changes in fuel temperature, were determined by a static critical calculation code.[2]

Then the capture cross sections were adjusted by interpolating the values at both boundaries of the FRED rod in and out, so that the reactivity change due to time variation in capture cross sections coincided with the data in Table 4.2.7 (which were fitted by the curve in Fig. 10 of Ref. (11)). The transport cross sections were assumed to change linearly with time between zero and 0.1 sec. This assumption is considered valid because the effect of changes in transport cross sections on the reactivity change is small, compared with that due to changes in capture cross sections. The Doppler feedback was obtained from changes in capture cross section and transport cross section, which were, in turn, calculated by a quadratic function and a linear function of fuel temperature, respectively.

The nuclear data at the initial state used in this analysis are summarized in Table 5.2.1 through 5.2.5. The values for β_i's and λ_i's are listed in Table 4.2.2.

The values of capture cross sections at the states of the FRED in and out of the reactor are summarized in Table 5.2.6 and those of transport cross sections are listed in Table 5.2.7. Changes in capture, fission and transfer cross section due to variations in temperature are listed in Table 5.2.8, 5.2.9 and 5.2.10, respectively.

Table 5.2.1 Group Structure and Properties

Group Number	Energy for Collapse	Average Neutron Speed (cm/sec)	Fisson Yield
1	10.5Mev-0.1 Mev	0.97029×10^{9}	0.98700
2	100kev-1.0 kev	0.20653×10^{9}	0.01300
3	1000ev-0.215ev	0.28216×10^{8}	0

Table 5.2.2 Diffusion Coefficient

Region / Group	1	2	3	4	5
1	2.3130	21.7590	1.5990	1.6000	1.5930
2	1.3530	14.2400	0.9426	0.9417	0.9373
3	0.6743	4.8700	0.7381	0.7375	0.7293

Region / Group	6	7	8	9	
1	3.0160	4.9580	2.3730	1.8440	
2	1.6830	3.8240	0.7937	1.3290	
3	1.0580	2.1740	0.3135	0.6821	

Table 5.2.3 Capture Cross Section

Region / Group	1	2	3	4	5
1	0.7233×10^{-2}	0.1318×10^{-2}	0.2741×10^{-2}	0.2744×10^{-2}	0.2649×10^{-2}
2	0.3291×10^{-1}	0.9279×10^{-3}	0.6553×10^{-2}	0.6577×10^{-2}	0.6663×10^{-2}
3	0.2006	0.4848×10^{-3}	0.2689×10^{-1}	0.2709×10^{-1}	0.3095×10^{-1}

Region / Group	6	7	8	9	
1	0.1735×10^{-2}	0.2505×10^{-2}	0.1972×10^{-2}	0.8290×10^{-2}	
2	0.1358×10^{-2}	0.2125×10^{-2}	0.1262×10^{-2}	0.2887×10^{-1}	
3	0.2157×10^{-2}	0.1934×10^{-2}	0.7048×10^{-2}	0.2805	

Table 5.2.4 Fission Cross Section

Region / Group	3	4	5
1	0.3471×10^{-2}	0.3474×10^{-2}	0.3452×10^{-2}
2	0.3259×10^{-2}	0.3266×10^{-2}	0.3307×10^{-2}
3	0.1560×10^{-1}	0.1576×10^{-1}	0.1876×10^{-1}

Table 5.2.5 Scattering Cross Section from GP into G
(Diagonal elements represent total removal cross sections)

Region	1			2		
G / GP	1	2	3	1	2	3
1	0.1554×10^{-1}	0.	0.	0.1656×10^{-2}	0.	0.
2	0.9417	0.3458×10^{-1}	0.	0.3380×10^{-3}	0.1050×10^{-2}	0.
3	0.	0.1668×10^{-2}	0.2006	0.	0.1221×10^{-3}	0.4848×10^{-3}

Region	3			4		
G \ GP	1	2	3	1	2	3
1	0.1338×10^{-1}	0.	0.	0.1338×10^{-1}	0.	0.
2	0.7168×10^{-2}	0.1152×10^{-1}	0.	0.7162×10^{-2}	0.1160×10^{-1}	0.
3	0.	0.1708×10^{-2}	0.4249×10^{-1}	0.	0.1757×10^{-2}	0.4285×10^{-1}

Region	5			6		
G \ GP	1	2	3	1	2	3
1	0.1335×10^{-1}	0.	0.	0.4582×10^{-2}	0.	0.
2	0.7249×10^{-2}	0.1206×10^{-1}	0.	0.2847×10^{-1}	0.3060×10^{-2}	0.
3	0.	0.2090×10^{-2}	0.4971×10^{-1}	0.	0.2248×10^{-2}	0.2157×10^{-2}

Region	7			8		
G \ GP	1	2	3	1	2	3
1	0.4552×10^{-2}	0.	0.	0.4877×10^{-2}	0.	0.
2	0.2047×10^{-2}	0.2583×10^{-2}	0.	0.2905×10^{-2}	0.5769×10^{-2}	0.
3	0.	0.7277×10^{-3}	0.1934×10^{-2}	0.	0.4507×10^{-2}	0.7048×10^{-2}

Region	9		
G \ GP	1	2	3
1	0.2169×10^{-1}	0.	0.
1	0.1340×10^{-1}	0.2980×10^{-1}	0.
3	0.	0.9318×10^{-3}	0.2805

Table 5.2.6 Capture Cross Section versus FRED Position

Region 1		
G	FRED In	FRED Out
1	0.7233×10^{-2}	0.1313×10^{-2}
2	0.3291×10^{-1}	0.9110×10^{-3}
3	0.2006	0.4582×10^{-3}

Table 5.2.7 Transport Cross Section versus FRED Position

Region 1		
G	FRED In	FRED Out
1	0.144113	0.013159
2	0.246366	0.020238
3	0.494340	0.058913

Table 5.2.8 Capture Cross Section versus Fuel Temperature

Region 3			
Temp / G	900°K	1300°K	1600°K
1	3.541×10^{-3}	3.540×10^{-3}	3.541×10^{-3}
2	8.466×10^{-3}	8.538×10^{-3}	8.466×10^{-3}
3	3.474×10^{-2}	3.620×10^{-2}	3.474×10^{-2}

Region 4			
G \ Temp	900°K	1300°K	1600°K
1	2.803×10^{-3}	3.550×10^{-3}	3.550×10^{-3}
2	8.497×10^{-3}	8.552×10^{-3}	8.577×10^{-3}
3	3.500×10^{-2}	3.634×10^{-2}	3.709×10^{-2}

Region 5			
G \ Temp	900°K	1300°K	1600°K
1	3.422×10^{-3}	3.426×10^{-3}	3.425×10^{-3}
2	8.608×10^{-3}	8.667×10^{-3}	8.705×10^{-3}
3	3.998×10^{-2}	4.155×10^{-2}	4.245×10^{-2}

$*\quad \Sigma c(T) = \Sigma c(Tt=_0) + \delta\Sigma$

$\delta\Sigma = F(T)-F(Tt=_0)$

Table 5.2.9 Fission Cross Section versus Fuel Temperature

Region	3		4		5	
G \ Temp	900°K	1600°K	900°K	1600°K	900°K	1600°K
1	0.3471×10^{-2}	0.3471×10^{-2}	0.3474×10^{-2}	0.3473×10^{-2}	0.3452×10^{-2}	0.3451×10^{-2}
2	0.3259×10^{-2}	0.3265×10^{-2}	0.3266×10^{-2}	0.3267×10^{-2}	0.3307×10^{-2}	0.3308×10^{-2}
3	0.1560×10^{-1}	0.1590×10^{-1}	0.1576×10^{-1}	0.1598×10^{-1}	0.1876×10^{-1}	0.1915×10^{-1}

Table 5.2.10 Transfer Cross Section versus Fuel Temperature

Region	3		4		5	
G \ Temp	900°K	1600°K	900 °K	1600°K	900 °K	1600°K
1	0.7168×10^{-2}	0.7168×10^{-2}	0.7162×10^{-2}	0.7169×10^{-2}	0.7249×10^{-2}	0.7258×10^{-2}
2	0.1708×10^{-2}	0.1718×10^{-2}	0.1757×10^{-2}	0.1734×10^{-2}	0.2090×10^{-2}	0.2064×10^{-2}
3	0.	0.	0.	0.	0.	0.

3. Results of One Dimensional Model Analysis

Two calculation cases for transient number 8 were performed by the one dimensional kinetics code, NAKIN, in order to evaluate the Doppler coefficient. The initial power level was set at 8 MW and the FRED worth was 1.257 $. In one case, a value of −0.0081 was used for the Doppler coefficient, $T\frac{dK}{dT}$, which was considered the most appropriate value for it. In the other case, a value of −0.0063 was used for $T\frac{dK}{dT}$. Figure 5.2.2. shows the power history result of calculation case 1. The power history calculation result was found to agree qualitatively with the experimental result of super-prompt critical transient 8 (Fig. 4.3.1) and that of the point reactor kinetics calculation. However, the second power peak level was proved to be higher in this calculation. This tendency is considered to be caused by the fitting result of the input reactivity vs. time, which, in this calculation, was simulated by the change in FRED capture cross section. Such influence is also seen in the net reactivity shown in Fig. 5.2.3.

Calculated results of neutron flux distributions of the initial state, the peak power level and at 0.3 sec after the test initiation are shown in Fig. 5.2.4, 5.2.5 and 5.2.6, respectively. A flux distortion due to the FRED insertion is seen on the distribution of group 3 in Fig. 5.2.4, but it is not dominant. An effect of the reflector can be found in the group 3 flux distribution in Figs. 5.2.4 to 5.2.6. This effect, however, is not strong enough to have a direct influence on the reactor power. Since the flux distribution shape during transient is, as a whole, invariable (see Figs. 5.2.4 to 5.2.6), it may be concluded that the transient can be sufficiently simulated by a point reactor kinetics model.

Fig. 5.2.2 Time Dependent Power for Super-Prompt Transient No.8
(Calculated by One Dimensional Kinetics Model)

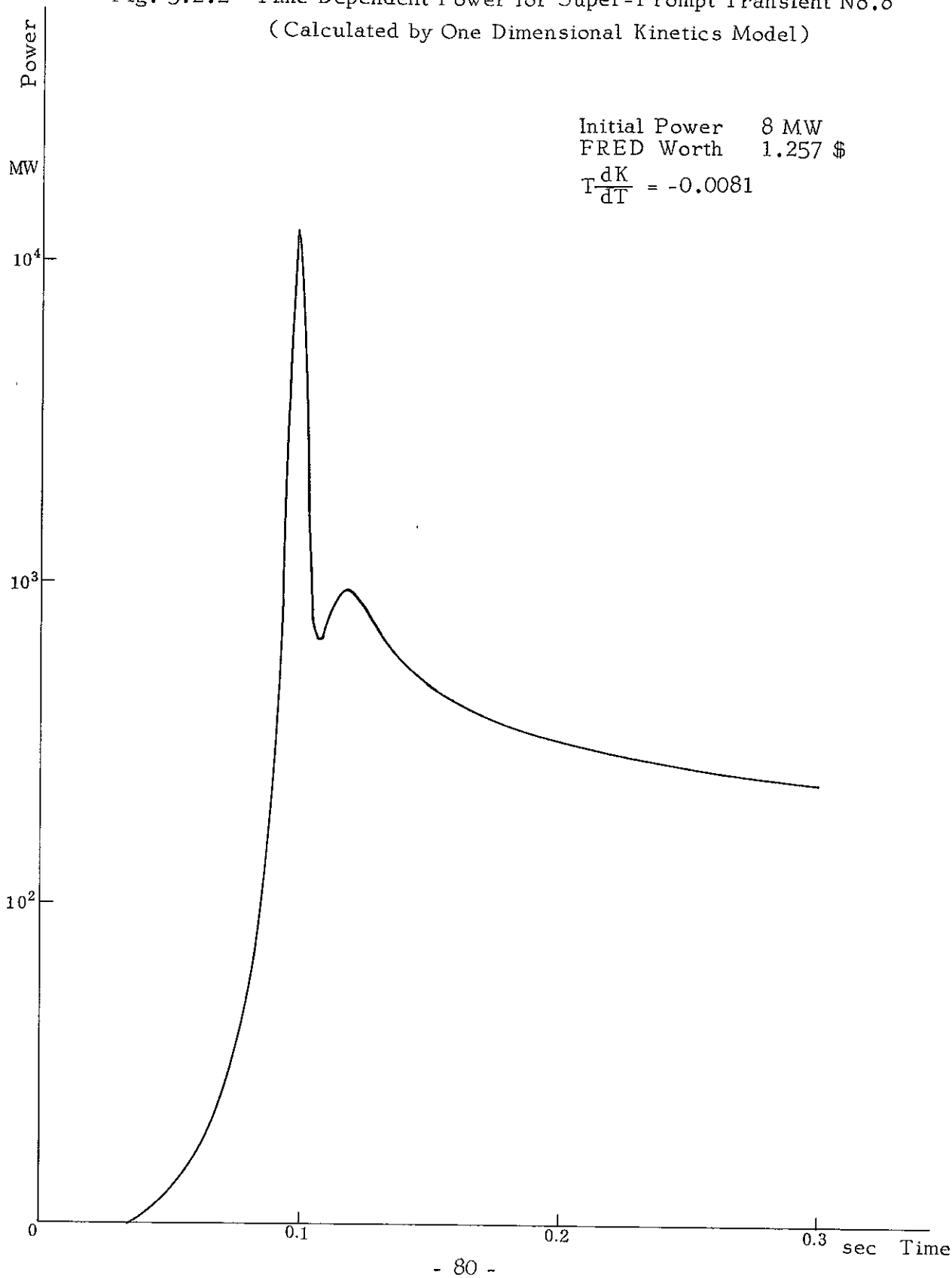

Fig. 5.2.3 Time Dependent Reactivities for Super-Prompt Transient No.8
(Calculated by One Dimensional Kinetics Model)

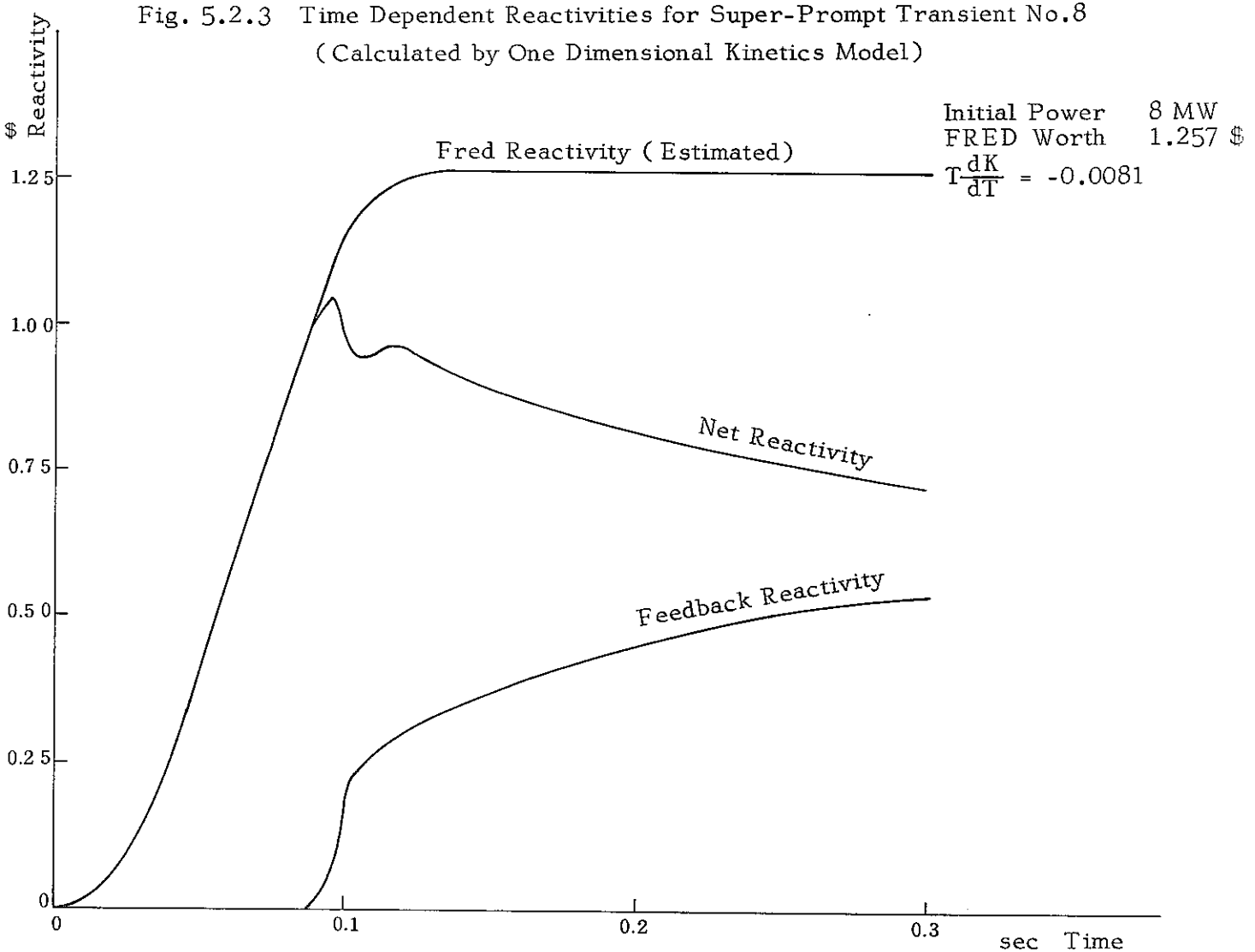

Fig. 5.2.4 Radial Neutron Flux Distribution for Super-Prompt Transient No.8
(at Initial State)

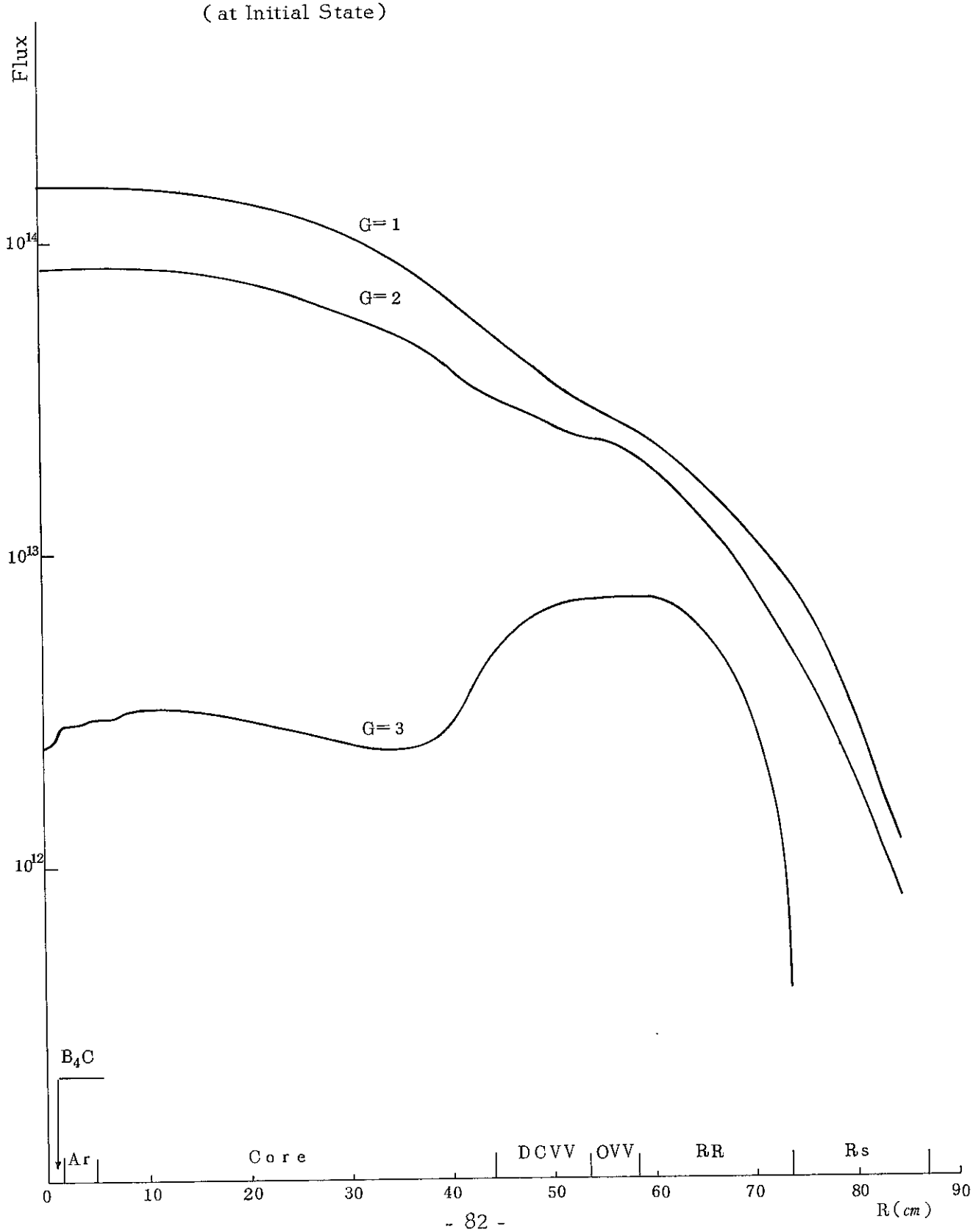

Fig. 5.2.5 Radial Neutron Flux Distribution for Super-Prompt Transient No.8
(at Peak Power Level)

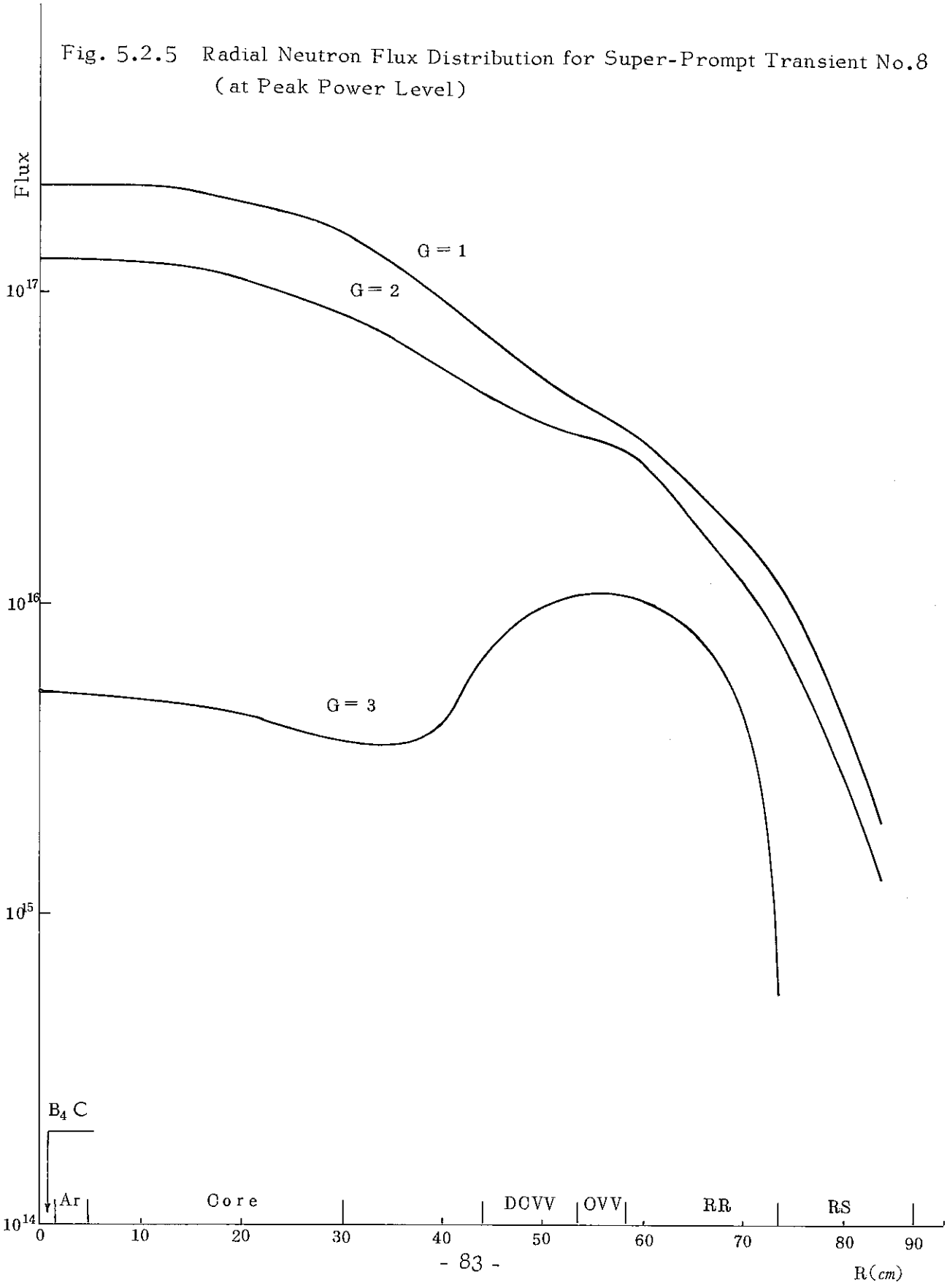

Fig. 5.2.6 Radial Neutron Flux Distribution for Super-Prompt Transient No.8
(at 0.3 sec after the Transient Initiation)

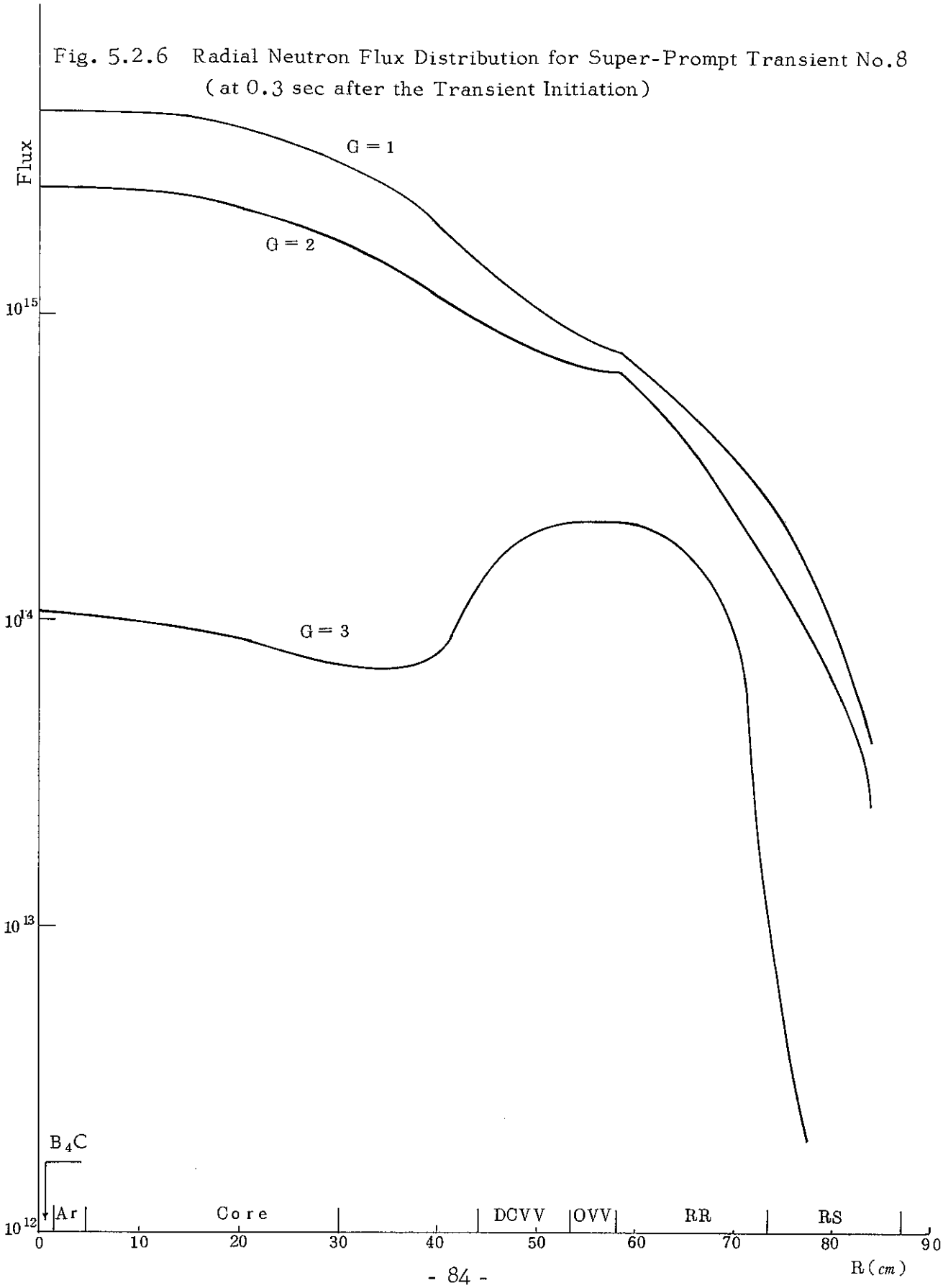

Fig. 5.2.7 Time Dependent Power for Super-Prompt Transient No.8
(Calculated by One Dimensional Kinetics Model)

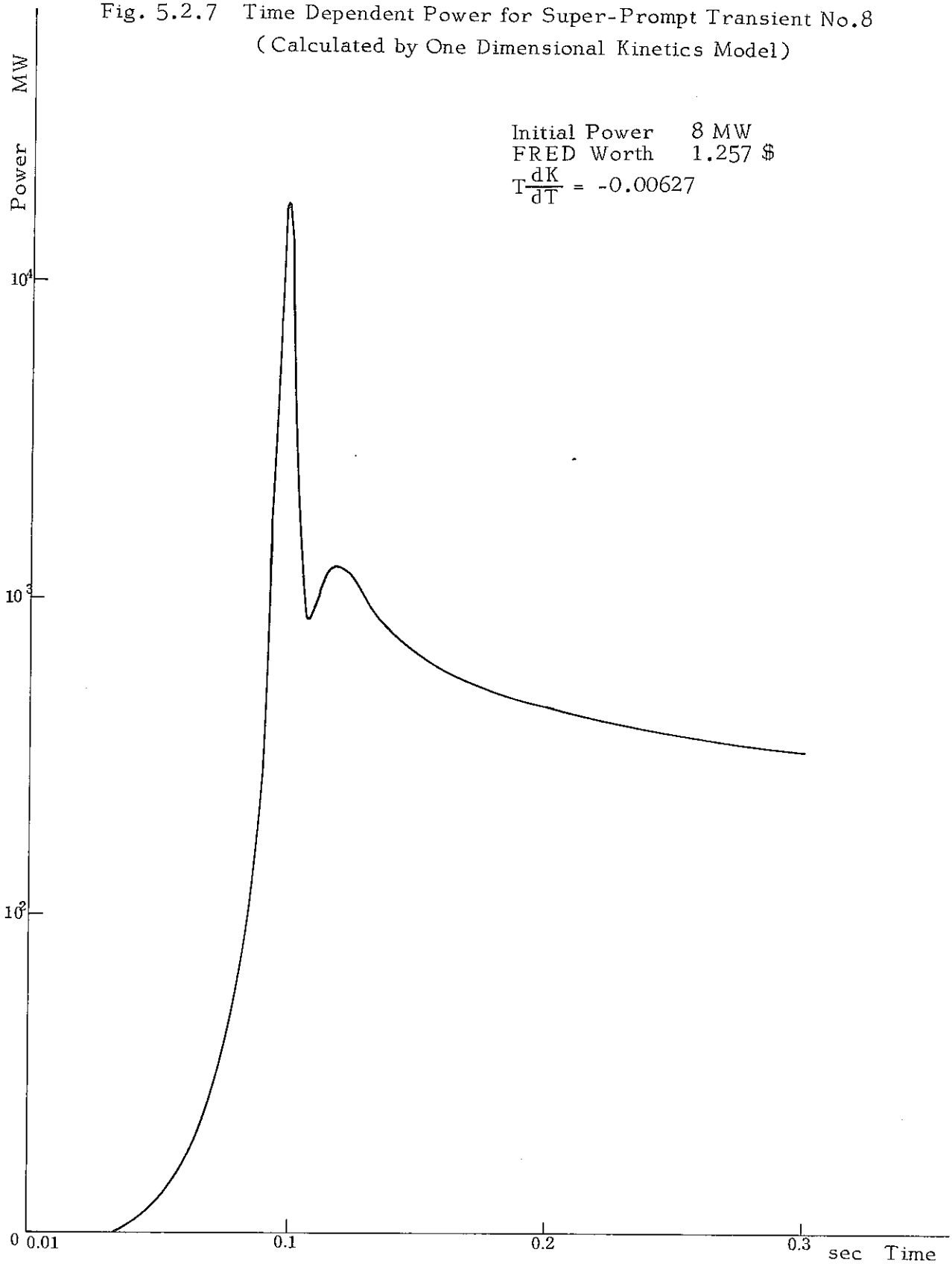

Fig. 5.2.8 Time Dependent Power for Super-Prompt Transient No.8
(Calculated by Point Reactor Kinetics Model)

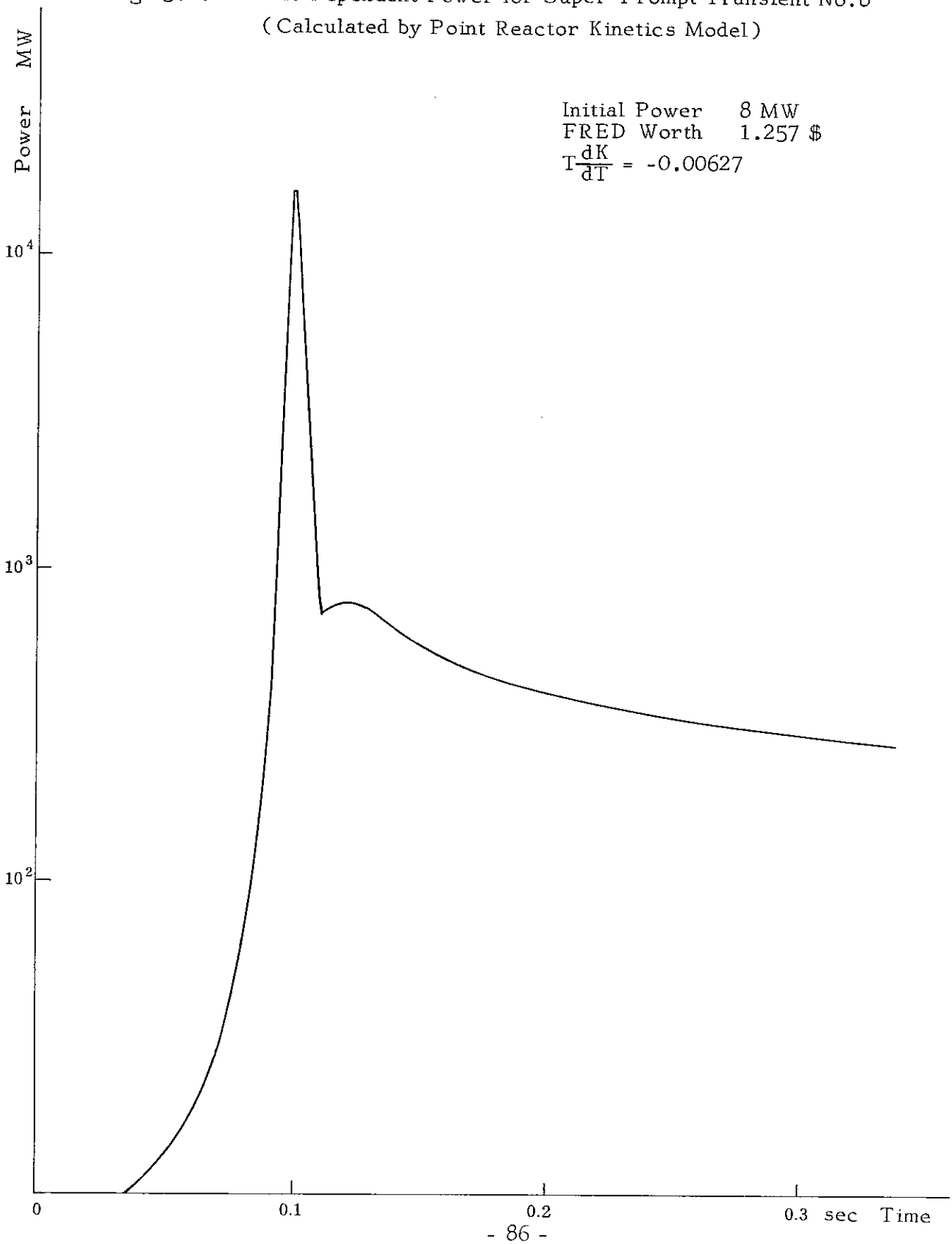

Fig. 5.2.9 Time Dependent Reactivities for Super-Prompt Transient No.8
(Calculated by One-Dimensional Kinetics Model)

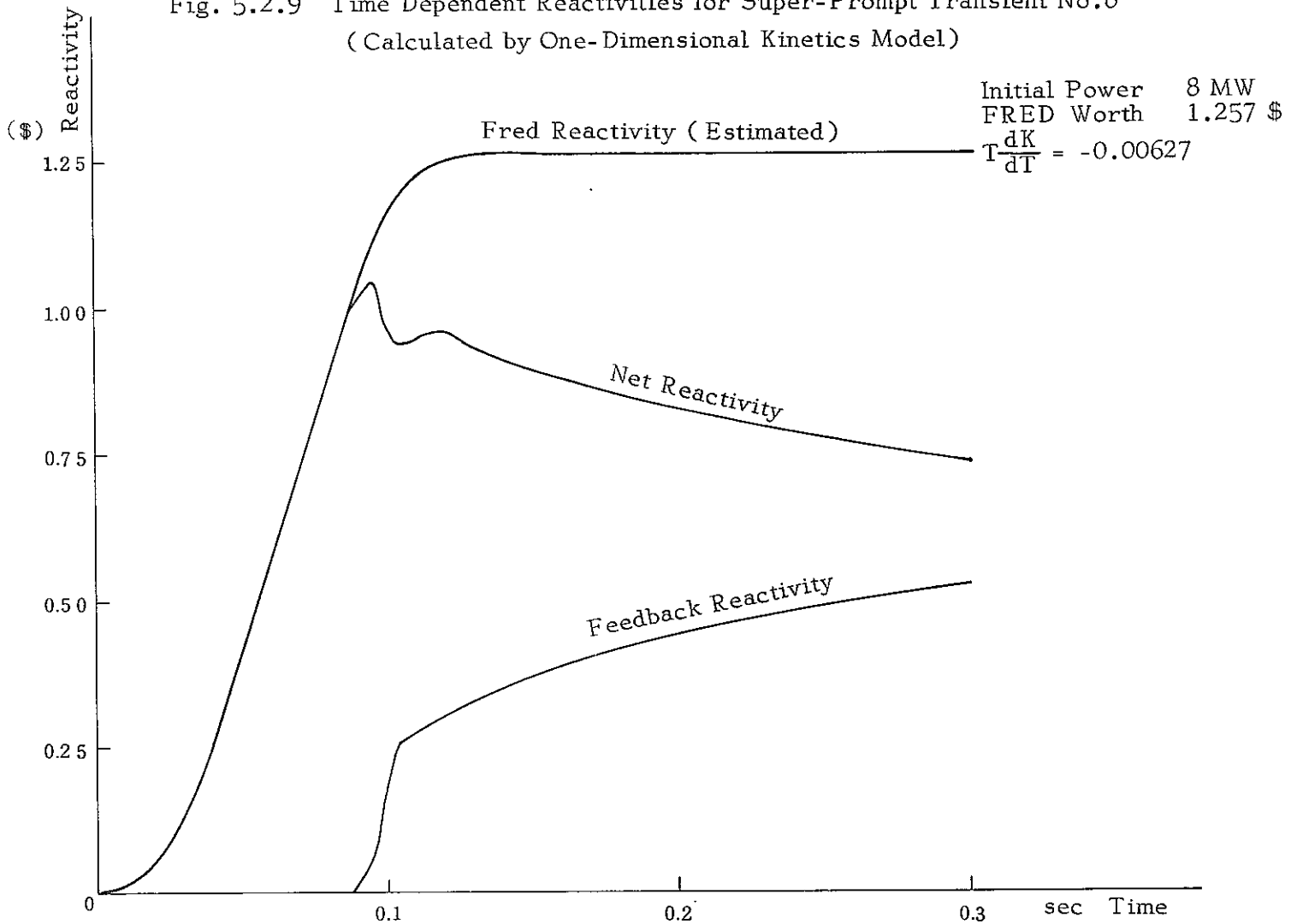

Fig. 5.2.10 Time Dependent Reactivities for Super-Prompt Transient No.8
(Calculated by Point Reactor Kinetics Model)

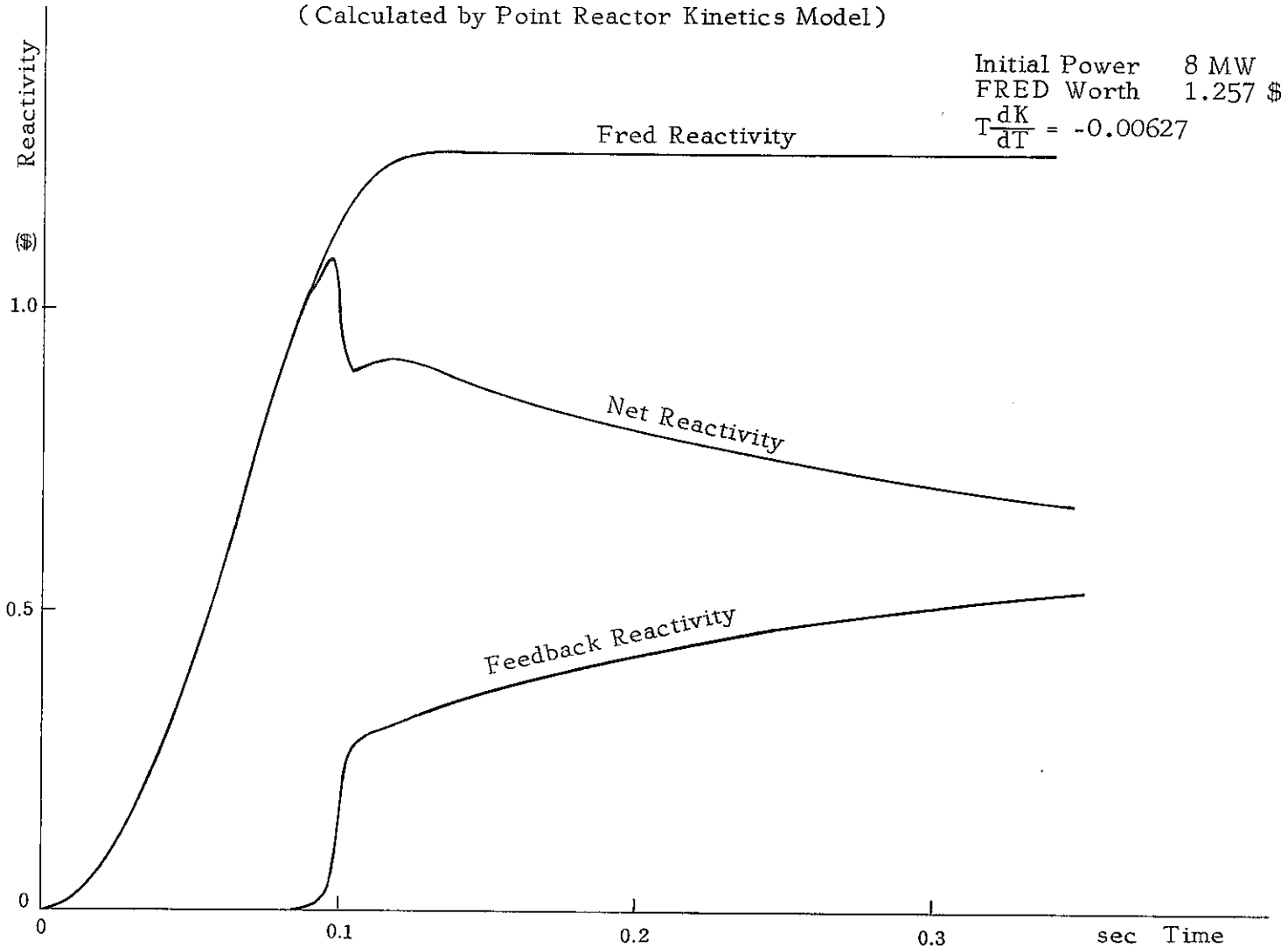

Calculated power history results for case 2 (with $T\frac{dK}{dT}$ of -0.0063), using NAKIN and the point reactor kinetics model, are shown in Figs. 5.2.7 and 5.2.8, respectively. Both results are greater in magnitude than the experimental power history. The calculated peak power levels are seen to be about twice as great in magnitude as the measurement values. From these results, the value of -0.0081 was confirmed to be reasonable for the Core I Doppler coefficient $T\frac{dK}{dT}$.

5-3. Application to "JOYO"

1. "JOYO" model

A one-dimensional sylindrical model was applied to "JOYO" (Japan Experimental Fast Reactor), in order to analyze the same hypothetical transient as in the case of SEFOR. The reactor was divided into 8 regions; of which four were in the fuel region, as shown in Fig. 5.3.1. Reactivity insertion was simulated by changing the neutron cross sections in Region 3, which was assigned to a control rod region. The reactivity insertion of this analysis was adjusted to be a ramp change from zero up to 1.18 $ during 0.1 sec.

Fig. 5.3.1 "JOYO" Core Configuration

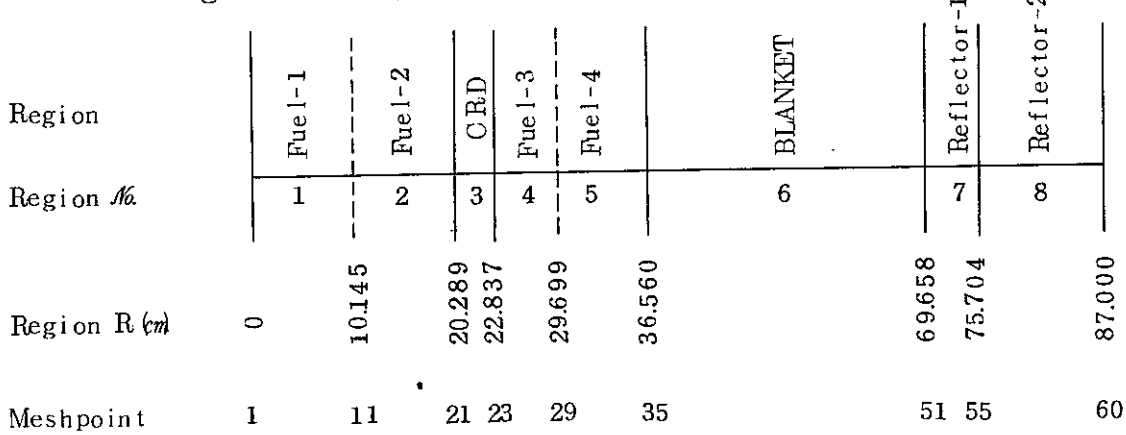

2. Data Used

Significant data on the "JOYO" reactor elements used in the calculation are summarized in Table 5.3.1. Similarly as in the previous section, nuclear data and various parameters are listed in Tables 5.3.2 through 5.3.12.

Table 5.3.1 "JOYO" Reactor Element Description

Reactor Thermal Power		50 MWt
Inlet Sodium Temperature		370 ℃
Outlet Sodium Temperature* (Fuel Region)		453 ℃
Outlet Sodium Temperature* (Blanket Region)		420 ℃
Core Height		60 cm
Extrapolation Distance (Radial)		30 cm
Fuel Rod		
Pellet Diameter	:	Core 5.4 mm, Blanket 13.6 mm
Clad Inner Diameter	:	5.6 mm, 13.8 mm
Clad Outer Diameter	:	6.3 mm, 15.0 mm
Volume Ratio		
Core Fuel/Na/SUS	:	0.3613/0.4013/0.2090
Blanket Fuel/Na/SUS	:	0.4798/0.3243/0.1817
Coolant Flow Rate		
Regions 1 and 2		350.8 cm/sec
Regions 4 and 5		290.0 cm/sec
Region 6		59.0 cm/sec

* These values were not used for calculation. Outlet sodium temperatures were calculated in the code through heat balce in the reactor.

Table 5.3.2 Delayed Neutron Fraction (β_i) and Decay Constant (λ_i)

i	β_i	λ_i (sec^{-1})
1	1.617×10^{-4}	0.0127
2	1.030×10^{-3}	0.0317
3	9.311×10^{-4}	0.1150
4	1.949×10^{-3}	0.3110
5	7.393×10^{-4}	1.4000
6	1.967×10^{-4}	3.8700
total	5.007×10^{-3}	

Table 5.3.3 Group Structure and Properties

Group Number	Energy for Collapse	Average Neutron Speed (cm/sec)	Fission Yield
1	10.5Mev − 0.1Mev	1.00761×10^{9}	0.9860
2	10.0Kev − 1.0 Kev	2.48807×10^{8}	0.0140
3	1000ev − 0.215ev	3.11026×10^{7}	0.

Table 5.3.4 Diffusion Coefficient

Region Group	1	2	3	4
1	1.9070	1.9070	4.0820	1.8870
2	1.1260	1.1260	2.5450	1.1150
3	0.8091	0.8091	1.8190	0.7993

region / group	5	6	7	8
1	1.8870	1.5420	1.7860	2.5560
2	1.1150	0.9847	1.1210	1.6100
3	0.7993	0.8723	0.4738	0.9282

Table 5.3.5 Capture Cross Section

G \ R	1	2	3	4
1	0.3540×10^{-2}	0.3540×10^{-2}	0.5964×10^{-2}	0.3496×10^{-2}
2	0.6160×10^{-2}	0.6160×10^{-2}	0.1011×10^{-1}	0.6349×10^{-2}
3	0.2787×10^{-1}	0.2787×10^{-1}	0.5066×10^{-1}	0.3069×10^{-1}

G \ R	5	6	7	8
1	0.3496×10^{-2}	0.2940×10^{-2}	0.1584×10^{-2}	0.1883×10^{-2}
2	0.6349×10^{-2}	0.6515×10^{-2}	0.1940×10^{-2}	0.1686×10^{-2}
3	0.3069×10^{-1}	0.1501×10^{-1}	0.3835×10^{-2}	0.2458×10^{-2}

Table 5.3.6 Fission Cross Section

G \ R	1, 2	4, 5	6
1	0.4672×10^{-2}	0.4641×10^{-2}	0.5649×10^{-3}
2	0.6037×10^{-2}	0.6198×10^{-2}	0.6212×10^{-4}
3	0.2989×10^{-1}	0.3251×10^{-1}	0.3944×10^{-3}

Table 5.3.7 Scattering Cross Section from GP into G
(Diagonal elements represent total removal cross sections)

R	1 , 2			3		
G \ GP	1	2	3	1	2	3
1	0.1276×10^{-1}	0.	0.	0.8363×10^{-2}	0.	0.
2	0.4548×10^{-2}	0.1279×10^{-1}	0.	0.2399×10^{-2}	0.1061×10^{-1}	0.
3	0.	0.5927×10^{-3}	0.5776×10^{-1}	0.	0.5052×10^{-3}	0.5066×10^{-1}

R	4 , 5			6		
G \ GP	1	2	3	1	2	3
1	0.1297×10^{-1}	0.	0.	0.1160×10^{-1}	0.	0.
2	0.4833×10^{-2}	0.1332×10^{-1}	0.	0.8155×10^{-2}	0.8267×10^{-2}	0.
3	0.	0.7734×10^{-3}	0.6320×10^{-1}	0.	0.1690×10^{-2}	0.1540×10^{-1}

R	7			8		
G \ GP	1	2	3	1	2	3
1	0.7961×10^{-2}	0.	0.	0.6672×10^{-2}	0.	0.
2	0.6377×10^{-2}	0.5262×10^{-2}	0.	0.4789×10^{-2}	0.4605×10^{-2}	0.
3	0.	0.3322×10^{-2}	0.3835×10^{-2}	0.	0.2919×10^{-2}	0.2458×10^{-2}

Table 5.3.8 Capture Cross Section versus Control Rod Position

Region 3		
G	Control Rod In	Control Rod Out
1	0.5964×10^{-2}	0.5537×10^{-2}
2	0.1011×10^{-1}	0.7795×10^{-2}
3	0.5066×10^{-1}	0.3487×10^{-1}

Table 5.3.9 Transport Cross Section versus Control Rod Position

Region 3		
G	Control Rod In	Control Rod Out
1	0.081659	0.079120
2	0.130976	0.126598
3	0.183251	0.165755

Table 5.3.10 Capture Cross Section versus Fuel Temperature

Region 1,2			
Temp / G	1080 °K	1280°K	1480°K
1	0.3542×10^{-2}	0.3542×10^{-2}	0.3542×10^{-2}
2	0.6176×10^{-2}	0.6189×10^{-2}	0.6191×10^{-2}
3	0.2793×10^{-1}	0.2828×10^{-1}	0.2856×10^{-1}

Region 4 , 5			
G \ Temp	1080 °K	1280°K	1480°K
1	0.3499×10^{-2}	0.3498×10^{-2}	0.3498×10^{-2}
2	0.6363×10^{-2}	0.6367×10^{-2}	0.6381×10^{-2}
3	0.3065×10^{-1}	0.3099×10^{-1}	0.3126×10^{-1}

Region 6			
G \ Temp	750°K	850°K	950°K
1	0.2944×10^{-2}	0.2944×10^{-2}	0.2943×10^{-2}
2	0.6517×10^{-2}	0.6546×10^{-2}	0.6570×10^{-2}
3	0.1501×10^{-1}	0.1528×10^{-1}	0.1553×10^{-1}

$*\quad \Sigma_c(T)=\Sigma_c(T_{t=0})+\delta\Sigma$

$\delta\Sigma = F(t)-F(T_{t=0})$

Table 5.3.11 Fission Cross Section versus Fuel Temperature

Region	1 , 2		4 , 5		6	
G \ Temp	1080°K	1480°K	1080°K	1480°K	750°K	950°K
1	4.671×10^{-3}	4.671×10^{-3}	4.640×10^{-3}	4.640×10^{-3}	5.640×10^{-4}	5.639×10^{-4}
2	6.052×10^{-3}	6.051×10^{-3}	6.209×10^{-3}	6.207×10^{-3}	6.214×10^{-5}	6.202×10^{-5}
3	2.996×10^{-2}	3.007×10^{-2}	3.247×10^{-2}	3.253×10^{-2}	3.944×10^{-4}	3.922×10^{-4}

Table 5.3.12 Transfer Cross Section versus Fuel Temperature

Region	1 , 2		4 , 5		6	
Temp / G	1080°K	1480°K	1080°K	1480°K	750°K	950°K
1	4.557×10^{-3}	4.557×10^{-3}	4.841×10^{-3}	4.842×10^{-3}	8.162×10^{-3}	8.163×10^{-3}
2	6.120×10^{-4}	6.084×10^{-4}	7.882×10^{-4}	7.816×10^{-4}	1.693×10^{-3}	1.672×10^{-3}
3	0.	0.	0.	0.	0.	0.

3. Analysis Results

NAKIN calculation for the "JOYO" reactor model was performed with an initial reactor power level of 50 MWt, a 1.18 $ input reactivity worth for the control rod and a Doppler coefficient, $T\frac{dK}{dT}$, of -0.002. As shown in Fig. 5.3.2, the maximum peak power level reached 500 times as high as the initial power level. The second power peak was seen on the downhill of the power history curve, which gave a marked contrast to the SEFOR case. The difference of the power history shapes is assumed to the dependent on the input reactivity time histories. The reactivity insertion curve applied to the "JOYO" model was not as smooth as that of SEFOR.

The reactivity curves in this case are shown in Fig. 5.3.3. A change in feedback reactivity is found to be sharp, compared with that of SEFOR. This is because of the "JOYO" fuel rod being thinner, its heat capacity being smaller, therefore the thermal conductance time constant in a fuel rod is smaller than the constants reported by the SEFOR tests. It is predicted that fuel temperature and reactivity feedback responses to a change in reactor power will be more rapid in the case of "JOYO".

Flux distributions during the transient are hardly seen to be affected by the control rod extraction, as shown in Figs. 5.3.4 through 5.3.6. The distortions in SEFOR flux distribution by the FRED were also not so distinguished. Since the neutron spectrum in "JOYO" is still harder, the effect of the control rod on the distortion in flux distribution is predicted to be smaller. Therefore, a point reactor kinetics model is thought to be adequate for an analysis of this kind.

The analytical results of the "JOYO" super-prompt critical transient demonstrated that the Doppler effect was capable of stopping the rapid power rise efficiently.

Fig. 5.3.2 Time Dependent Power for "JOYO" Super-Prompt Transient
(Calculated by One-Dimensional Kinetics Model)

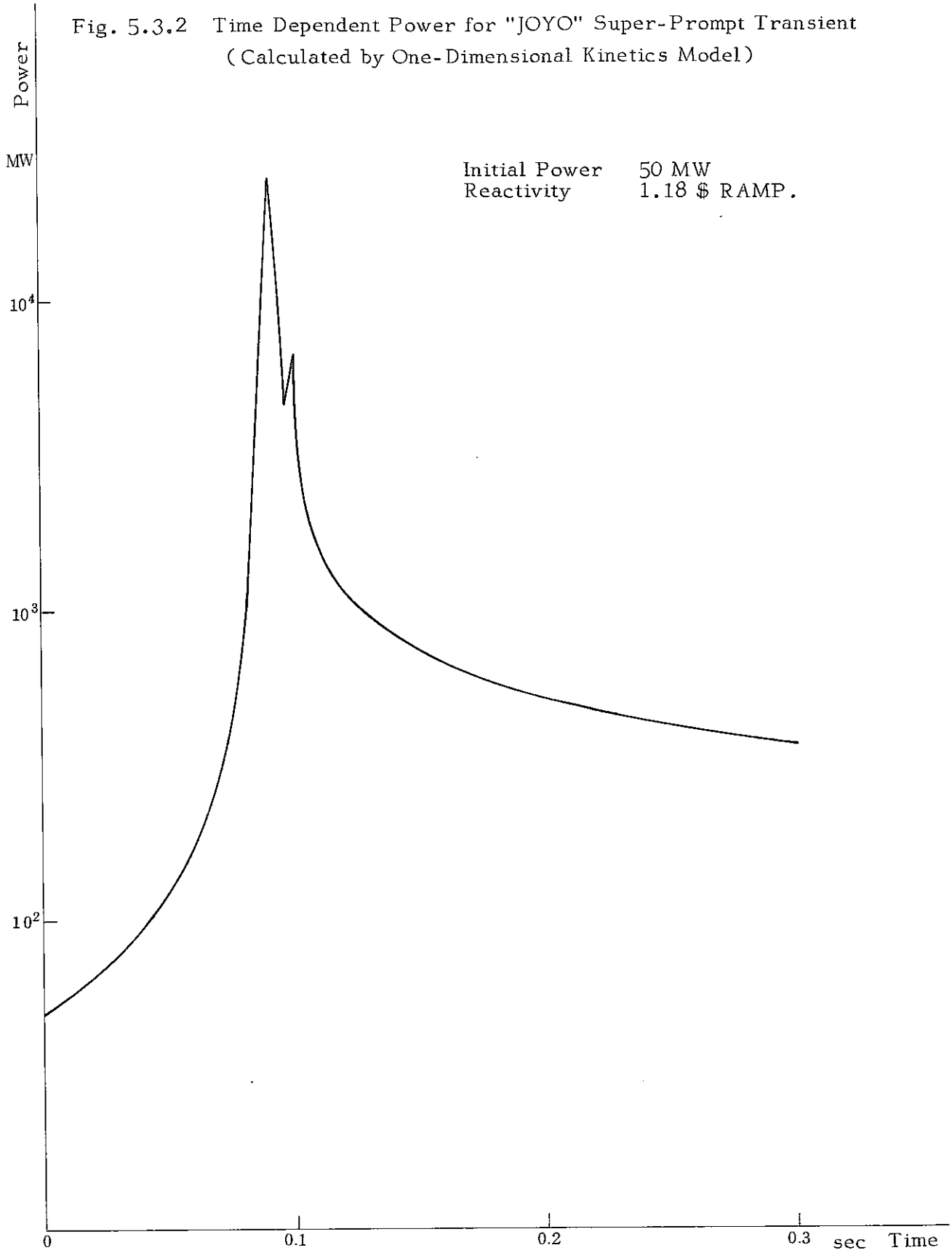

Fig. 5.3.3 Time Dependent Reactivities for "JOYO" Super-Prompt Transient
(Calculated by One-Dimensional Kinetics Model)

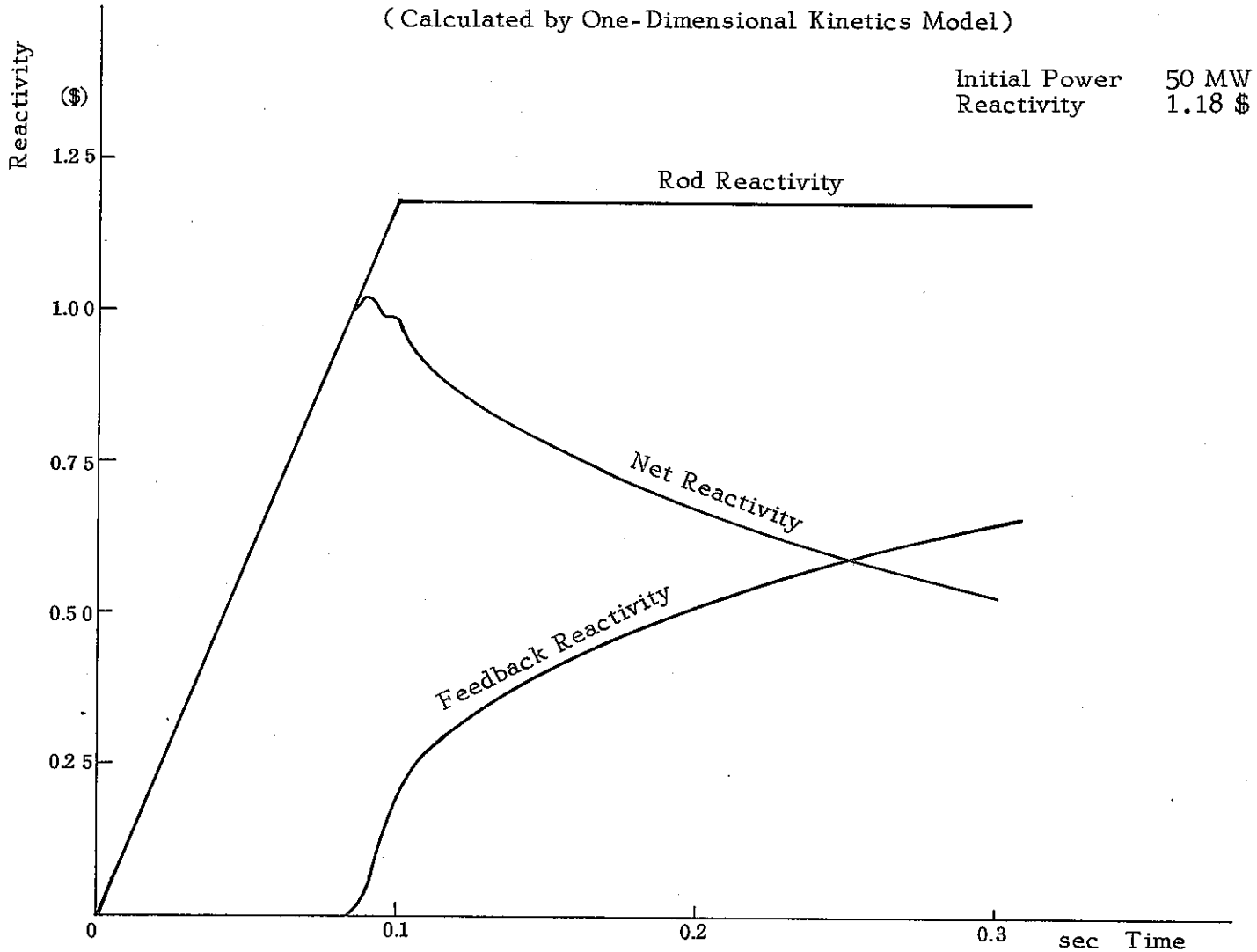

Fig. 5.3.4 Radial Neutron Flux Distribution for "JOYO" Super-Prompt Transient
(at Initial State)

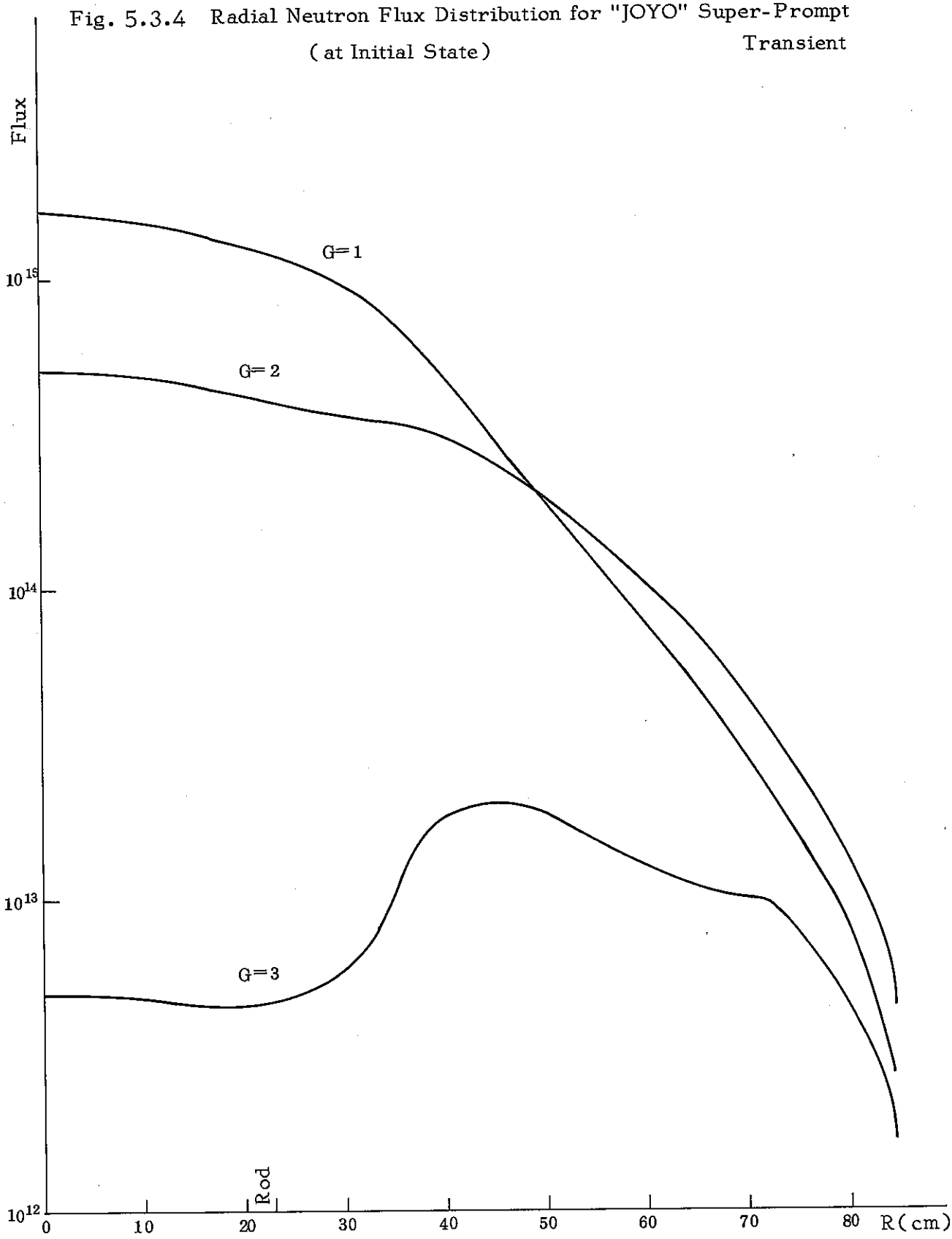

Fig. 5.3.5 Radial Neutron Distribution for "JOYO" Super-Prompt Transient (at Peak Power Level)

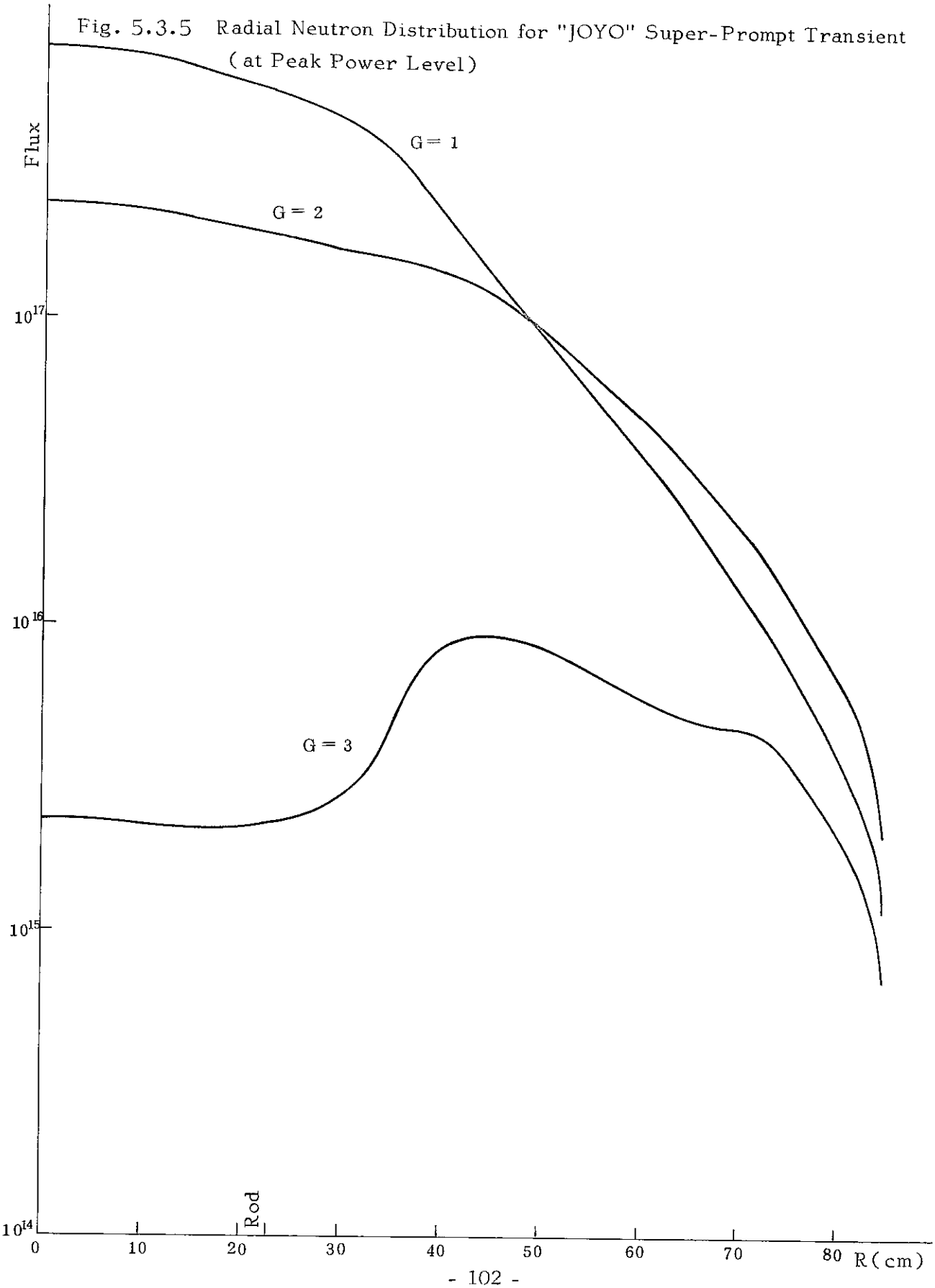

Fig. 5.3.6 Radial Neutron Flux Distribution for "JOYO" Super-Prompt Transient
(at 0.3 sec after the Transient Initiation)

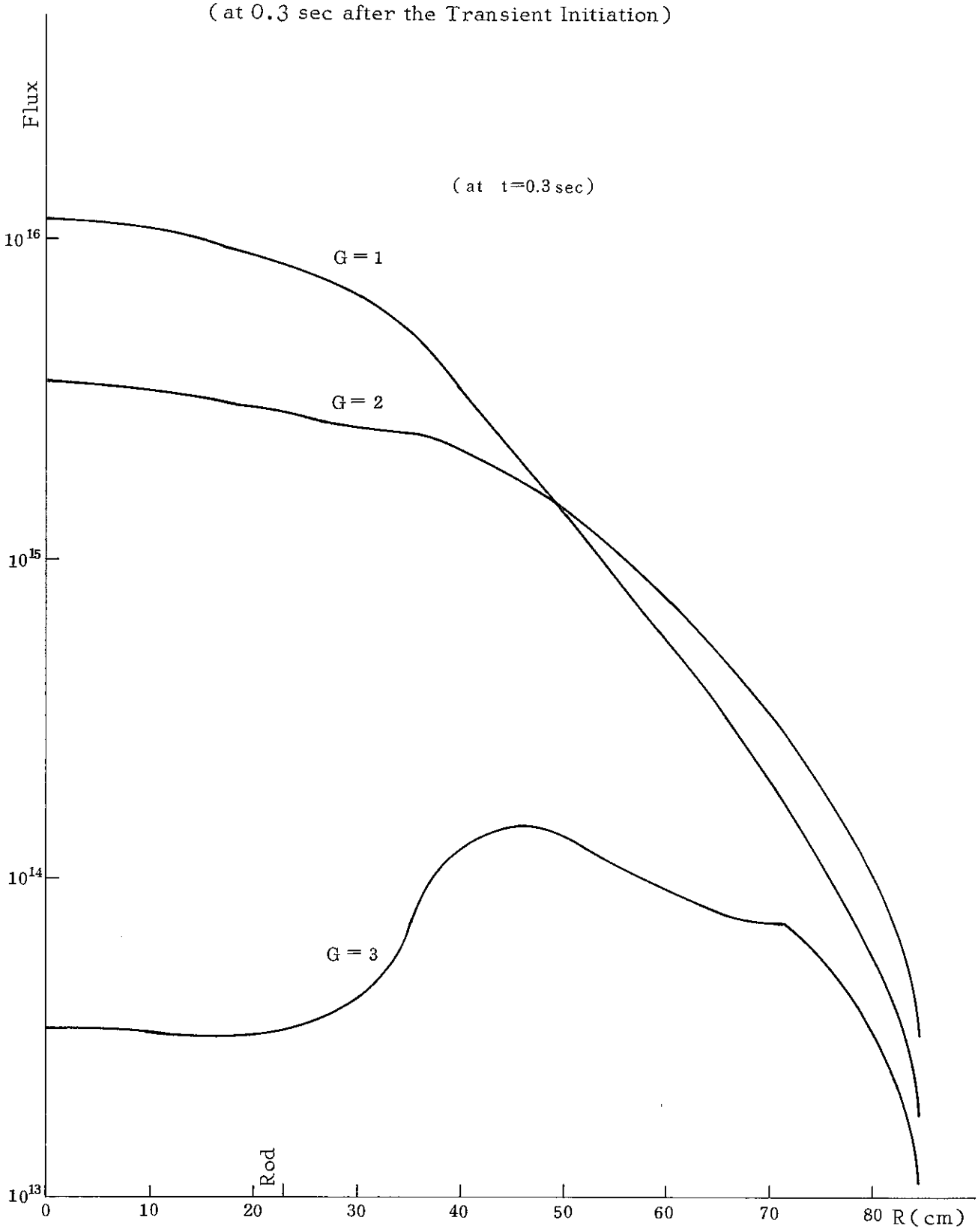

6. Discussion on Results

The purpose of this study was to evaluate the usual method of dynamic analysis for these severe transients by comparing analytical results with experimental data. Also, the purpose was to clarify the parameters and the method of approximation which have an important effect on the analysis.

The results of analysis performed with the point reactor kinetics model are described in Section 4. The calculated results were quantitatively in good agreement with the experimental data.

It was found that the calculated results of reactivity energy coefficient, peak power level, energy release and fuel temperature were affected especially by the values of thermodynamic parameters and β_{eff}, and by the method of calculating the average fuel temperature.

In evaluation of the feedback reactivity, a better approximation was found to take the weight of flux distribution (flux importance) into account. The method using the unweighted, volume average fuel temperature resulted in a smaller feedback reactivity, which was considered on a safety side in the analysis of reactor accident. However, good agreement was never reached with the experimental data. This was also shown to be true in the static analysis of the Doppler reactivity.[2]

The delayed neutron fraction has an important effect on the dynamic calculations of this kind through the relationship used to calibrate the reactivity values. The β_{eff} values are fairly different from one another, depending on the source data of the delayed neutron precursor yields. The keeping data were used throughout the SEFOR experimental program. Also, in this analysis, the keeping data were used to adjust the standard β_{eff} value.

Thermodynamic parameters had effects on the calculation of fuel temperatures at the initial state and during transients. There were many uncertainties in thermodynamic parameters to be adjusted for this analysis. Throughout the analysis, it was found that the initial fuel temperature had been calculated lower, especially in the cases with the low initial power level, as compared with the experimental data and the calculated results in the other reports.[2] That the difference between the calculated and measured reactivity energy coefficients was greater when the initial power level was low, was considered to be due to the effect of estimation of the initial fuel temperature. The low initial fuel temperature resulted, in turn, from the high estimation of the fuel thermal conductivity and/or the fuel-clad heat transfer coefficient. These factors should be examined in more detail.

The thermodynamic parameters, such as thermal conductivity and heat transfer coefficient, have many uncertainties from their nature. So far, in the reactor safety analysis and in design calculations, probable values obtained from various experiments have been used for such parameters according to the various situations. From the safety point of view, smaller values for them are usually used to confirm to the upper limit of the accident. The decrease in thermodynamic parameters causes an increase in initial fuel temperature and, as a result of the T^{-1} Doppler dependence of $\frac{dK}{dT}$ (for the SEFOR, a T^{-1} dependence of $\frac{dK}{dT}$ was indicated by calculation as in LMFBR's[16]), the Doppler reactivity feedback is calculated smaller. Therefore, the peak power level becomes higher and an increase in temperature at the center of the fuel rod results. This is a usual procedure for the safety analysis.

In most LMFBR's, such a great reactivity insertion rate as in the SEFOR experiments (~10 $/sec) is hardly considered. The reactivity insertion is usually well controlled to be a reasonable value (~ a few cents/sec) by the reactor control mechanism and, therefore, it is very difficult to imagine an actual occurrence of such a super-prompt critical accident. Sufficient means are provided on a timely basis to prevent the reactor from being in such a critical state through the reactor safety and protection system. On the other hand, it is not realistic to deny the possibility of a reactivity accident caused by a large scale fuel melting or sodium boiling or void. Therefore, from the reactor design and operation point of view, sufficiently careful means should be taken to prevent the occurrence of such an accident as sudden failure of sodium pumps, loss of coolant from the core, or establishment of excessively high ratio of the reactor power to coolant flow rate, which would lead to a reactivity accident.

In a severe accident analysis, to assure the safety of the system, the thermodynamic parameters are chosen so as to make sure of the upper limits of the plant variables, such as reactor peak power level and fuel temperature. As the accuracy of these parameters becomes betters, more realistic analyses will be performed. Therefore, it is necessary to enhance the reliability of these parameters for analytical use in the future. Thus, it is important to evaluate the various parameters such as thermodynamic properties to be used in calculation, through accumulation of experimental data from such experiments as the SEFOR program, and through comparison between the measured and calculated data.

Calculated results of the point reactor kinetics model agreed well with the analytical results by the one-dimensional kinetics model

calculated under the same conditions. Since the effect of the distortion in flux distribution is not considered so remarkable in a small reactor core like the size of the one used in SEFOR, it is concluded that such an analysis as this is sufficiently performed by the use of a point reactor kinetics model.

7. Conclusion

The SEFOR Core I experimental data were analyzed, mainly focused on the super-prompt critical transients, through simulation by using a point reactor kinetics model and a one-dimensional space-time model. It was found that the analytical results of reactor power, feedback reactivity and energy release by both methods agreed well with one another in quality, and that the dynamic analysis model and the theory of Doppler coefficient were sound.

In the analysis with the point reactor kinetics model, the reactivity energy coefficient was defined in order to evaluate and compare the measured and calculated Doppler reactivity effects. Both the calculated and measured reactivity energy coefficients agreed with one another when the initial power level was 8 MW, but were in less agreement in the case with lower initial power level under the same conditions.

For the maximum peak power level, a better coincidence was shown in the cases of lower initial power level. It can be said that good analytical results were obtained on the whole through this analysis.

Further, getting and examining more data in detail and choosing more reliable parameters for analyses, the Doppler reactivity effect and the pattern of reactor power change will be possible to be investigated with higher reliability.

8. Acknowledgement

The authors are grateful to Mr. K. Kinjo of the PNC for providing many materials, which contained valuable data necessary for this work and for many valuable discussions during the course of this work.

The authors are also indebted to Messrs. T. Yoshida and M. Kawashima of Nippon Atomic Industry Group Co., for their considerable assistance in nuclear data collapsing work.

9. References

(1) Y. Matsuno, et al., Compilation of Fast Critical Experiments (SEFOR) Analysis of Doppler Experiment (I) J201 72-15, May, 1972

(2) Y. Matsuno, et al., Analysis of Doppler Experiment (II) (SEFOR) J201 73-03, Feb., 1973 (in Japanese)

(3) G.R. Pflasterer, et al., SEFOR Development Program the 29th Quarterly Report, GEAP 10010-29, Aug. 1971

(4) G.R. Pflasterer, et al., SEFOR Development Program the 30th Quarterly Report, GEAP 10010-30, Nov. 1971

(5) G.R. Pflasterer, et al., SEFOR Development Program the 31st Quarterly Report, GEAP 10010-31, Feb., 1970

(6) L.D. Noble, et al., Results of SEFOR Zero Power Experiments, GEAP - 13588, March, 1970

(7) R.A. Meyer, et al., Design and Analysis of SEFOR Core I. GEAR - 13598, June, 1970

(8) L.D. Noble, et al., SEFOR Core I Test Results to 20 MW, GEAP - 13702, March, 1971

(9) L.D. Noble, et al., SEFOR Core I Transients GEAP - 13837, Aug. 1972

(10) D.D. Freeman, SEFOR Experimental Results and Applications to LMFBR's, GEAP - 13929, January, 1973

(11) R.A. Harris, et al., SEFOR - Core I Doppler Constant Analysis, HEDL - TME 72-78, April, 1972

(12) R.A. Harris, Analysis of the Doppler Constants of Core I and II of SEFOR, HEDL - TME 73-42, May, 1973

(13) W.A. Rhoades, Calculated Kinetics Parameters for the SEFOR Assemblies I-P, II-A and II-C, ORNL-TM-4244, May, 1973

(14) G.H. Golden, et al., Thermophysical Properties of Sodium, ANL-7323, Aug. 1967

(15) K.F. Hansen, et al., GAKIN: A One Dimensional Multigroup Kinetics Code, GA-7543, Aug. 1967

(16) D.D. Freeman, et al., GE SEFOR: Verification of the Doppler Transient Shutdown Capability of LMFBR's Sept. 1972

(17) F.G. Lether, The Use of Richardson Extrapolation in One-Step Methods with Variable Step Size, Mathematics of Computation, vol. 20 No.95, July, 1966

(18) C.B. Jackson, et al., Liquid Metals Handbook, July, 1955

(19) Thomson & Garelis, ACS Monograph Series, No. 133, 1956

(20) D. Bermann, et al., Weighted Doppler Analysis Code WEDOP, GEAP-5543, July, 1967